ANALYSIS OF SLOT-TYPE RADIATORS

A Dissertation

Presented to the Faculty of Graduate Studies

The University of Manitoba

In Partial Fulfillment

of the Requirements for the Degree

Doctor of Philosophy

in

Electrical Engineering

by

ABDOLMAJID HADIDI

B. Sc., Elec. Eng., 1983, University of Tehran, Iran

M. Sc., Elec. Eng., 1985, University of Manitoba, Canada

ISBN 0-315-47845-4

ANALYSIS OF SLOT-TYPE RADIATORS

BY

ABDOLMAJID HADIDI

A thesis submitted to the Faculty of Graduate Studies of
the University of Manitoba in partial fulfillment of the requirements
of the degree of

DOCTOR OF PHILOSOPHY

ABSTRACT

The problem of slot-type radiators including the cavity-backed slots is analyzed. A general formulation is given for the electric field in an arbitrary shaped aperture in a conducting screen and specialized to the case of a narrow slot. The electric field in the slot aperture satisfies Pocklington's equation for which a novel numerical technique based on the method of moments and Fourier transform is presented. Once the voltage distribution along the slot aperture is known one may easily obtain the radiation and circuit parameters of the antenna including the input impedance, resonance frequency and bandwidth.

The electromagnetic fields produced by sources in a bounded region, as well as the appropriate electric and magnetic-type dyadic Green's functions are derived and the results are used in formulating the general problem of an aperture backed by a conducting enclosure of arbitrary shape. A system of coupled integro-differential equations is obtained for the electric field along the aperture. The special case of a rectangular cavity-backed slot is examined in detail for which the Galerkin method with piecewise sinusoidal basis and testing functions is used to numerically solve for the voltage distribution along the slot. The effect of various parameters on the circuit quantities of the antenna are discussed and the case of probe-fed excitation of the cavity is also investigated.

It is shown that it is possible to obtain a Gaussian field distribution in the slot aperture by using a cavity of proper shape. To this end, the fields in the cavity are expressed as a superposition of plane waves and the beam-wave condition is applied to write approximate expressions for the fields that decay exponentially off the axial direction. The field amplitudes are then expanded in terms of Gauss-Hermite functions and the appropriate boundary condition is used to obtain the equation for the shape of the cavity back-wall. The structure is excited by a current source connected to the slot edges and an integral equation is derived for the voltage distribution along the slot which is solved numerically by using entire-domain basis and testing functions of the Gauss-Hermite type.

ACKNOWLEDGEMENTS

The author wishes to express sincere appreciation to his advisor Professor M. Hamid for his interest and encouragement. Thanks are also due to Professor L. Shafai of the University of Manitoba for a number of profitable discussions, and to the University of Manitoba Faculty of Graduate Studies, for the financial assistance in the form of fellowship which made this research possible.

TABLE OF CONTENTS

LIST OF FIGURES

CHAPTER 1

INTRODUCTION

The purpose of this thesis is to investigate the properties of slot-type radiators of electromagnetic waves. These include open slots in a conducting screen and slots backed by cavity resonators of various shapes for which two important types namely, rectangular and Gaussian geometries are analyzed in detail. In the following, we first present a survey of the literature relevant to the subjects covered in the work and then explain the contributions and organization of the thesis.

The problem of interaction between electromagnetic fields and an aperture in a conducting screen has attracted the attention of many workers ever since it was stated by Lord Rayleigh [1] some 90 years ago. A substantial part of the research in this area has been devoted to the diffraction of plane waves by apertures and a review paper which includes an extensive bibliography of the works prior to 1954 is given by Bouwkamp [2]. A review of the present status of the subject can be found in [3] and [4, pp. 117-172]. It should be pointed out that except for the case of circular apertures no analytical solution is available for this simplest of aperture problems [5]. Assuming D to be the largest dimension of the aperture, there exist asymptotic and approximate methods in the high ($D \gg \lambda$) and low ($D \ll \lambda$) frequency limits [6-16]. However, in the resonance region where $D \simeq \lambda$, which is incidentally of the greatest importance to microwave applications, all other approaches seem to break down and one usually has to resort to numerical methods.

Wilton and Dunaway [17] derived a set of integral equations for the magnetic current in an aperture of arbitrary shape and applied the method of moments to cast the integral equation to a matrix equation. Harrington and Mautz [18] introduced a generalized network formulation for aperture problems and in another paper [19], they obtained an operator equation for the magnetic current in the aperture and used the moments method to solve this equation for a rectangular aperture. It should be pointed out that in the above numerical

methods the matrix size and computer time for evaluating the matrix elements increase with the size of the aperture. At present this can cause severe computational limitations if both dimensions of the aperture are of the order of the wavelength λ or larger. Fortunately in antenna applications apertures are usually in the form of slots with one dimension much less than λ and therefore one should be able to apply the available numerical methods.

For the slot problem, Suzuki [20] considered the case of an incident plane wave and used the variational method to calculate the transmission coefficient. Butler [21] formulated the same problem and derived an integral equation for the electric field in the slot. The case of a slot antenna has often been treated in the literature [22] as the complementary of a strip dipole by applying Babinet's principle as generalized by Booker [23].

An open slot antenna, i.e. a slot in a conducting screen which is free to radiate from both sides, has limited applications. A practical alternative is the so-called cavity-backed slot (CBS) antenna where the slot is cut in the wall of a conducting enclosure in the form of a cavity resonator. These types of radiators satisfy the requirements of flush mounting as well as small size and light weight at lower operating frequencies (through dielectric loading) and therefore are most useful in airborne applications. On the other hand, CBS when used in an array configuration, produces small mutual effects and is thus a suitable element for large antenna systems such as phased arrays.

In one of the earliest treatments of CBS, Cohen [24] considered a square waveguide shorted at one end and radiating into half space at the other end. He assumed a single waveguide mode in the cavity and a TE_{10} mode for the tangential electric field in the aperture. The cavity was treated as a transmission line with terminals at the aperture whose admittance is known for the mode excited in the waveguide. He used the oscillation condition of the cavity to calculate the complex frequency from which the quality factor of the nth mode was defined. Galejs [25] obtained a variational expression for the admittance of a rectangular CBS where the slot was excited at the center by a delta current source. This expression is in terms of the unknown voltage distribution along the slot and is stationary with respect to small variations of the voltage distribution which was assumed to be

sinusoidal. It is possible in general to expand the unknown field in terms of a set of suitable functions and use the stationarity property of the admittance to obtain a system of nonlinear equations for the expansion coefficients. However, only two terms of such an expansion were considered by Galejs and the calculations were only for the ratio of their coefficients.

In a later paper, Adams [26] derived a variational expression for the aperture admittance of a loaded semi-infinite rectangular waveguide radiator and used the result in calculating the aperture admittance for the case of an aperture plane iris. The computations were performed for the waveguide dominant mode and thus a sinusoidal aperture field was assumed. The results were then applied to a shorted waveguide excited by a coaxial probe. An equivalent circuit was presented and used to calculate parameters such as resonance frequency, bandwidth and efficiency. The possibility of tuning the ferrite loaded cavity by applying a dc magnetic field was also shown experimentally. In this work the emphasis was on loading the cavity by dielectric and ferrite material which can significantly reduce the size of the antenna for a given frequency at the expense of reduction in bandwidth.

The calculation of the input admittance of a rectangular CBS is also the subject of a paper by Cockrell [27]. He applied the complex Poynting theorem to the small volume formed by the slot with a current source across its center and obtained the admittance for vanishing screen thickness with the assumption of a single propagating mode in the cavity and a sinusoidal field distribution in the slot. Extensive experimental measurements of the input impedance of a rectangular CBS were performed by Long [28]. In these experiments the slot was fed by a coaxial cable connected to the center of the slot and the cavity cross section was chosen such that only the dominant mode could propagate. The cases of dielectric filled cavity and a waveguide with inductive post to replace the shorting plate were also considered. In another paper [29] based on the experimental data in [28], Long derived a formula for the admittance of CBS as a function of frequency and cavity depth for a specific cavity cross section and slot size and within a certain range of frequencies.

In some applications such as radar and tracking, it is very important to suppress the side lobes in the radiation pattern of the antenna. This can be achieved in principle by

producing a Gaussian field distribution in the radiating slot aperture which in turn can be obtained by using a cavity of proper shape to back the slot. Such a so-called Gaussian cavity resonator operating at microwave frequencies should support fields that decay exponentially in a certain direction and in this respect it resembles the laser at optical frequencies. The appropriate field solution which is usually known as a wave beam because of its localized and directional nature, was first introduced by Goubau and Schwering for the circularly symmetric case [30]. These authors expressed the field as a set of elementary wave beams which were characterized by Laguerre polynomials and pointed out the possibility of reiterating and guiding the waves by reconstituting the cross-sectional phase distribution at certain intervals to construct a beam waveguide which is an open structure and does not need the metallic side walls to confine the fields. Experimental results based on this theory were subsequently reported by Christian and Goubau for low-loss transmission of millimeter waves [31]. Further development of beam waveguides for optical frequencies can be found in [32-34].

The wave beam of rectangular symmetry was studied by Schwering [35] and he expressed the fields in terms of Hermite polynomials. To construct a Gaussian resonator one needs only to short circuit two appropriate constant phase surfaces of a beam waveguide by metallic reflectors. This resonator is essentially open from all sides; however, for beams of rectangular symmetry one may use two parallel conducting plates to restrict the size of the resonator in one direction. Brauer [36] used this type of resonator to make a line source antenna by cutting a row of closely spaced small holes in the front wall. For the electric field in the aperture, he used the magnetic dipole moment of the holes and assumed a delta function dependence for the transverse variable. The results reported in [36] indicated very low side-lobe levels in the radiation pattern and the possibility of obtaining aperture field distribution in the form of a Gaussian and the derivative of a Gaussian.

In Chapter 2 we obtain general equations for the tangential electric field in an aperture of arbitrary shape located in a planar conducting screen. The results are then reduced to an integro-differential equation for the special case of a narrow slot. A method based on a

combination of moments method and Fourier transform is proposed for efficient numerical solution of this equation [37]. A knowledge of the correct voltage distribution along the slot is necessary for accurate prediction of the antenna performance both as an electromagnetic radiator and as a circuit element. The latter aspect is emphasized by investigating the effect of various parameters such as slot length, slot width and feed point location on the slot voltage distribution, input impedance, resonance frequency and bandwidth.

The fields produced by electric and magnetic sources in an enclosure with conducting walls which contain radiating apertures are derived in Chapter 3. The fields are expanded in terms of irrotational and solenoidal eigenvectors and the results are written in the form of volume and surface integrals over the sources and boundaries respectively. General expressions for the electric and magnetic-type dyadic Green's functions of a bounded region are also obtained and specialized to the case of a rectangular cavity resonator. Most of the results and developments in this Chapter are reported elsewhere [38] and are extensively used in the rest of the thesis.

Regarding the problem of cavity-backed slot radiators, in spite of the rather large number of papers on this subject, no general and satisfactory treatment of the problem is available. For example in all the references mentioned earlier, the cavity has been considered as a shorted waveguide and no attempt is made to independently formulate the problem for the general case. Also a sinusoidal field distribution is assumed in the slot which corresponds to the presence of a single propagating mode in the cavity and is not correct in general. Furthermore, all the previous works fail to include the effect of one or more of the various parameters such as the cavity and slot dimensions, location of the excitation source, characteristics of the material in the cavity, etc. on the slot field distribution. In Chapter 4 we therefore derive general equations for the electric field in the aperture of a cavity-backed aperture radiator of arbitrary shape and specialize the results to the case of a narrow slot backed by a rectangular cavity. The structure is excited by a current source connected to the slot edges and hence the cavity can be considered as a load. The method of moments with piecewise sinusoidal basis and testing functions is used to numerically solve the integral

equation for the field in the slot. Subsequently, the effect of various parameters on the voltage distribution along the slot and impedance of the antenna as well as the resonance frequency and bandwidth are examined. The case where the cavity is excited by a coaxial-line probe and the slot acts as a load is investigated in Chapter 5. The calculation of the input impedance for this problem is rather involved and an approximate method based on the Poynting theorem is used for this purpose.

As far as the problem of Gaussian CBS is concerned, no rigorous solution for the electric field in the slot aperture could be found in the literature and therefore the subject has been treated in detail in Chapter 6. A general solution of the source free Maxwell's equations applied to the region between two conducting parallel plates is presented in terms of a continuous spectrum of elementary plane waves. Next, the wave beam condition is used to obtain an approximate solution for waves which are confined to a small solid angle about the principal axis of the system. A cavity resonator is formed by placing reflecting surfaces on two suitable constant-phase planes. The fields in the cavity are then expanded in terms of Gauss-Hermite functions whose orthogonality property is used to obtain the expansion coefficients. A radiating slot is cut in the front wall of the cavity and the structure is excited by a current source on the slot aperture. An integral equation is derived for the tangential electric field in the slot and entire-domain basis and testing functions are utilized in its numerical evaluation. The restrictions imposed on the cavity dimensions by the wave beam assumption are also discussed and the equation for the surface of the cavity back-wall is obtained and solved numerically.

CHAPTER 2

APERTURES IN A PLANAR CONDUCTING SCREEN

In this Chapter we first present a general formulation for the problem of diffraction by an arbitrary shape aperture in a perfectly conducting screen and then specialize the results to the case of a narrow slot. The resulting equation for the electric field in the slot aperture is in the form of an integro-differential equation and a technique based on the moments method and Fourier transform is proposed for its efficient numerical evaluation. The slot is excited by either a current source on the aperture or an incident plane wave which correspond to the radiation and diffraction problems, respectively. Once the electric field, and hence the voltage distribution, in the slot aperture is known it is easy to calculate the radiation and circuit parameters of the antenna. Booker's extension of Babinet's principle and its limitations are also discussed. Finally, typical numerical results for the voltage distribution, input impedance, resonance frequency and bandwidth are given.

2.1 - Formulation of the problem

The geometry of the fundamental problem to be considered in this section is shown in Fig. 2.1. The arbitrary shaped aperture is excited by specified impressed sources $\vec{J}^i$, $\vec{M}^i$ (or incident fields $\vec{E}^i$, $\vec{H}^i$) in region (1) as well as a surface current density $\vec{J}_s^a$ on the aperture. The screen is perfectly conducting, vanishingly thin and of infinite extent and is located in the $x-y$ plane. Regions (1) and (2) are homogeneous with parameters (μ_1, ε_1) and (μ_2, ε_2) respectively. The loss in the medium can be accounted for through replacing ε by $\varepsilon - j\,\frac{\sigma}{\omega}$. All source and field quantities are assumed to vary harmonically with time as $e^{j\omega t}$ which factor is suppressed throughout.

The fields in regions (1) and (2) should satisfy the following boundary conditions:

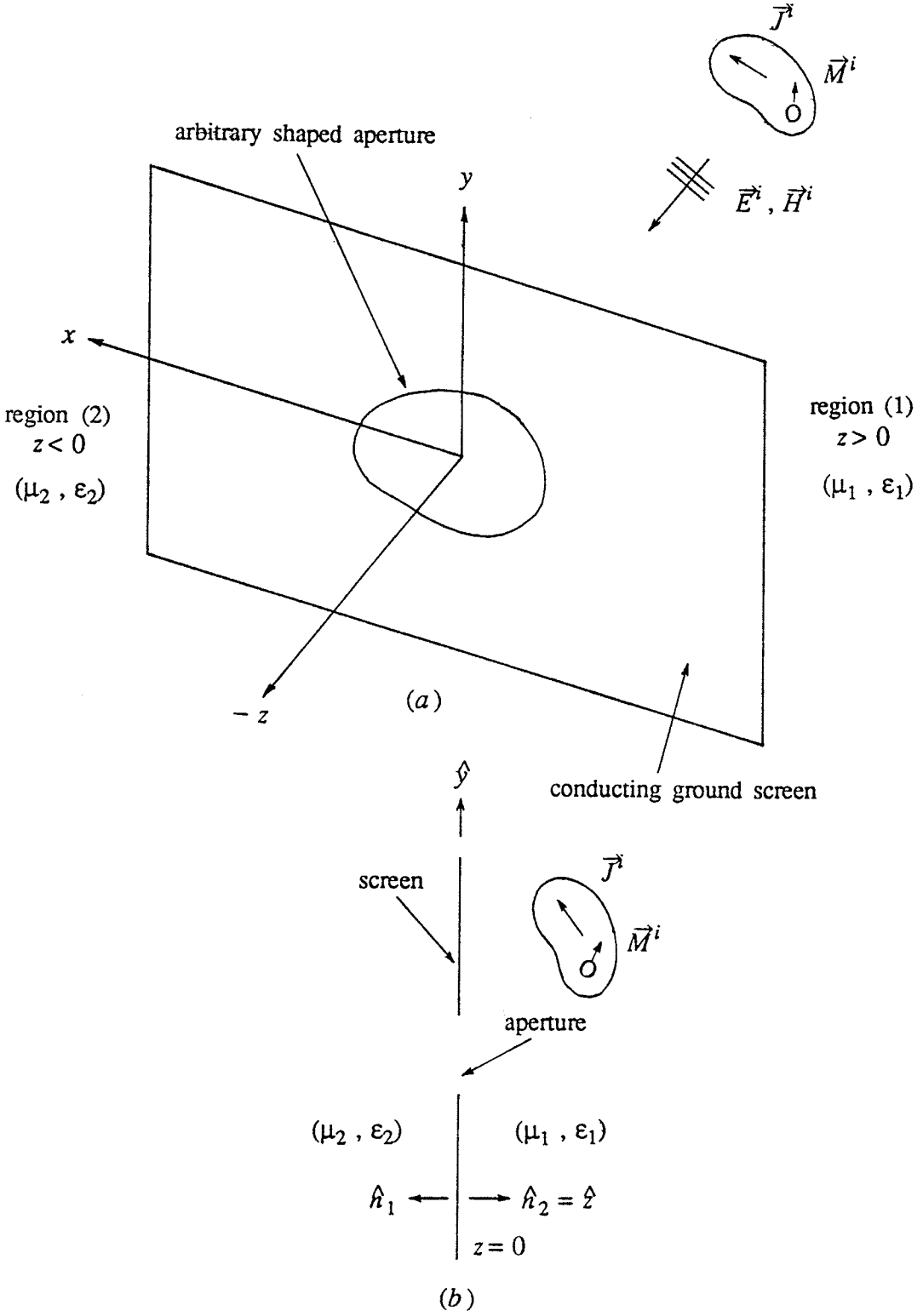

Fig. 2.1- An arbitrary shaped aperture in a planar conducting ground screen (a) and its cross-sectional view (b).

i) $\hat{n}_1 \times \vec{E} = 0$ on the surface of the ground screen,

ii) continuity of $\hat{n}_1 \times \vec{E}$ in the aperture,

iii) a discontinuity of $\hat{n}_1 \times \vec{H}$ in the aperture equal to $\vec{J}_s^a$.

We apply the surface equivalence principle [39] to replace the aperture and obtain a simple structure in each region. For convenience in the pictorial representations, we will assume in the following that the impressed current on the aperture $\vec{J}_s^a$ is zero; but it will be included in the final results. Considering for the moment only the fields in region (1) i.e. $z > 0$, it is clear from the equivalence principle that we can replace the entire ground screen, the aperture, and the half-space $z < 0$ by an imaginary surface in the $x-y$ plane on which the equivalent surface current densities $\vec{J}_s^{(1)} = \vec{H} \times \hat{n}_1$ and $\vec{M}_s^{(1)} = \hat{n}_1 \times \vec{E} \mid_A$ flow without affecting the fields in the half-space $z > 0$. Here A is the aperture area and quantities in the $z > 0$ region are denoted by the superscript (1). Note that the boundary condition *i* implies that $\vec{M}_s^{(1)}$ is non-zero only over that portion of the $x-y$ plane originally occupied by the aperture.

The application of the surface equivalence principle causes zero fields to exist in region (2), i.e. the half-space $z < 0$. Therefore as far as the fields in region (1) are concerned, it does not matter what material exists in region (2). Consequently we may fill this region by a perfect electric conductor immediately behind the surface currents in the $x-y$ plane. This eliminates the contribution of the electric surface current density $\vec{J}_s^{(1)}$ to the fields in region (1), as may be easily seen from considering the image of $\vec{J}_s^{(1)}$ due to the infinite ground screen. The above developments are represented in Figs. 2.2a and 2.2b. By further application of the image theorem, the original problem takes a simple form which is valid only for $z > 0$ as shown in Fig. 2.2c. Using the same procedures as explained above one obtains an equivalent magnetic surface current density $\vec{M}_s^{(2)} = \hat{n}_2 \times \vec{E} \mid_A$ for the equivalent system of region (2) which is shown in Fig. 2.3. Application of the boundary condition *ii* along with the fact that unit normal vectors are oppositely directed for the two half-spaces, leads to the conclusion that $\vec{M}_s = \vec{M}_s^{(1)} = -\vec{M}_s^{(2)}$ with $\vec{M}_s = -\hat{z} \times \vec{E}^a$ and $\vec{E}^a$ is the electric field in the aperture.

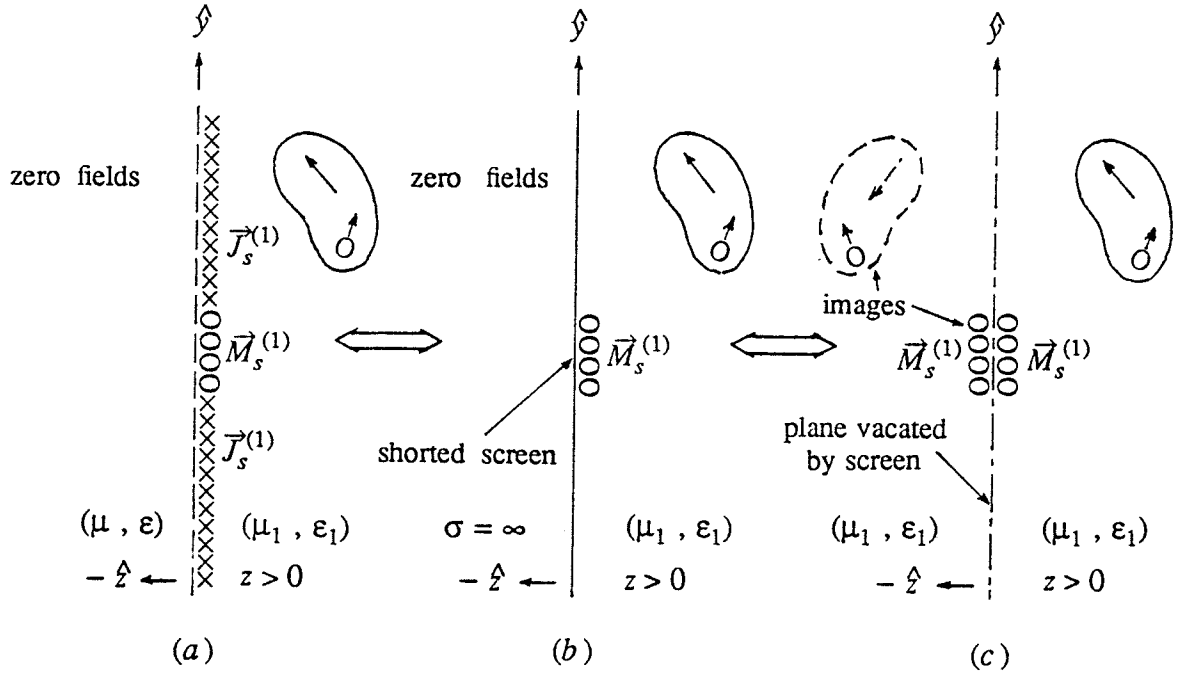

Fig. 2.2- Equivalent system of the problem, valid for $z > 0$.

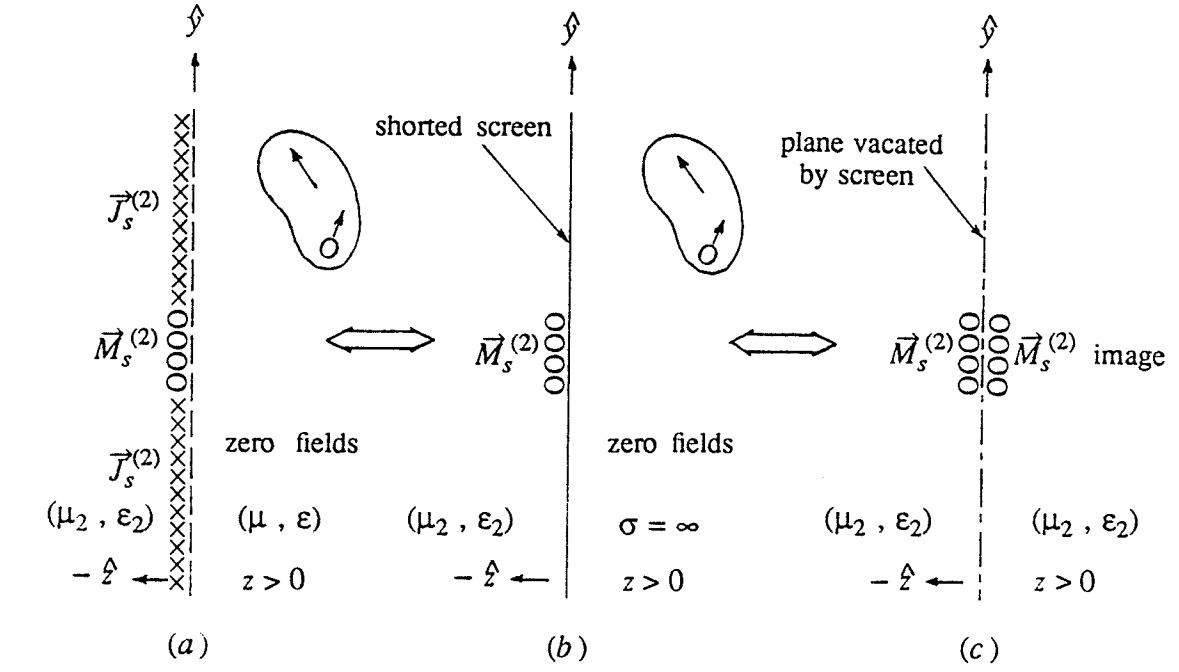

Fig. 2.3- Equivalent system of the problem, valid for $z < 0$.

The quantities $\vec{J}^i$ and $\vec{M}^i$ in Figs. 2.1 to 2.3 represent independent sources of the electromagnetic fields. The total fields $\vec{E}^{(1)}$ and $\vec{H}^{(1)}$ in region (1) are composed of incident fields $\vec{E}^i$ and $\vec{H}^i$ due to the independent sources which would exist in free space (i.e. in the absence of the screen) plus fields $\vec{E}^r$ and $\vec{H}^r$ reflected from the infinite non-perforated ground screen, and scattered fields $\vec{E}^{s(1)}$ and $\vec{H}^{s(1)}$ radiated by the equivalent surface current $\vec{M}_s^{(1)}$ in the presence of the shorted screen. The sum of the incident field and the reflected field may be considered as a short-circuit field, written as

$$\vec{E}^{sc} = \vec{E}^i + \vec{E}^r \tag{2.1a}$$

$$\vec{H}^{sc} = \vec{H}^i + \vec{H}^r \tag{2.1b}$$

In region (2) the total fields $\vec{E}^{(2)}$ and $\vec{H}^{(2)}$ are simply the scattered fields $\vec{E}^{s(2)}$ and $\vec{H}^{s(2)}$ radiated by the equivalent magnetic surface current density $\vec{M}_s^{(2)}$ in the presence of the shorted ground screen. The fact that $\vec{M}_s^{(1)} = -\vec{M}_s^{(2)}$ implies that we need only solve for $\vec{M}_s$. From the above considerations, the equivalent systems obtained for regions (1) and (2) satisfy the boundary conditions i and ii. The remaining condition (iii) will be used to determine the actual distribution of the equivalent current $\vec{M}_s$ in the aperture. In order to enforce this condition we must find the fields $\vec{H}^{s(1)}$ and $\vec{H}^{s(2)}$ produced by $\vec{M}_s$ which is the subject of the next section.

2.1.1- Calculation of the magnetic fields

The magnetic field due to a magnetic surface current density $\vec{M}_s$ is given by

$$\vec{H}(\vec{r}) = -\frac{j\omega\varepsilon}{4\pi}\int_S \overleftrightarrow{G}_0(\vec{r}' \mid \vec{r}) \cdot \vec{M}_s(\vec{r}')\, ds' \tag{2.2}$$

where the integration is over the magnetic current surface and $\overleftrightarrow{G}_0(\vec{r}' \mid \vec{r})$ is the dyadic Green's function of an unbounded region given by [40]

$$\overleftrightarrow{G}_0(\vec{r}' \mid \vec{r}) = \left(\overleftrightarrow{I} + \frac{1}{k^2}\nabla\nabla\right) G_0(\vec{r}' \mid \vec{r}) \tag{2.3}$$

In this equation $\overleftrightarrow{I} = \hat{x}\hat{x} + \hat{y}\hat{y} + \hat{z}\hat{z}$ is the unit dyadic and

$$G_0(\vec{r}' \mid \vec{r}) = \frac{e^{-jkR}}{R} \quad , \qquad k = \omega(\mu\varepsilon)^{1/2} \tag{2.4}$$

with

$$R = [(x - x')^2 + (y - y')^2 + z^2]^{1/2} \tag{2.5}$$

and the primed quantities are those of the source points.

In the equivalent system of Fig. 2.2c (Fig. 2.3c) we employed the image theorem, removed the infinite ground screen and replaced its effect in region $z > 0$ by an image magnetic surface current density identical to the original and located an infinitesimally small distance away. This leaves, in effect, a magnetic surface current distribution $2\vec{M}_s^{(1)}$ (or $2\vec{M}_s^{(2)}$ if $z < 0$) which is non-zero only over the surface S, which resides in free space, and which together with the incident fields and their images yield the correct fields for $z > 0$ and zero fields for $z < 0$.

With the above development, an expression for $\vec{H}^s$ is easily obtained in each region by using (2.2) with the appropriate current density. The total fields are then

$$\vec{H}^{(1)} = \vec{H}^{s(1)} + \vec{H}^{sc} \tag{2.6}$$

$$\vec{H}^{(2)} = \vec{H}^{s(2)} \tag{2.7}$$

The condition *iii* on the tangential magnetic fields on the aperture requires that

$$\lim_{z \to 0^+} \hat{z} \times \vec{H}^{(1)} - \lim_{z \to 0^-} \hat{z} \times \vec{H}^{(2)} = \vec{J}_s^a \tag{2.8}$$

where $\vec{J}_s^a$ is the specified impressed current distribution on the aperture. On the surface of the electric conductor the condition $\hat{z} \times (\vec{H}^i - \vec{H}^r) = 0$ must be satisfied and therefore from (2.1b) we obtain

$$\hat{z} \times \vec{H}^{sc} = 2\, \hat{z} \times \vec{H}^i \tag{2.9}$$

Expansion of (2.6) to (2.9) yields the following system of equations for the unknown magnetic surface current density $\vec{M}_s$ on the aperture

$$H_x^{(2)} - H_x^{(1)} = - J_y^a \, , \qquad z \to 0 \tag{2.10a}$$

$$H_y^{(2)} - H_y^{(1)} = J_x^a \,, \qquad z \to 0 \tag{2.10b}$$

where

$$H_x^{(1)}(x,y) = 2H_x^i - \frac{j\omega\varepsilon_1}{2\pi k_1^2}\int_A [M_x(x',y')\,(k_1^2 + \frac{\partial^2}{\partial x^2})G_0 + M_y(x',y')\frac{\partial^2}{\partial x\,\partial y}G_0]\,ds' \tag{2.11a}$$

$$H_y^{(1)}(x,y) = 2H_y^i - \frac{j\omega\varepsilon_1}{2\pi k_1^2}\int_A [M_x(x',y')\frac{\partial^2}{\partial y\,\partial x}G_0 + M_y(x',y')\,(k_1^2 + \frac{\partial^2}{\partial y^2})G_0]\,ds' \tag{2.11b}$$

and

$$H_x^{(2)}(x,y) = \frac{j\omega\varepsilon_2}{2\pi k_2^2}\int_A [M_x(x',y')\,(k_2^2 + \frac{\partial^2}{\partial x^2})G_0 + M_y(x',y')\,\frac{\partial^2}{\partial x\,\partial y}G_0]\,ds' \tag{2.12a}$$

$$H_y^{(2)}(x,y) = \frac{j\omega\varepsilon_2}{2\pi k_2^2}\int_A [M_x(x',y')\,\frac{\partial^2}{\partial y\,\partial x}G_0 + M_y(x',y')\,(k_2^2 + \frac{\partial^2}{\partial y^2})G_0]\,ds' \tag{2.12b}$$

From the above results and for the case where both regions are free space, i.e. $\mu_1 = \mu_2 = \mu_0$, $\varepsilon_1 = \varepsilon_2 = \varepsilon_0$ and thus $k_1 = k_2 = k_0$, we obtain, after re-arranging terms, two coupled integro-differential equations for the components of $\vec{M}_s$ given by

$$(k_0^2 + \frac{\partial^2}{\partial x^2})\,F_x + \frac{\partial^2}{\partial x\,\partial y}\,F_y = -\,j\pi\omega\mu_0\,(2H_x^i - J_y^a)\,, \qquad z = 0 \tag{2.13}$$

$$(k_0^2 + \frac{\partial^2}{\partial y^2})\,F_y + \frac{\partial^2}{\partial y\,\partial x}\,F_x = -\,j\pi\omega\mu_0\,(2H_y^i + J_x^a)\,, \qquad z = 0 \tag{2.14}$$

where

$$F_x(\vec{r}) = \int_A M_x(\vec{r}')\,G_0(\vec{r}'\,|\,\vec{r})\,ds' \tag{2.15a}$$

$$F_y(\vec{r}) = \int_A M_y(\vec{r}')\,G_0(\vec{r}'\,|\,\vec{r})\,ds' \tag{2.15b}$$

It is possible, in principle, to transform a system of coupled integral equations to a system of simultaneous algebraic equations and compute the resulting matrix elements by available numerical methods. However, because of the differential operators in Eqs. (2.13)

and (2.14) this direct approach will result in considerable numerical difficulties. In an attempt to solve this problem one may use the two dimensional Fourier transform defined by the relation:

$$F\{f(x,y)\} = \tilde{f}(\alpha,\beta) = \int_{-\infty}^{+\infty}\int_{-\infty}^{+\infty} f(x,y)\, e^{-j(\alpha x + \beta y)}\, dx\, dy \tag{2.16}$$

Application of this transform and using its well-known properties to (2.13) and (2.14), the differential operators reduce to algebraic quantities in the spectral domain where a numerical procedure such as the method of moments can be used efficiently. The details of this approach are given in the next section for the special case of a narrow slot.

2.2- Special case of a narrow slot

Equations (2.13) and (2.14) are very general and can be applied to any arbitrary aperture shape and impressed sources. However, in antenna applications we are more interested in apertures in the form of narrow slots. The slot shown in Fig. 2.4 is of length $2L$, width $2w$ and is excited by sources either outside the aperture to construct a diffraction problem, or by a current source on the aperture itself with the slot acting as a radiator. Assuming a narrow slot, i.e. $w \ll \lambda$, $w \ll L$ and for the type of excitations to be considered here, the axial component of the unknown electric field in the slot is negligible, i.e. $E_x^a(x,y) \simeq 0$ and the transverse component of the electric field can be written in the separable form

$$E_y^a(x,y) = X(x)\, Y(y) \tag{2.17}$$

with

$$Y(y) = \frac{1/\pi}{\sqrt{w^2 - (y - y_c)^2}} \tag{2.18}$$

where y_c is the ordinate of the slot center. This choice for the Y function is based on the knowledge of the field in a narrow slot of infinite length and incorporates the proper field behavior at the edges [21]. The unknown function $X(x)$ satisfies the following integral equation with differential operator in the integrand,

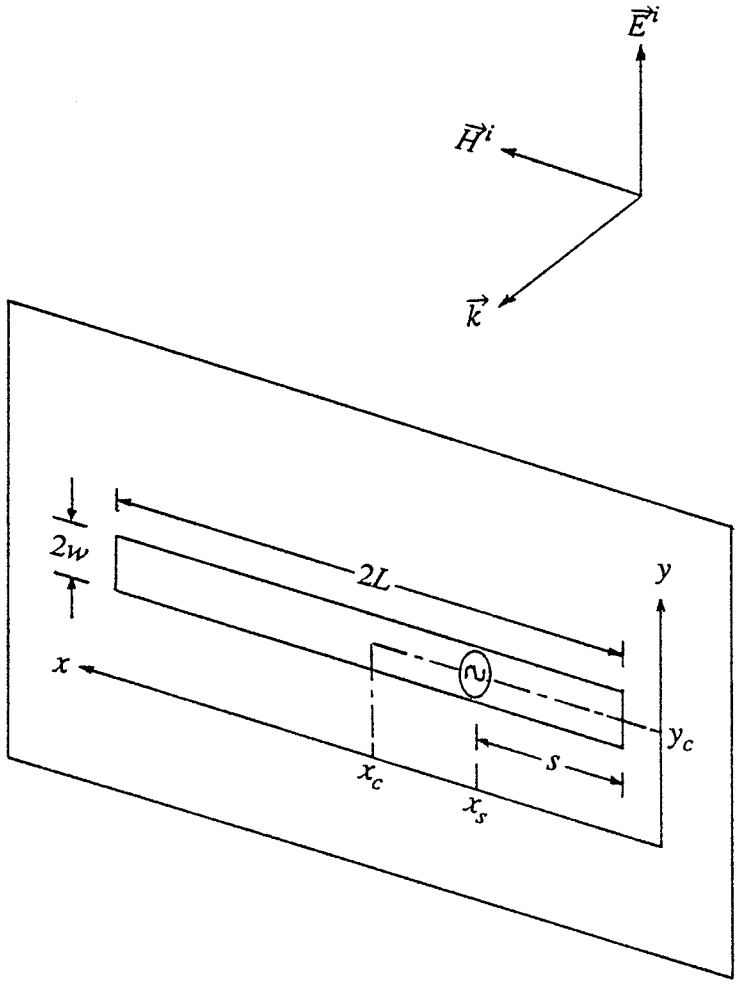

Fig. 2.4- Narrow slot excited by a current source and an incident plane wave.

$$\int_{x_c-L}^{x_c+L} X(x')\,(k^2+\frac{\partial^2}{\partial x^2})\,G(x-x')\,dx' = g(x, y_c) \tag{2.19}$$

$$G(\xi) = \frac{2}{\pi}\int_0^{\pi/2} \frac{e^{-jk[\,\xi^2+(w\sin\theta)^2\,]^{1/2}}}{[\,\xi^2+(w\sin\theta)^2\,]^{1/2}}\,d\theta \tag{2.20}$$

where $g(x, y_c)$ is the forcing function to be discussed in Sec. 2.4 and $k = k_0$ is the wavenumber.

2.3- Numerical solution of the integral equation

Equation in (2.19) is similar to the so-called Pocklington's equation for the current distribution along a wire in the theory of linear antennas and scatterers. This equation, which is in the form of a Fredholm integral equation of the first kind, is basically an integro-differential equation and due to the presence of derivatives in the integrand as well as the singular nature of the kernel its numerical evaluation requires a special treatment.

In the past the method of moments has been used to solve Pocklington's equation and several approaches are introduced to eliminate the differential operator and these may be categorized as follows:

1) writing the integro-differential equation in the form of a harmonic differential equation whose solution is used to form a simple integral equation of Hallen's type which is then solved for the unknown function;

2) applying piecewise linear or sinusoids for basis and/or testing functions in the moments method and using integration by parts twice to eliminate the second derivative resulting in a difference equation;

3) replacing the second derivative in the equation by a finite difference approximation and thus obtain an integro-difference equation.

In particular the last two methods are equivalent to Hallen's equation with point matching as shown elsewhere [41].

While all the above approaches are aimed at removing the differential operator from Pocklington's equation, very little analytical work has been done to treat the singularity of the integral which can result in serious difficulties in numerical computations. A popular solution to this problem is to use the well known reduced kernel approximation which is valid only for very thin wires and narrow slots. In yet another approach, the integrand is made smooth by isolating the singularity of the kernel and integrating the singular part separately [4, pp. 3-55]. However, the operations are rather involved and numerically inefficient as they include a number of double integrations.

We apply the method of moments to the problem and use the Fourier transform to obtain simple and numerically efficient expressions for the matrix elements without resorting to any of the above mentioned methods or approximations. This approach eliminates the differential operator in Pocklington's equation without imposing any restriction on the choice of basis and testing functions, thus making it possible to use the simple pulse expansion and point matching. Furthermore, the singular kernel in the space domain turns to a smooth function in the Fourier domain and no additional effort is required to handle the singularity. Finally, the matrix elements are expressed in terms of a single integral in comparison with a double integral for the case of exact kernel in other methods.

We consider a solution of (2.19) in the form

$$X(x) \simeq \sum_{n=1}^{N} V_n \, X_n(x) \tag{2.21}$$

where $X_n(x)$ are known basis functions and V_n are unknown constant coefficients. Thus

$$\sum_{n=1}^{N} V_n \, F_n(x) \simeq g(x, y_c) \tag{2.22}$$

where

$$F_n(x) = (k^2 + \frac{\partial^2}{\partial x^2}) \, A_n(x) \tag{2.23}$$

and

$$A_n(x) = \int_{x_c - L}^{x_c + L} X_n(x') \, G(x - x') \, dx' \tag{2.24}$$

Since the tangential electric field vanishes on the conducting screen, we can extend the limits of the integral in (2.24) to infinity and write

$$A_n(x) = \int_{-\infty}^{+\infty} X_n(x') \, G(x - x') \, dx' \tag{2.25}$$

To obtain a system of N linear equations for the N unknowns in (2.22), we form the inner products of both sides with a testing function ${W_m}^*(x)$ where * denotes complex conjugate. The result may be written in matrix form

$$[a_{mn}] \, [V_n] \simeq [b_m] \tag{2.26}$$

where

$$a_{mn} = \int_{-\infty}^{+\infty} {W_m}^*(x) \, F_n(x) \, dx \tag{2.27}$$

$$b_m = \int_{-\infty}^{+\infty} {W_m}^*(x) \, g(x, y_c) \, dx \tag{2.28}$$

From (2.20), (2.23), (2.25) and (2.27), it is seen that the matrix elements a_{mn} contain triple integrals with differential operator in the integrand and a singular kernel which makes the computations even more prohibitive. In the next section we present a method that removes the derivative and gives a_{mn} as only a single integral with a well behaved integrand.

2.3.1- Calculation of the matrix elements

Using Parseval's identity, the integral in (2.27) can be written in the Fourier domain as

$$a_{mn} = \frac{1}{2\pi} \int_{-\infty}^{+\infty} \tilde{W}_m^*(\alpha) \, \tilde{F}_n(\alpha) \, d\alpha \tag{2.29}$$

where α is the Fourier transform variable and $\tilde{}$ denotes the Fourier domain quantities.

Since the integral in (2.25) is in the form of a convolution integral, the convolution theorem and the well-known properties of the Fourier transform lead to

$$\tilde{F}_n(\alpha) = (k^2 - \alpha^2)\, \tilde{X}_n(\alpha)\, \tilde{G}(\alpha) \tag{2.30}$$

where from (2.20) (see Appendix A)

$$\tilde{G}(\alpha) = 2\, J_0(j\frac{w}{2}\sqrt{\alpha^2 - k^2})\, K_0(\frac{w}{2}\sqrt{\alpha^2 - k^2}) \tag{2.31}$$

and K_0 is the modified Bessel function of the second kind and zero order. Thus, the matrix elements become

$$a_{mn} = \frac{1}{\pi}\int_{-\infty}^{+\infty} (k^2 - \alpha^2)\, \tilde{X}_n(\alpha)\, \tilde{W}_m^*(\alpha)\, J_0(j\frac{w}{2}\sqrt{\alpha^2 - k^2})\, K_0(\frac{w}{2}\sqrt{\alpha^2 - k^2})\, d\alpha \tag{2.32}$$

At this point it is appropriate to investigate the effect of using the reduced kernel approximation on the calculations in the Fourier domain. With this approximation, the kernel given in (2.20) reduces to

$$G(\xi) \approx \frac{e^{-jk\sqrt{\xi^2 + (w/2)^2}}}{\sqrt{\xi^2 + (w/2)^2}} \tag{2.33}$$

and its transform becomes

$$\bar{G}(\alpha) = 2\, K_0(\frac{w}{2}\sqrt{\alpha^2 - k^2}) \tag{2.34}$$

where the bar indicates quantities related to the reduced kernel approximation. Thus the matrix elements are given by

$$\bar{a}_{mn} = \frac{1}{\pi}\int_{-\infty}^{+\infty} (k^2 - \alpha^2)\, \tilde{X}_n(\alpha)\, \tilde{W}_m^*(\alpha)\, K_0(\frac{w}{2}\sqrt{\alpha^2 - k^2})\, d\alpha \tag{2.35}$$

It is interesting to note that this approximation significantly increases the convergence rate of the integral, as can be observed by comparing the asymptotic behavior of $I_0(x)K_0(x)$ in (2.32) and $K_0(x)$ in (2.35) with $x = \frac{w}{2}\sqrt{\alpha^2 - k^2}$ for $\alpha > k$, namely [42, p. 378]

$$I_0(x)\,K_0(x) \approx \frac{1}{x}\left(a_0 + \frac{a_1}{x} + \frac{a_2}{x^2} + \frac{a_3}{x^3} + \cdots\right) \tag{2.36}$$

which decreases as the inverse power of x, while

$$K_0(x) \approx \frac{e^{-x}}{\sqrt{x}}\left(b_0 + \frac{b_1}{x} + \frac{b_2}{x^2} + \frac{b_3}{x^3} + \cdots\right) \tag{2.37}$$

decreases exponentially with x.

2.3.2- The basis and testing functions

For the basis and testing functions, one may choose any of the commonly used sub-domain functions shown in Fig. 2.5. These are

a) rectangular pulse or piecewise constant function

$$f_n(x) = \begin{cases} 1, & \text{for} \quad |x - x_n| \le \dfrac{\Delta}{2} \\ 0, & \text{for} \quad |x - x_n| > \dfrac{\Delta}{2} \end{cases} \tag{2.38a}$$

$$\tilde{f}_n(\alpha) = \Delta\, e^{-jx_n\alpha}\left[\frac{\sin(\frac{\Delta}{2}\alpha)}{\frac{\Delta}{2}\alpha}\right] \tag{2.38b}$$

b) triangular pulse or piecewise linear function

$$f_n(x) = \begin{cases} 1 - \dfrac{|x - x_n|}{\Delta}, & \text{for} \quad x_{n-1} \le x \le x_{n+1} \\ 0, & \textit{otherwise} \end{cases} \tag{2.39a}$$

$$\tilde{f}_n(\alpha) = \frac{\Delta}{2}\, e^{-jx_n\alpha}\left[\frac{\sin(\frac{\Delta}{4}\alpha)}{\frac{\Delta}{4}\alpha}\right]^2 \tag{2.39b}$$

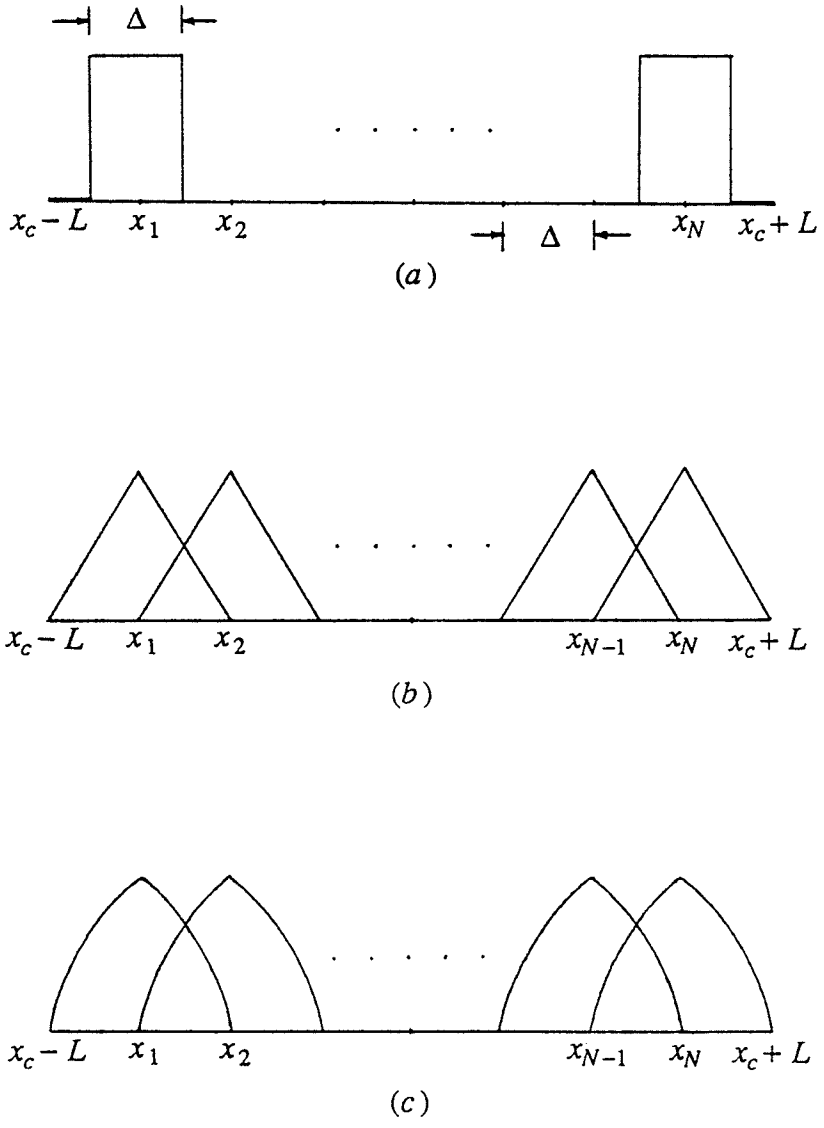

Fig. 2.5- Sub-domain functions commonly used as basis and testing functions; a) rectangular pulse, b) triangular pulse, c) sinusoidal pulse.

c) sinusoidal pulse or piecewise sinusoid function

$$f_n(x) = \begin{cases} \dfrac{\sin[k(\Delta - |x - x_n|)]}{\sin(k\Delta)}, & \text{for } x_{n-1} \le x \le x_{n+1} \\ 0, & \textit{otherwise} \end{cases} \tag{2.40a}$$

$$\tilde{f}_n(\alpha) = \frac{2ke^{-jx_n\alpha}}{\sin(k\Delta)} \left[\frac{\cos(k\Delta) - \cos(\Delta\alpha)}{\alpha^2 - k^2} \right] \tag{2.40b}$$

In these equations $x_n = x_c - L + n\Delta$, $n = 1, 2, \cdots, N$ and $\Delta = 2L/(N+1)$; while $x_{n-1} = x_n - \Delta$ and $x_{n+1} = x_n + \Delta$. For point matching at points $x_m = x_c - L + m\Delta$, $m = 1, 2, \cdots, N$ the testing function is

$$W_m(x) = \delta(x - x_m) \tag{2.41a}$$

$$\tilde{W}_m^*(\alpha) = e^{jx_m\alpha} \tag{2.41b}$$

We may use any of the above functions in (2.32) or (2.35) to calculate the matrix elements. From these equations it is clear that when both the basis and testing functions are the same, i.e. Galerkin's method, the convergence of the integral is faster than point matching, as can be seen from the power of α in the denominator. For the same reason, sinusoidal or triangular pulses result in faster convergence than the rectangular pulse. In all the cases, the integral in the matrix elements has a well behaved integrand over the entire range of integration and can be performed numerically without difficulty. As an example we choose the rectangular pulse as basis function along with point matching. Substitution from (2.38b) and (2.41b) into (2.35) yields the matrix elements as

$$\bar{a}_{mn} = \frac{4}{\pi} \int_0^\infty \frac{(k^2 - \alpha^2)}{\alpha} K_0\left(\frac{w}{2}\sqrt{\alpha^2 - k^2}\right) \cos[(m-n)\Delta\alpha] \sin\left(\frac{\Delta}{2}\alpha\right) d\alpha \tag{2.42}$$

Note that the matrix elements depend on $|m - n|$ and therefore the moments matrix is of the Toeplitz type [43]. Hence, we only need to compute the elements of one row (column) and the other elements are just repetition of these values. This property significantly reduces the filling time of the moment matrix. To evaluate the matrix elements in (2.42), due to the branch point at $\alpha = k$ we split the integral and write

$$\bar{a}_{mn} = \frac{4}{\pi} \left[\int_0^k h_1(\alpha)\, d\alpha + \int_k^\infty h_2(\alpha)\, d\alpha \right] \tag{2.43}$$

where $h_1(\alpha)$ and $h_2(\alpha)$ constitute the integrand of (2.42) for $\alpha < k$ and $\alpha > k$, respectively. The finite integral in (2.43) can be easily computed by numerical integration. To perform the infinite integral, we write it in the form

$$\int_k^\infty h_2(\alpha)\, d\alpha = I_1 + I_2 - I_3 \tag{2.44a}$$

where

$$I_1 = \int_k^M h_2(\alpha)\, d\alpha \tag{2.44b}$$

$$I_2 = \int_0^\infty h(\alpha)\, d\alpha \tag{2.44c}$$

$$I_3 = \int_0^M h(\alpha)\, d\alpha \tag{2.44d}$$

Here $h(\alpha)$ is the approximation of $h_2(\alpha)$ for $\alpha \gg k$, i.e.

$$h(\alpha) = -\alpha\, K_0(\frac{w}{2}\alpha)\, \cos[(m-n)\Delta\alpha]\, \sin(\frac{\Delta}{2}\alpha) \tag{2.45}$$

and M is a number chosen such that $h(M) \approx h_2(M)$ which is normally true for $M > 10k$. The integrals I_1 and I_3 are finite and a 20 point Gaussian quadrature is used for their numerical evaluation, while the infinite integral I_2 can be calculated analytically by using Eq. 6.691 in [44], i.e.

$$\int_0^\infty x\, K_0(ax)\, \sin(bx)\, dx = \frac{\pi b}{2}\, (a^2 + b^2)^{-3/2}$$

2.4- Calculation of the source vector elements

For the general case where the slot is excited by an incident plane wave with its magnetic field $\vec{H}^i$ as well as a known surface current distribution $\vec{J}_s^a = J_y^a(x)\hat{y}$ on the slot aperture, the forcing function $g(x, y_c)$ in (2.19) may be written in the form

$$g(x, y_c) = j\pi\omega\mu \left[J_y^a(x) - 2\, H_x^i(x, y_c) \right], \qquad z = 0 \tag{2.46}$$

where ω is the radian frequency and μ is the permeability of the medium. In the following we will obtain the source vector elements b_m for each type of excitation separately.

2.4.1- Current source excitation

For this case the forcing function in (2.46) reduces to

$$g(x) = j\pi\omega\mu\, J_y^a(x) \tag{2.47}$$

Practical examples of such a source are coaxial or two-wire lines connected to the slot edges. Due to the fact that $w \ll \lambda$, the current distribution over the feed line in the slot is essentially uniform. On the other hand, to avoid blocking the radiation it is desirable to keep the width (or radius) of the feed line in the slot to a minimum. Thus one can assume the slot to be excited by a delta current source of amplitude I_0 applied at the point $x = x_s$. We model the delta function by a pulse of width Δ and unit area. Hence, the current distribution of the excitation source on the slot aperture is given by

$$J_y^a(x) = \begin{cases} \dfrac{I_0}{\Delta}, & \text{for} \quad |x - x_s| \le \dfrac{\Delta}{2} \\ 0, & \text{for} \quad |x - x_s| > \dfrac{\Delta}{2} \end{cases} \tag{2.48}$$

and from (2.28) the source vector elements become

$$b_m = \begin{cases} j\pi\omega\mu \dfrac{I_0}{\Delta}, & \text{for} \quad |x_m - x_s| \le \dfrac{\Delta}{2} \\ 0, & \text{for} \quad |x_m - x_s| > \dfrac{\Delta}{2} \end{cases} \tag{2.49}$$

2.4.2- Plane wave excitation

For excitation of the slot by an incident plane wave ($\vec{E}^i$, $\vec{H}^i$), the forcing function in (2.46) reduces to

$$g(x, y_c) = -j2\pi\omega\mu\, H_x^i(x, y_c)\,, \qquad z = 0 \tag{2.50}$$

In general, for a uniform plane wave incident in a direction specified by the angles θ^i and ϕ^i, the x component of the magnetic field is given by

$$H_x^i(x, y, z) = \frac{1}{\omega\mu}(k_y\, E_{0z}^i - k_z\, E_{0y}^i) \exp\left[-j(k_x x + k_y y + k_z z)\right] \tag{2.51}$$

where $k_x = k\sin\theta^i\cos\phi^i$, $k_y = k\sin\theta^i\sin\phi^i$ and $k_z = k\cos\theta^i$. For normal incidence i.e. $\theta^i = 0$, from (2.50) and (2.51) the source vector elements b_m turn out to be independent of the parameter m and we obtain

$$b_m = j2\pi k\, E_{0y}^i \tag{2.52}$$

2.5- Circuit quantities of the slot radiator

From the circuit point of view an antenna can be characterized by quantities such as input impedance, resonance frequency and bandwidth. With the slot excited by a source with uniform current distribution of a total current I_0, the input impedance is defined as

$$Z_{in} = \frac{V(x_s)}{I_0} \tag{2.53}$$

where $V(x_s)$ is the voltage across the feed point. The voltage distribution along the slot is given by

$$V(x) = -\int_{y_c - w}^{y_c + w} E_y^a(x, y)\, dy \tag{2.54}$$

From (2.17), (2.18) and (2.21) it is easy to show that

$$V(x) \simeq \sum_{n=1}^{N} V_n \, X_n(x) \tag{2.55}$$

where for pulse expansion the basis functions $X_n(x)$ are defined by (2.38a). Thus the complex values of V_n obtained from (2.26) give the actual amplitude and phase of the voltage at the matching points x_m, $m = 1, 2, \cdots, N$. This data can then be used to find the voltage at other points of the slot by interpolation.

The resonance frequency f_r is defined as the frequency at which the imaginary part of the input impedance vanishes, i.e. $X(f_r) = 0$. The useful bandwidth of an antenna is that range of frequencies over which the antenna satisfies certain requirements of impedance, radiation pattern and directivity or polarization characteristics. Since these requirements vary according to each particular application, there is no unique definition for the bandwidth of any antenna. Here we define the bandwidth as the frequency range over which the *VSWR* remains below a specified value, namely 2:1. With the input impedance of the antenna as a function of frequency given, one can easily find the *VSWR* versus frequency and from there determine the bandwidth. For this purpose and to provide a reference point we assume that the antenna is perfectly matched to the generator at the resonance frequency.

2.6- Booker's extension of Babinet's principle

Booker [23] generalized Babinet's principle of optics to take into account the vector nature of the electromagnetic fields. This extension which has often been applied to the case of a slot antenna shows that the impedance Z of any planar antenna and the impedance Z' of its complement i.e. the antenna for which the area of the conducting screen and that of the aperture are reversed, satisfy the relation $Z\,Z' = (Z_0/2)^2$ where Z_0 is the characteristic impedance of the surrounding medium. However, there are a number of basic assumptions that must be made before Babinet's principle can strictly be applicable; namely, the screen must be perfectly conducting, flat and infinite in size, and vanishingly thin. Of course some results obtained from Babinet's principle may be approximately correct for a practical case where the screen is only highly conducting and large and thin compared to

the wavelength. In addition, it is possible to take into account the effect of finite thickness of the screen from a conformal mapping solution of the static case. The region outside the slot can be mapped to that outside an infinitesimally thin one by the Schwartz-Christoffel transformation [45] with the result reducing to complete elliptic integrals of the first and second kind [42]. Application of this method shows that the effective width of the slot is less than the actual size [28]. One can also consider the small change in the effective length of the slot due to the finite thickness of the screen.

The validity of the Booker's assumptions to obtain the impedance of a slot antenna from those of a linear dipole were examined experimentally by Long [28]. In these experiments a slot of one-half the desired width was cut in the edge of a ground plane and mounted on a highly conducting imaging plane. With this arrangement one is able to place the feed system and measuring equipment behind the image plane and thus allow the slot to radiate freely on both sides of the screen.

2.7- Numerical results

A knowledge of the voltage distribution along the slot is necessary for determining the circuit and radiation properties of the antenna. To confirm the validity of the approach presented in this Chapter for solving Pocklington's equation and thus the voltage distribution in the slot, we compare our results with those based on available methods. In Figs. 2.6–2.7 we have used the abbreviation FD/PP to indicate the calculation of the matrix elements in Fourier domain with pulse expansion and point matching. Similarly, SD/GS is used to identify the solution in space domain using Galerkin method with sinusoidal functions for basis and testing which is based on method 3 mentioned in Sec. 2.3. Unless otherwise stated, the ratio of the slot width to slot length is 0.04 and the antenna is operating at $f = 3\ GHz$ in all the examples. The slot is excited either by a delta current source of amplitude $I_0 = 1\ mA$ located at the point $x = x_s$ or by a normally incident plane wave with $E^i_{0y} = 1\ V/m$. Fig. 2.6a shows the amplitude and phase of the voltage distribution along a slot of length $\lambda/2$ and $s = L$ while in Fig. 2.6b the slot length is λ and $s = L/2$.

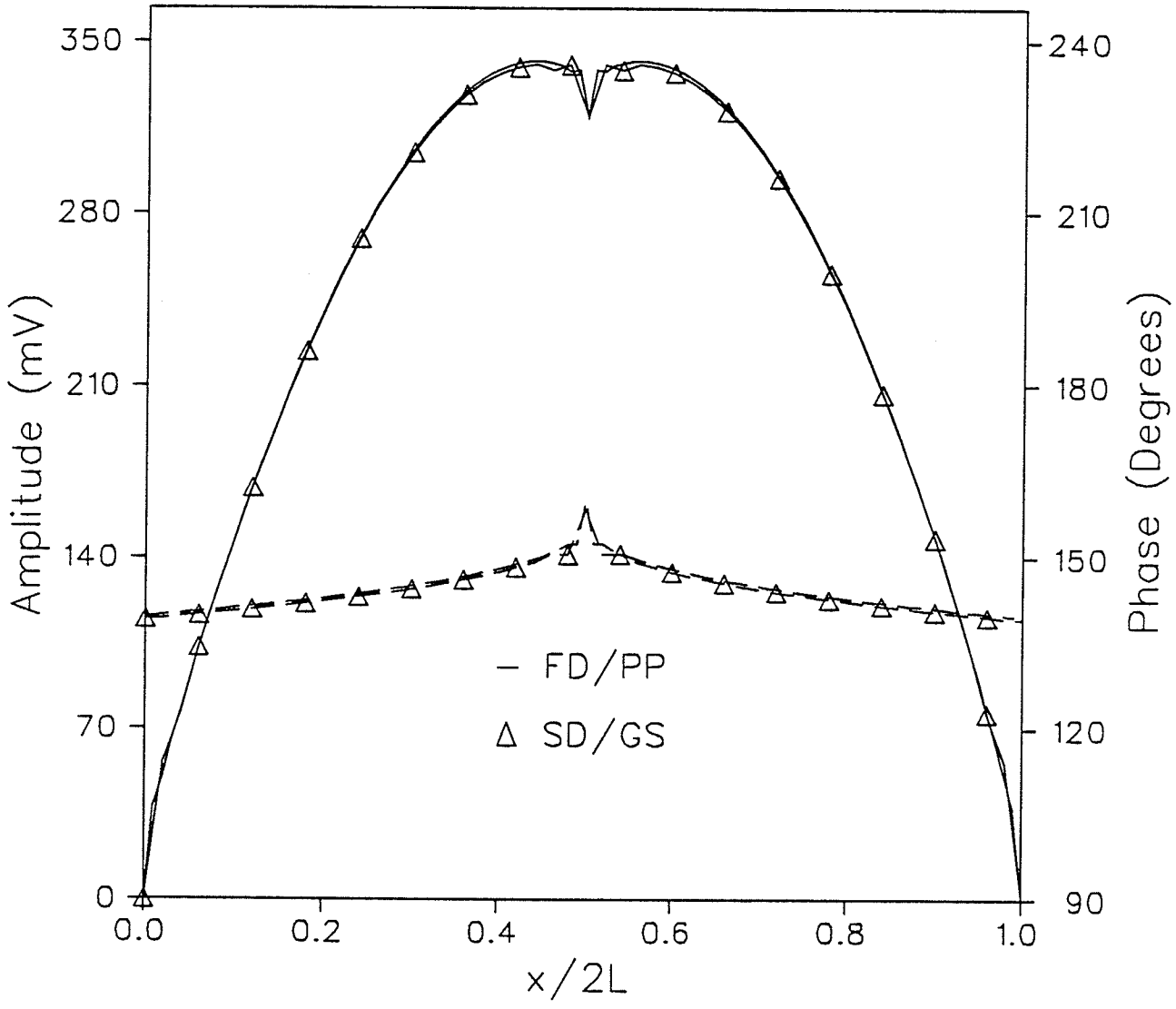

Fig. 2.6a- Comparison of the computed results for the voltage distribution along a slot of length $2L = \lambda/2$ and current source excitation at $s = L$.

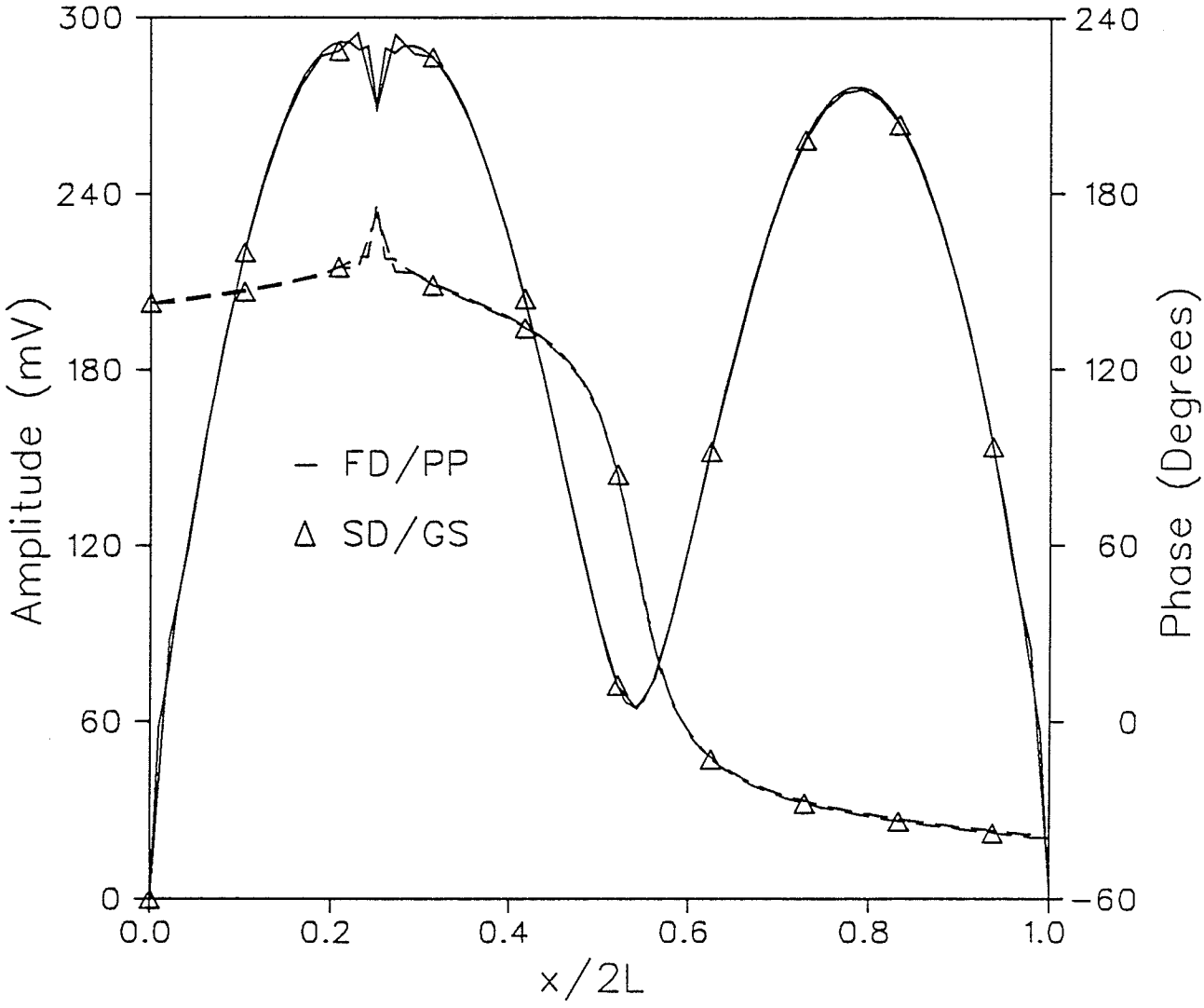

Fig. 2.6b- Comparison of the computed results for voltage distribution along a slot of length $2L = \lambda$ and current source excitation at $s = L/2$.

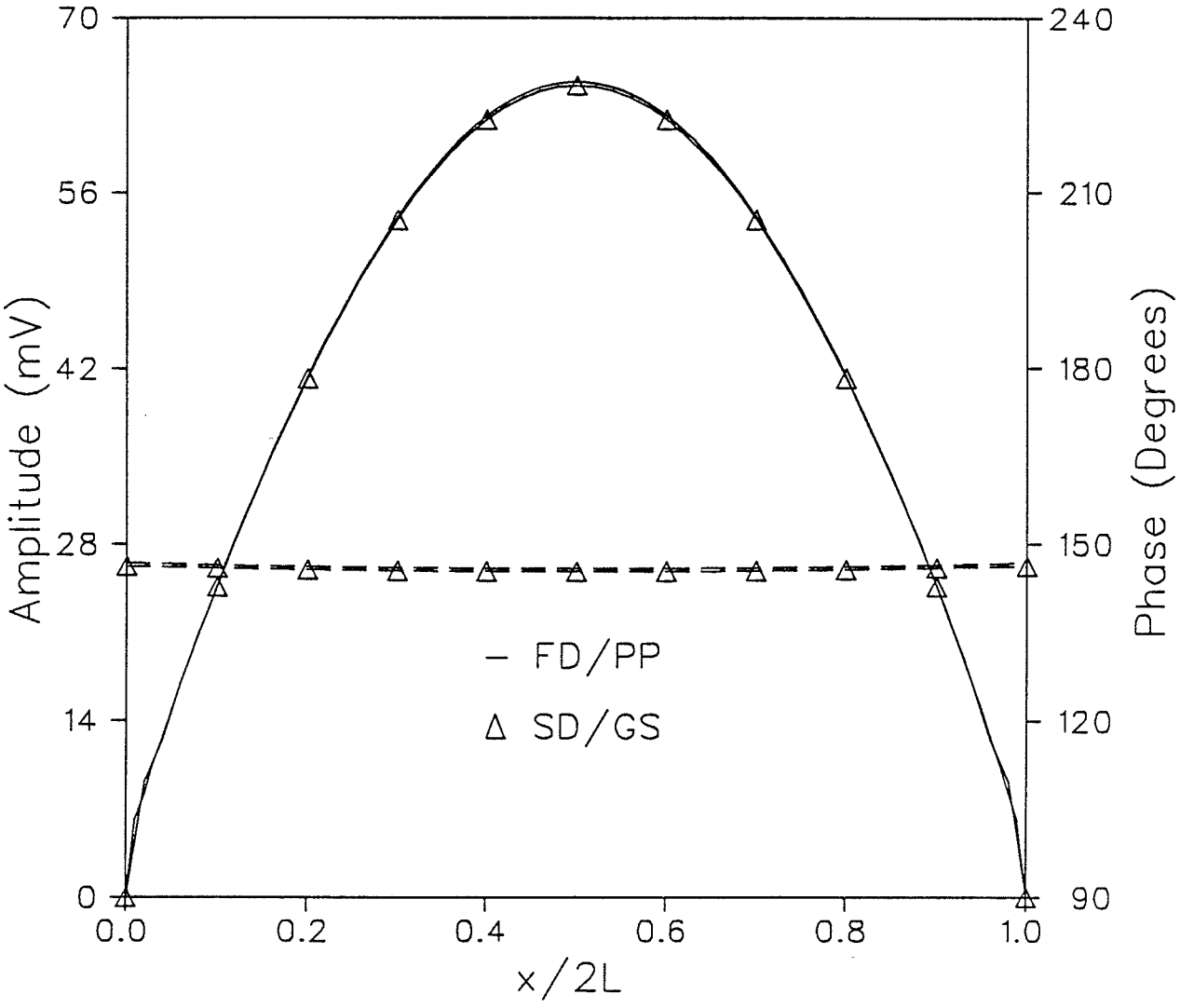

Fig. 2.7a- Comparison of the computed results for the induced voltage distribution along a slot of length $2L = \lambda/2$ illuminated by a normally incident plane wave.

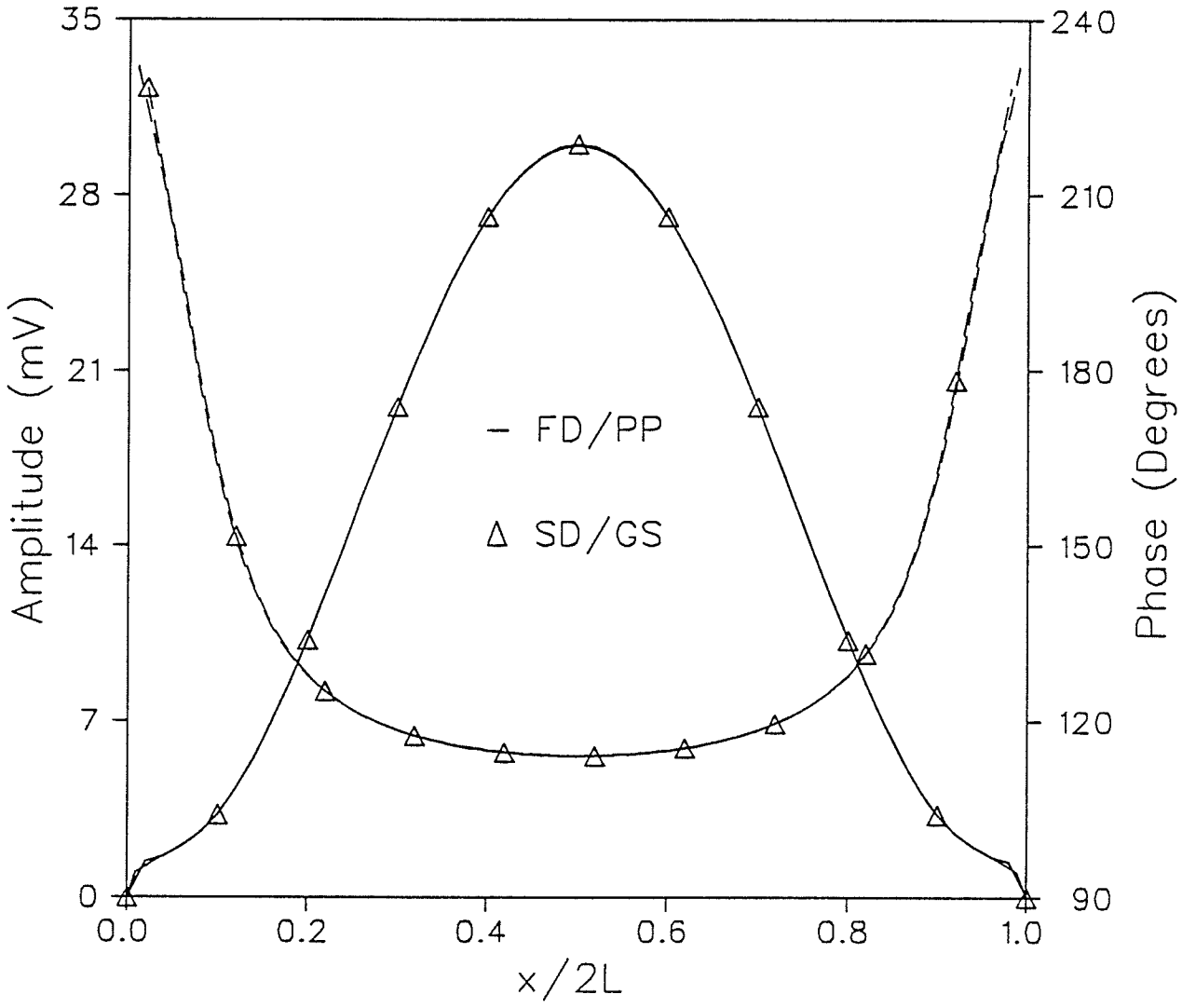

Fig. 2.7b- Comparison of the computed results for the induced voltage distribution along a slot of length $2L = \lambda$ illuminated by a normally incident plane wave.

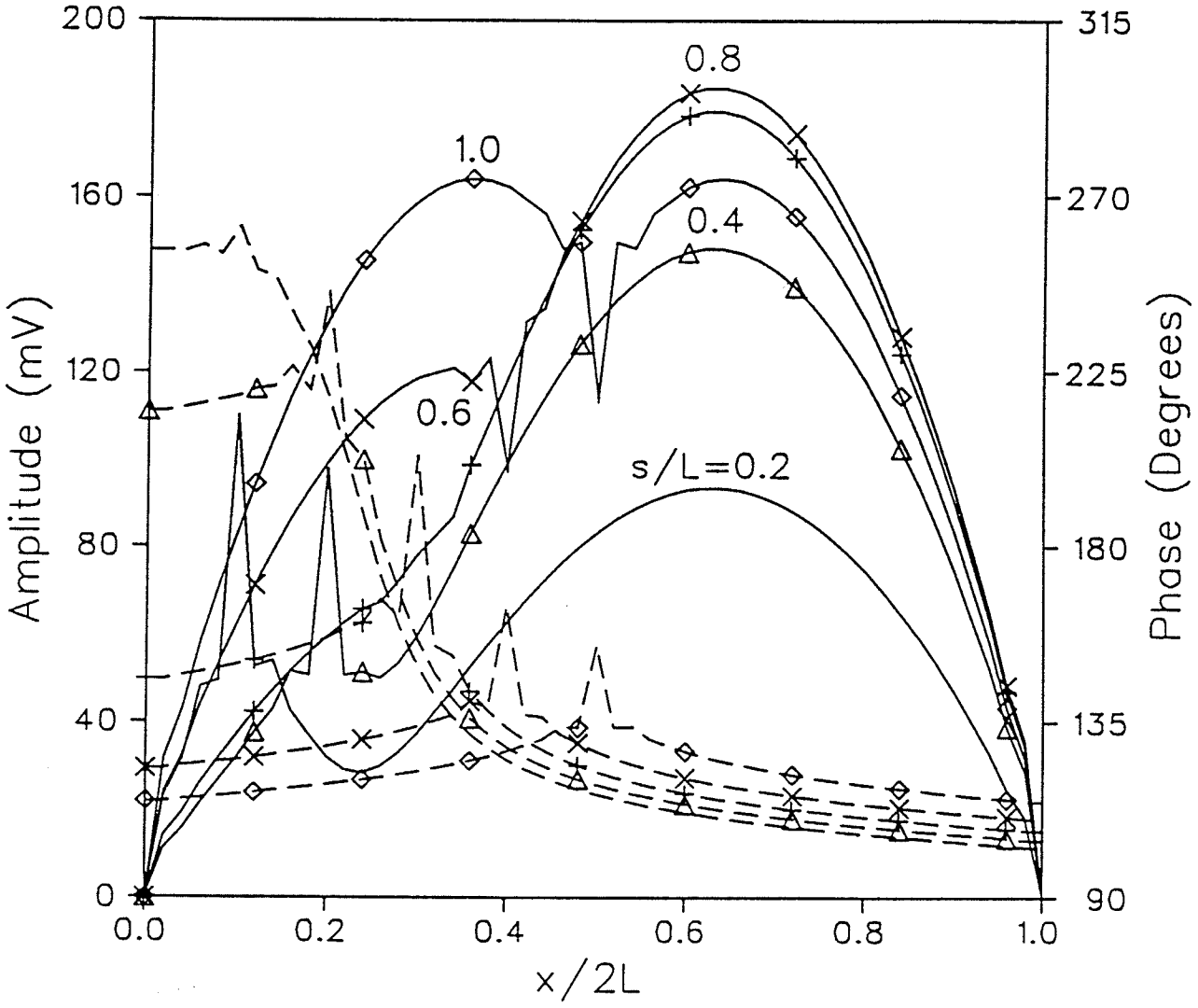

Fig..2.8- Amplitude and phase (dashed lines) of the voltage distribution for a slot with $2L/\lambda = 0.6$, $w/L = 0.04$ and feed-point locations $s/L = 0.2$ (1.0) 0.2.

In these figures the dashed line is used to denote the phase variation. For the case where the slot is illuminated by a plane wave, the amplitude and phase of the induced voltage are shown in Figs. 2.7a and 2.7b for $2L = \lambda/2$ and λ, respectively. From the above results it is seen that the agreement between the two methods is very good. The feed-point location s has significant effect on the voltage distribution along the slot and thus the input impedance. This point is demonstrated in Fig. 2.8 for a slot of length $0.6\ \lambda$ and $s/L = 0.2\ (1.0)\ 0.2$. The corresponding impedances are also given in Table 2.1.

Table 2.1

s/L	$R\ (\Omega)$	$X\ (\Omega)$
0.2	14.9	109.2
0.4	41.8	88.4
0.6	71.5	31.0
0.8	94.5	− 25.5
1.0	103.2	− 48.7

The resistance R and reactance X of a center-fed slot of length 25 *cm* and width 1 *cm* versus frequency are calculated from the moments method and compared in Fig. 2.9 with the results obtained from application of Babinet's principle as well as the experimental measurement [28]. In this and the following figures the dashed lines represent the reactance or susceptance. It is observed that the sinusoidal current distribution which was assumed on the complementary center-fed dipole in using the Babinet's principle [46] results in substantial error in the impedance values at frequencies higher than the resonance frequency as expected. The difference between the moments method solution results and those obtained from measurement data can be attributed to the fact that in the analytical solution we have assumed a perfectly conducting screen of infinite extent and vanishingly thin, while in the experiment the slot is cut in a screen of finite conductivity, size and thickness.

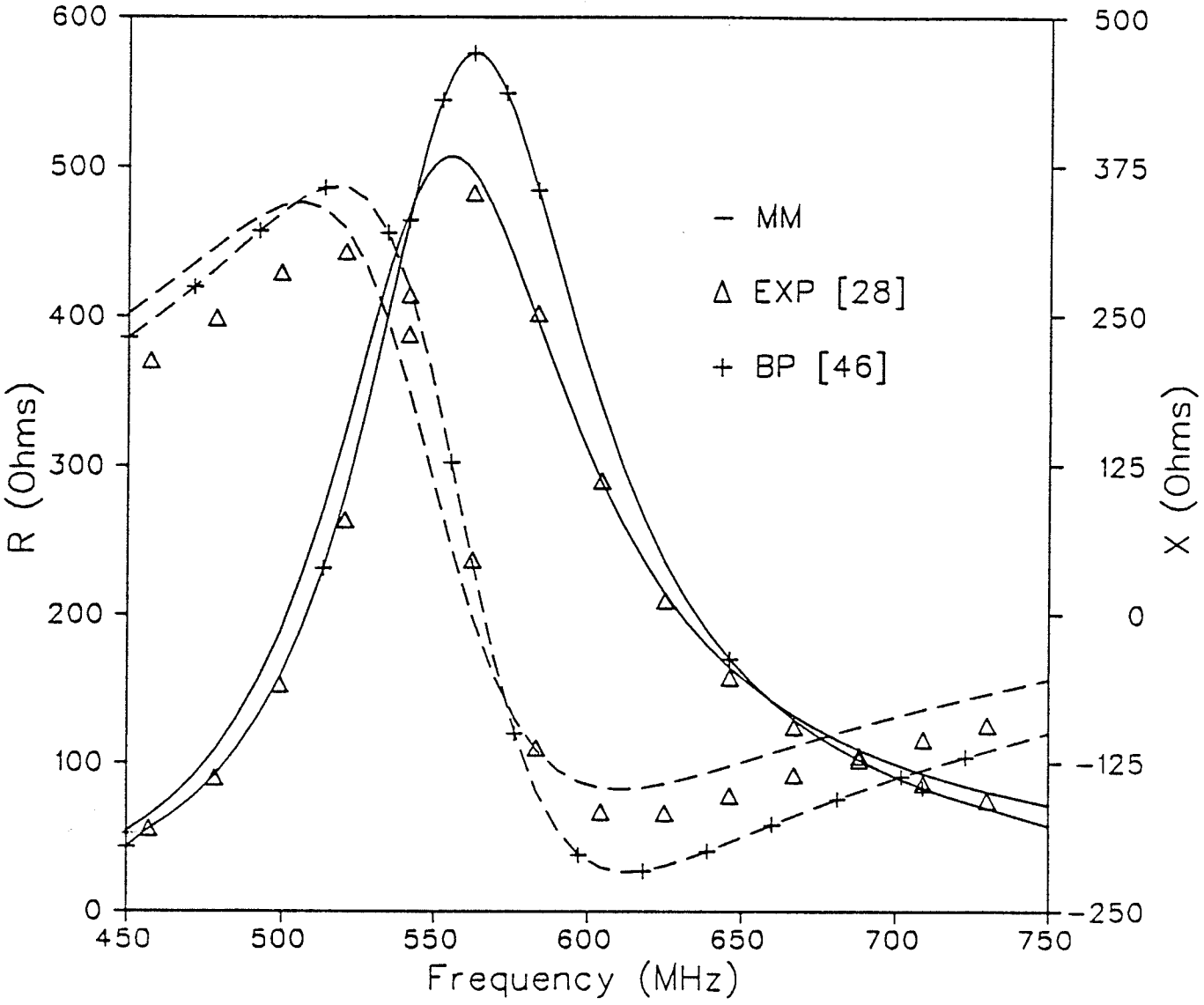

Fig. 2.9- Comparison of the resistance R and reactance X versus frequency, obtained from Moments Method (MM), experimental measurements (EXP) and Babinet's Principle (BP) for a center-fed slot of length $2L = 25\ cm$ and width $2w = 1\ cm$.

The effect of the feed-point location on the slot impedance is shown in Fig. 2.10 for various slot lengths. This figure suggests a convenient way for matching the antenna to the generator by choosing the proper location for connecting the feed line. The admittance of the slot versus $2L/\lambda$ is shown in Fig. 2.11 for $w/L = 0.02$, 0.04 and 0.06 while Fig. 2.12 presents the impedance as a function of frequency for slot lengths $2L = 4$, 5 and 6 cm. Fig. 2.13 shows the resonant length $2L_r$ namely the slot length at which resonance occurs, for a center-fed slot. The slot width has no appreciable effect on the resonance frequency which is mainly determined by the slot length. The radiation resistance R_r as a function of the slot resonant width $2w_r/\lambda$ is shown in Fig. 2.14. The computed results indicate that for a given slot width the value of R_r is essentially independent of the slot length. Fig. 2.15 shows the bandwidth versus $2L/\lambda$ for various slot widths. It is observed that in general a shorter and wider slot has a wider bandwidth and lower radiation resistance.

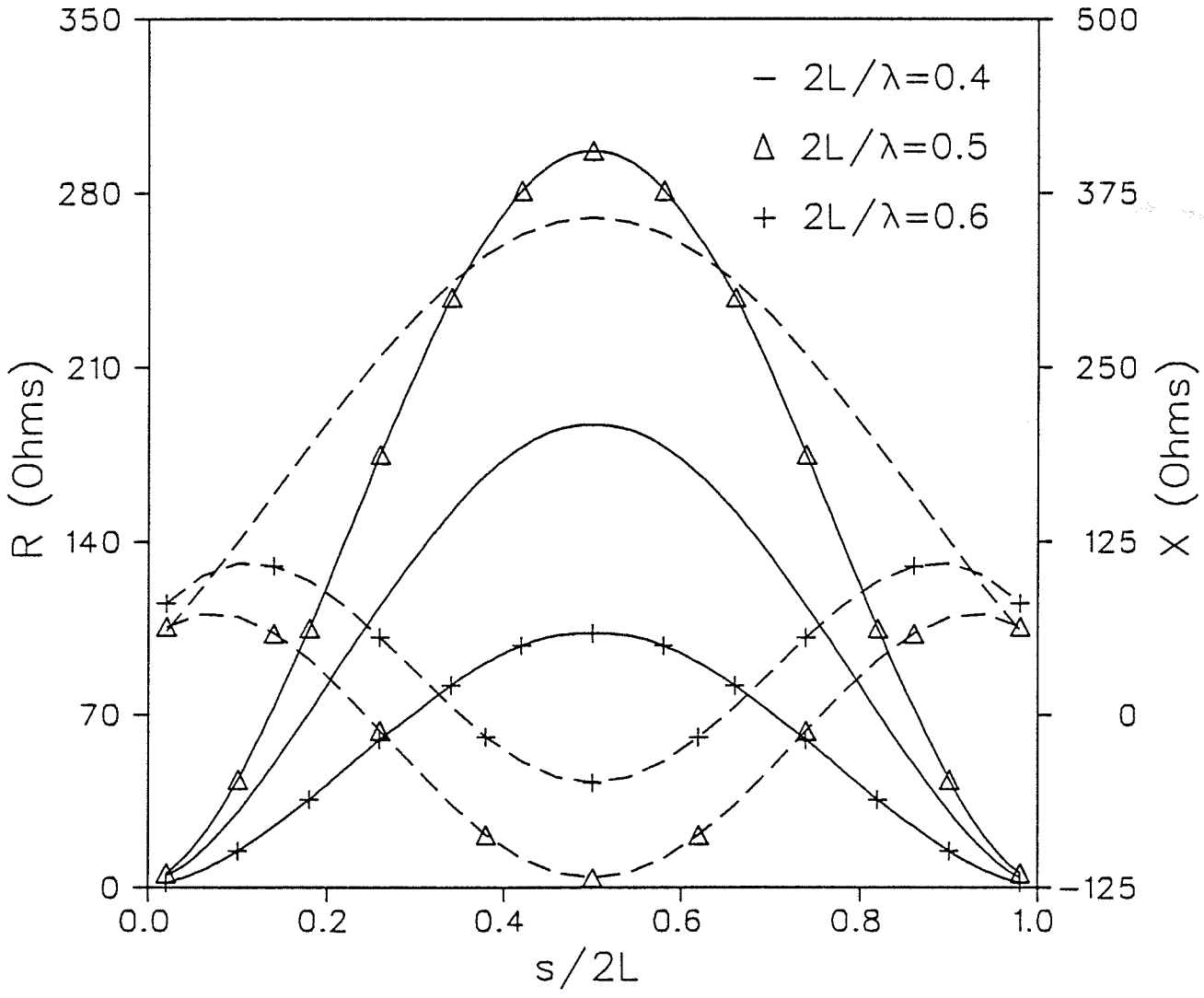

Fig. 2.10- Resistance R and reactance X (dashed lines) versus feed-point locations $s/2L$ for a slot of width $w/L = 0.04$ and lengths $2L/\lambda = 0.4$, 0.5 and 0.6.

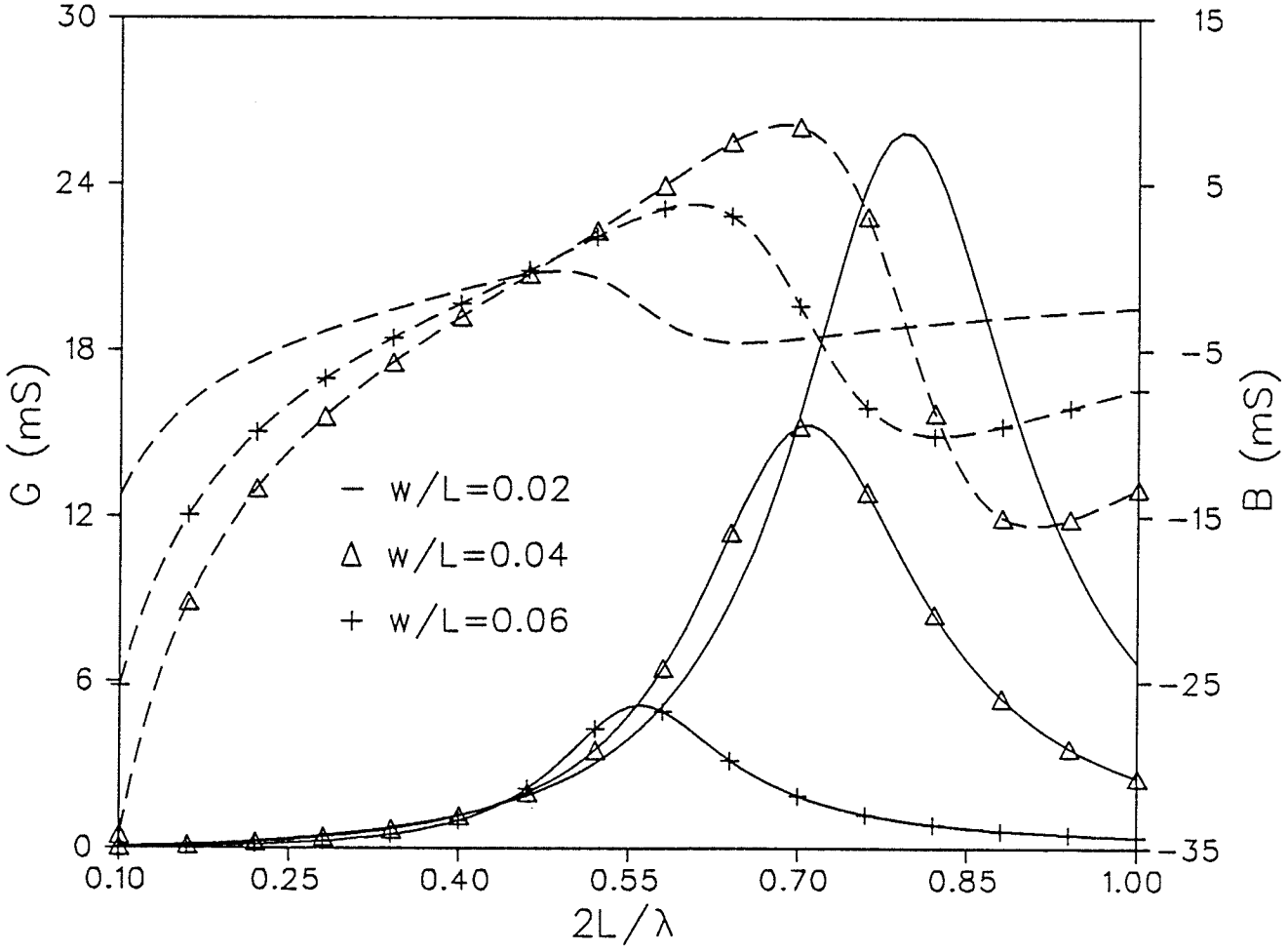

Fig. 2.11- Conductance G and susceptance B (dashed lines) versus slot length $2L/\lambda$ for normalized slot widths $w/L = 0.02$, 0.04 and 0.06.

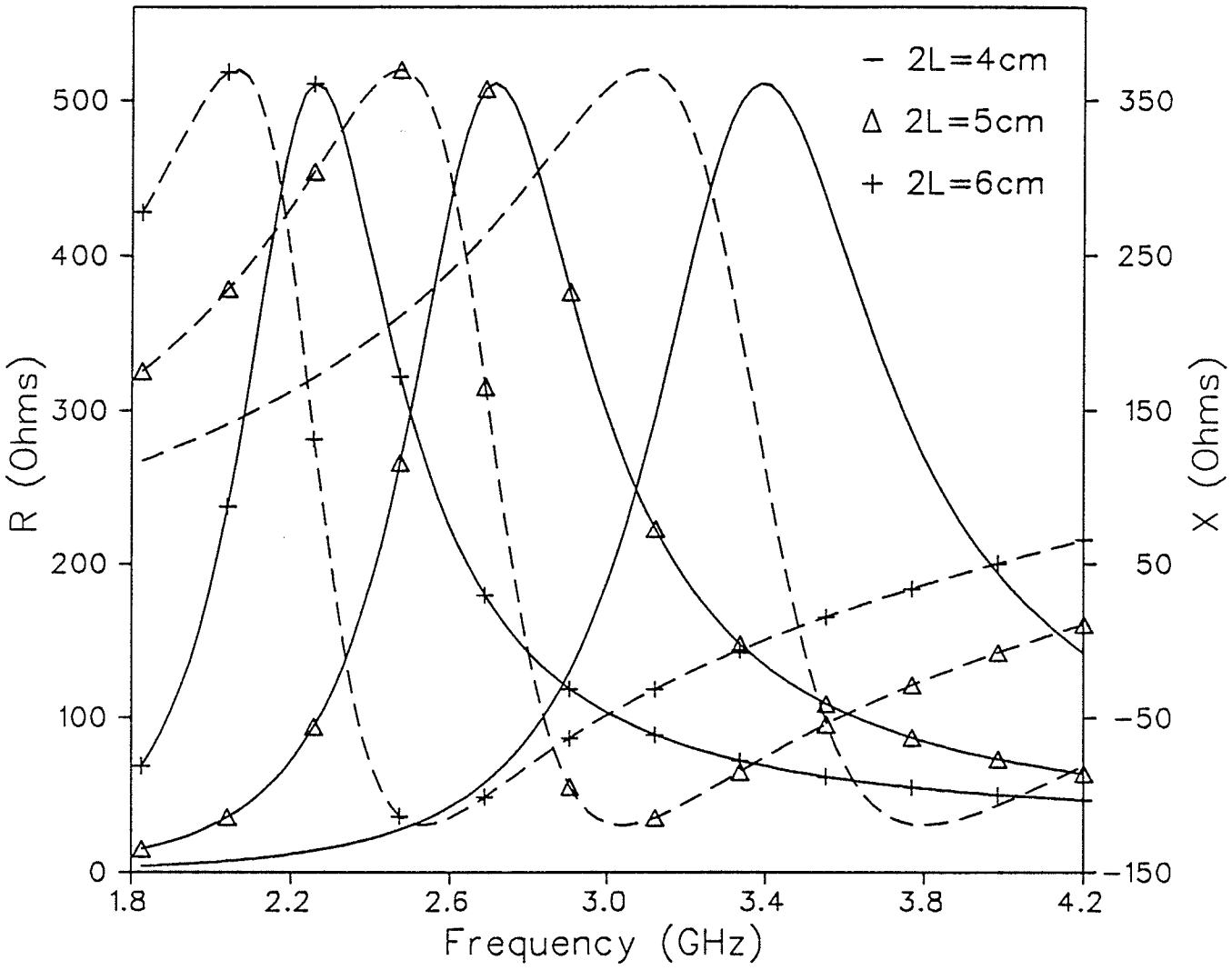

Fig. 2.12- Resistance R and reactance X (dashed lines) as a function of frequency for a slot with $w/L = 0.04$ and lengths $2L = 4$, 5 and 6 cm.

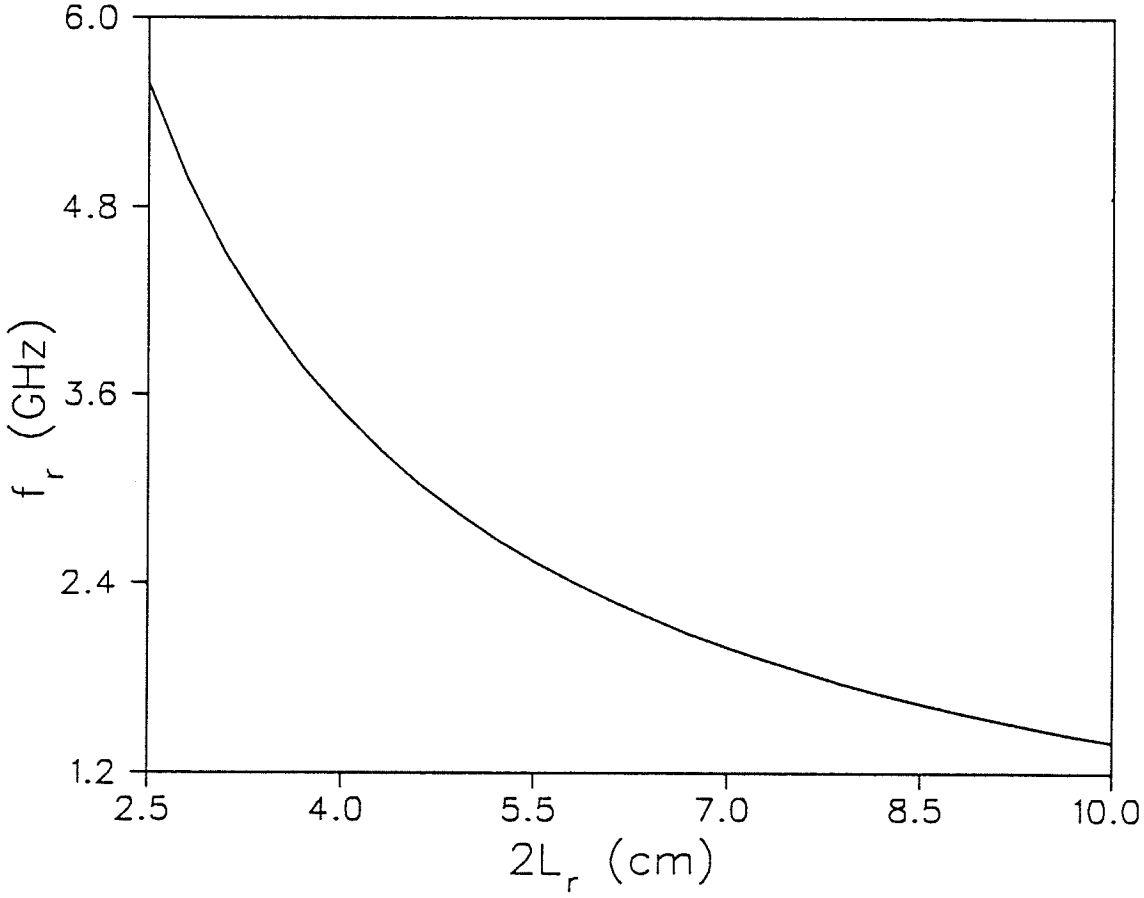

Fig. 2.13- The resonant length $2L_r$ of a center-fed slot with $w/L = 0.04$.

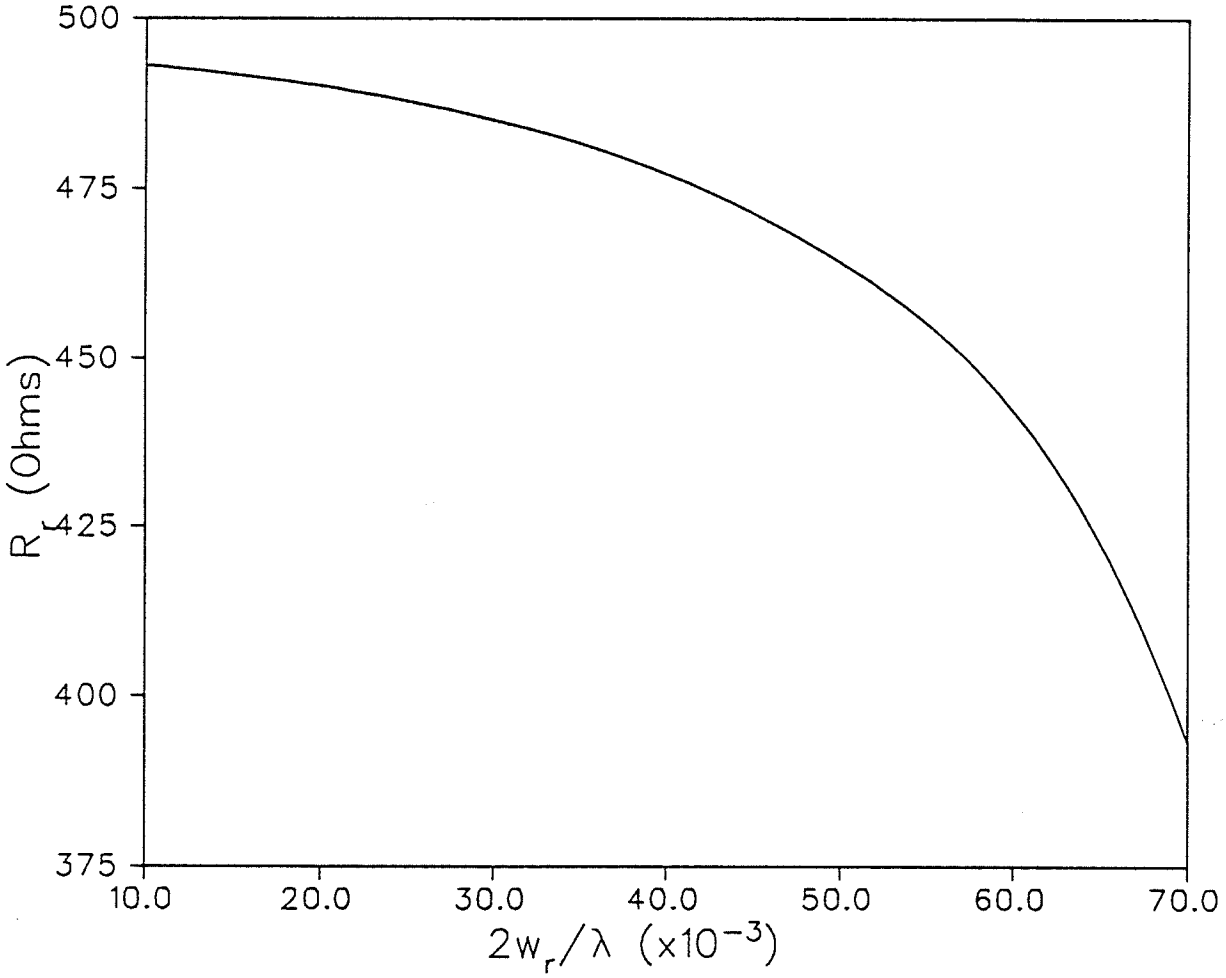

Fig. 2.14- Radiation Resistance R_r versus resonant slot width $2w_r/\lambda$ for a center-fed slot of length $2L = \lambda/2$.

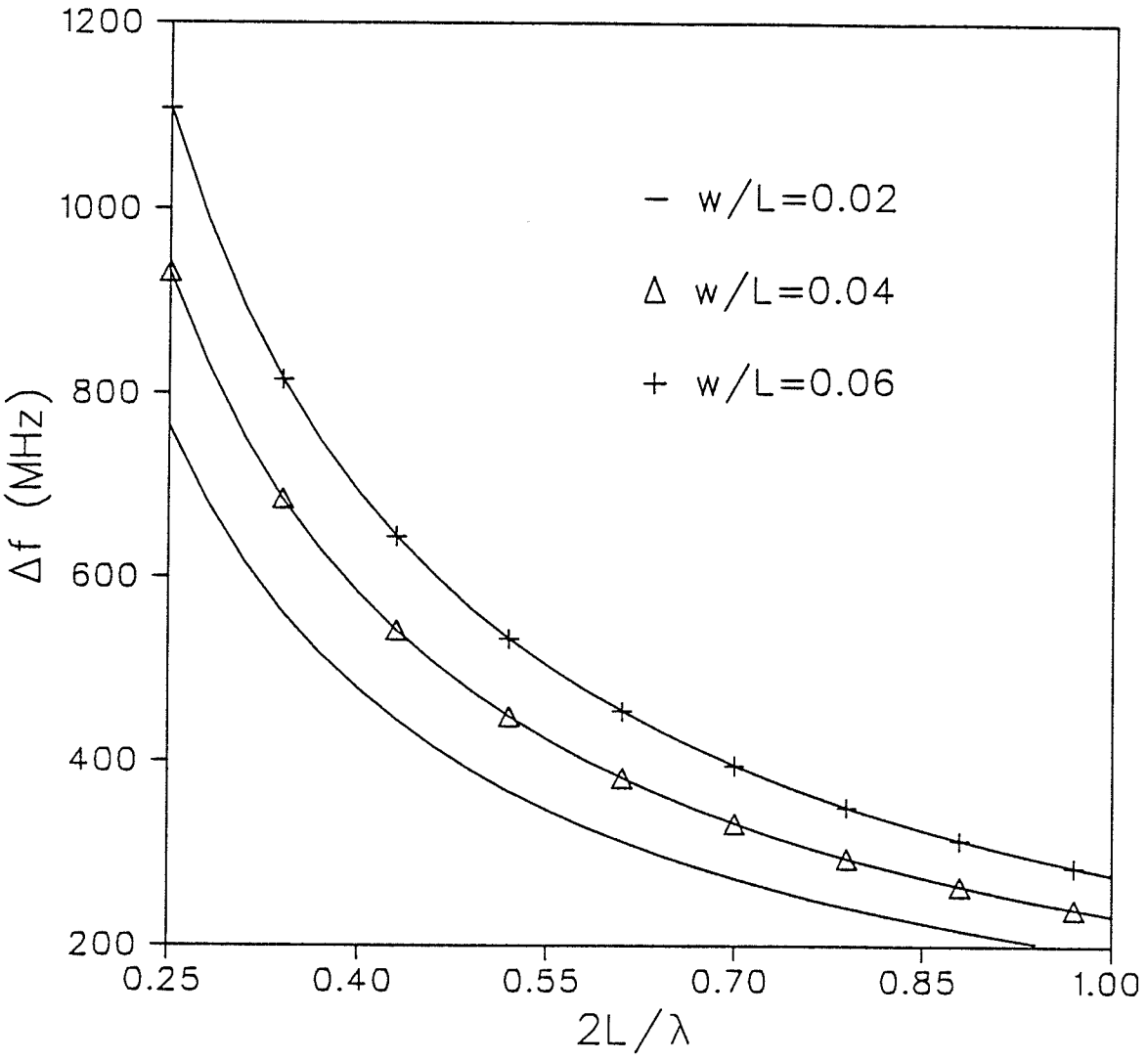

Fig. 2.15- Bandwidth Δf versus slot length $2L/\lambda$ for normalized slot widths $w/L = 0.02$, 0.04 and 0.06.

CHAPTER 3

ELECTROMAGNETIC FIELDS IN BOUNDED REGIONS

The open slot radiator discussed in the previous Chapter is free to radiate from both sides. However, in most applications the radiation should be restricted to one side only, which may be achieved by using a conducting enclosure to back the slot. In the problem of cavity-backed apertures to be analyzed in Chapter 4 we need the fields produced by volume or surface current distributions in a closed region of space. This problem is solved here by expanding the fields in terms of the irrotational and solenoidal eigenvectors. Although the method of field expansion is not new and has been used in different ways by many authors [47-50], the developments made in this Chapter were not found in the literature and seem to be new. First we obtain the solution in the form of volume integrals over the sources and surface integrals over the boundaries. Next, by re-arranging the terms in the integrals and writing them in the convenient dyadic form, general expressions for the dyadic Green's functions of an arbitrary closed region are extracted. The reduced form of these expressions for the important case of rectangular cavities is also derived and those pertinent to a cylindrical cavity can be found in [38]. Finally, the subject of resonant modes is discussed in detail.

3.1- Derivation of the fields and dyadic Green's functions

The expansion of the fields in terms of orthogonal eigenvectors (or normal modes) is based on the mathematical statement of the Helmholtz theorem [51]. According to this theorem an arbitrary continuous vector field with continuous derivatives in a region of space V and boundary S can be expressed in terms of gradient of a scalar function and curl of a vector function. Thus the field can be expanded in a series of irrotational (zero curl) and solenoidal (zero divergence) eigenvectors.

From Maxwell's equations the fields must satisfy

$$\nabla\times\nabla\times\vec{E} - k^2\vec{E} = -j\omega\mu\vec{J} - \nabla\times\vec{M} \tag{3.1a}$$

$$\nabla\times\nabla\times\vec{H} - k^2\vec{H} = \nabla\times\vec{J} - j\omega\varepsilon\vec{M} \tag{3.1b}$$

In these equations, $\vec{J}$ and $\vec{M}$ are the electric and magnetic source current distributions, while the $e^{j\omega t}$ harmonic time dependence is assumed and suppressed throughout. We consider the solution

$$\vec{E}(\vec{r}) = \sum_{\nu} A_\nu^e\ \vec{e}_\nu(\vec{r}) + \sum_{\nu} B_\nu^e\ \vec{E}_\nu^{TE}(\vec{r}) + \sum_{\nu} C_\nu^e\ \vec{E}_\nu^{TM}(\vec{r}) \tag{3.2a}$$

$$\vec{H}(\vec{r}) = \sum_{\nu} A_\nu^h\ \vec{h}_\nu(\vec{r}) + \sum_{\nu} B_\nu^h\ \vec{H}_\nu^{TE}(\vec{r}) + \sum_{\nu} C_\nu^h\ \vec{H}_\nu^{TM}(\vec{r}) \tag{3.2b}$$

where A, B, and C are unknown expansion coefficients and ν stands for a set of triple indices (m, n, p). In the above equations, $\vec{e}_\nu$ and $\vec{h}_\nu$ are the irrotational electric and magnetic eigenvectors, respectively, defined by

$$\vec{e}_\nu = \nabla\ \phi_\nu^e \tag{3.3}$$

with

$$\nabla^2\phi_\nu^e + (k_\nu^e)^2\phi_\nu^e = 0\ , \quad in\ V \tag{3.4a}$$

$$\phi_\nu^e = 0\ , \quad (or\ \hat{n}\cdot\vec{e}_\nu = 0\ ,\ \hat{n}\times\vec{e}_\nu = 0) \quad on\ S \tag{3.4b}$$

and

$$\vec{h}_\nu = \nabla\ \phi_\nu^h \tag{3.5}$$

with

$$\nabla^2\phi_\nu^h + (k_\nu^h)^2\phi_\nu^h = 0\ , \quad in\ V \tag{3.6a}$$

$$\frac{\partial\phi_\nu^h}{\partial n} = 0\ , \quad (or\ \ \hat{n}\cdot\vec{h}_\nu = 0) \quad on\ S \tag{3.6b}$$

where $\hat{n}$ is the outward normal to the boundary.

For the case $k_\nu^e = 0$ in (3.4a), the function ϕ_ν^e satisfies Laplace's equation $\nabla^2\phi_\nu^e = 0$ and can thus be considered as an electrostatic potential with $\vec{e}_\nu$ representing the electrostatic field. This case corresponds to a region which consists of two or more separate boundaries, as for example the space between two concentric spheres. On the other hand, $k_\nu^h = 0$ in (3.6a) corresponds to the case of a multiply connected region, i.e. regions in which there are contours that cannot be shrunk away to nothing. An example of such a region is the space between two coaxial cylinders closed at both ends. In this case $\vec{h}_\nu$ corresponds to the magnetic field produced by the *dc* current flowing through the circuit which consists of the center conductor, the shorted ends and the outer conductor.

The quantities $\vec{E}_\nu^{TE}$ and $\vec{E}_\nu^{TM}$ in (3.2a) are the solenoidal electric-field eigenvectors and are the two independent and mutually orthogonal solutions of the following homogeneous vector wave equation

$$\nabla\times\nabla\times\vec{E}_\nu - k_\nu^2\,\vec{E}_\nu = 0\,, \quad in\ V \tag{3.7a}$$

$$\hat{n}\times\vec{E}_\nu = 0 \quad on\ S\,, \quad \nabla\cdot\vec{E}_\nu = 0 \quad in\ V \tag{3.7b}$$

It is easy to show that the above solutions are of the form

$$\vec{E}_\nu^{TE} = \nabla\times(\psi_\nu^{TE}\,\vec{c}) \tag{3.8}$$

$$\vec{E}_\nu^{TM} = \frac{1}{k_\nu^{TM}}\,\nabla\times\nabla\times(\psi_\nu^{TM}\,\vec{c}) \tag{3.9}$$

where $\vec{c}$ is an arbitrary constant vector, and the generating functions ψ_ν^{TE} and ψ_ν^{TM} are solutions of the scalar wave equation

$$\nabla^2\,\psi_\nu + k_\nu^2\,\psi_\nu = 0 \tag{3.10}$$

with appropriate boundary conditions derived from (3.7b). Similarly $\vec{H}_\nu^{TE}$ and $\vec{H}_\nu^{TM}$ in (3.2b) are the solenoidal magnetic-field eigenvectors and are the independent and mutually orthogonal solutions of

$$\nabla\times\nabla\times\vec{H}_\nu - k_\nu^2\,\vec{H}_\nu = 0\,, \quad in\ V \tag{3.11a}$$

$$\hat{n}\times\nabla\times\vec{H}_\nu = 0 \quad \text{and} \quad \hat{n}\cdot\vec{H}_\nu = 0 \quad on\ S\ , \quad \nabla\cdot\vec{H}_\nu = 0 \quad in\ V \tag{3.11b}$$

These solutions are given by

$$\vec{H}_\nu^{TE} = \frac{1}{k_\nu^{TE}}\nabla\times\nabla\times(\psi_\nu^{TE}\,\vec{c}) \tag{3.12}$$

$$\vec{H}_\nu^{TM} = \nabla\times(\psi_\nu^{TM}\,\vec{c}) \tag{3.13}$$

It should be pointed out that in all the above equations, as yet, the superscripts TE and TM have no specific meaning and are merely used to denote two independent quantities. However, we will show later that with a proper choice of the constant vector $\vec{c}$, these superscripts actually represent the transverse electric and transverse magnetic components of the fields, respectively.

From the physical point of view, the boundary conditions defined for the irrotational and solenoidal eigenvectors correspond to the boundary conditions of an enclosure bounded by perfectly conducting walls. Therefore, it is appropriate to call these eigenvectors the short-circuit modes. The following orthogonality relations exist for these modes [49]:

$$\int_V \begin{Bmatrix}\vec{E}_\mu\\ \vec{H}_\mu\end{Bmatrix}\cdot\begin{Bmatrix}\vec{E}_\nu\\ \vec{H}_\nu\end{Bmatrix} dv = 0\ , \qquad \mu\neq\nu \tag{3.14a}$$

$$\int_V \begin{Bmatrix}\vec{e}_\mu\\ \vec{h}_\mu\end{Bmatrix}\cdot\begin{Bmatrix}\vec{e}_\nu\\ \vec{h}_\nu\end{Bmatrix} dv = 0\ , \qquad \mu\neq\nu \tag{3.14b}$$

$$\int_V \begin{Bmatrix}\vec{e}_\mu\\ \vec{h}_\mu\end{Bmatrix}\cdot\begin{Bmatrix}\vec{E}_\nu\\ \vec{H}_\nu\end{Bmatrix} dv = 0\ , \qquad \forall\ \mu\ ,\ \nu \tag{3.14c}$$

In the above relations, $\begin{Bmatrix}\vec{E}\\ \vec{H}\end{Bmatrix}$ is either $\begin{Bmatrix}\vec{E}^{TE}\\ \vec{H}^{TE}\end{Bmatrix}$ or $\begin{Bmatrix}\vec{E}^{TM}\\ \vec{H}^{TM}\end{Bmatrix}$. Furthermore

$$\int_V \begin{Bmatrix}\vec{E}_\mu^{TE}\\ \vec{H}_\mu^{TE}\end{Bmatrix}\cdot\begin{Bmatrix}\vec{E}_\nu^{TM}\\ \vec{H}_\nu^{TM}\end{Bmatrix} dv = 0\ , \qquad \forall\ \mu\ ,\ \nu \tag{3.14d}$$

and the following relations exist between the solenoidal electric and magnetic eigenvectors:

$$\nabla\times \begin{Bmatrix} \vec{E}_\nu^{TE} \\ \vec{H}_\nu^{TE} \end{Bmatrix} = k_\nu^{TE} \begin{Bmatrix} \vec{H}_\nu^{TE} \\ \vec{E}_\nu^{TE} \end{Bmatrix} \tag{3.15a}$$

$$\nabla\times \begin{Bmatrix} \vec{E}_\nu^{TM} \\ \vec{H}_\nu^{TM} \end{Bmatrix} = k_\nu^{TM} \begin{Bmatrix} \vec{H}_\nu^{TM} \\ \vec{E}_\nu^{TM} \end{Bmatrix} \tag{3.15b}$$

For the fields defined in (3.2) to be actual solutions of (3.1), they must satisfy the specific boundary conditions dictated by the problem at hand as well as Maxwell's equations, i.e.

$$\nabla\times \vec{E} = -j\omega\,\mu\,\vec{H} - \vec{M} \tag{3.16a}$$

$$\nabla\times \vec{H} = j\omega\,\varepsilon\,\vec{E} + \vec{J} \tag{3.16b}$$

We use these equations to obtain the unknown coefficients in (3.2) in terms of the sources $\vec{J}$ and $\vec{M}$ in volume V, and also the tangential electric field on the boundary surface S. However, it should be noted that because the specified boundary conditions are, in general, different from those of the short-circuit modes, the fields in (3.2) are not uniformly convergent at the boundary and thus the derivatives of the fields are not the sum of the derivatives of the short-circuit modes. In other words, one cannot directly use Maxwell's equations to solve for the unknown coefficients. One way of circumventing this problem is through integration of the vector identity

$$\nabla\cdot \vec{A}\times \vec{B} = \nabla\times \vec{A}\cdot \vec{B} - \nabla\times \vec{B}\cdot \vec{A}$$

over the volume V. Application of this relation to various combinations of the fields and eigenvectors yields

$$\int_V \nabla\cdot \vec{E}\times \begin{Bmatrix} \vec{H}_\mu \\ \vec{h}_\mu \end{Bmatrix} dv = \int_V \nabla\times \vec{E}\cdot \begin{Bmatrix} \vec{H}_\mu \\ \vec{h}_\mu \end{Bmatrix} dv - \int_V \nabla\times \begin{Bmatrix} \vec{H}_\mu \\ \vec{h}_\mu \end{Bmatrix} \cdot \vec{E}\, dv \tag{3.17a}$$

$$\int_V \nabla\cdot \begin{Bmatrix} \vec{E}_\mu \\ \vec{e}_\mu \end{Bmatrix} \times \vec{H}\, dv = \int_V \nabla\times \begin{Bmatrix} \vec{E}_\mu \\ \vec{e}_\mu \end{Bmatrix} \cdot \vec{H}\, dv - \int_V \nabla\times \vec{H}\cdot \begin{Bmatrix} \vec{E}_\mu \\ \vec{e}_\mu \end{Bmatrix} dv \tag{3.17b}$$

In these equations, $\vec{E}_\mu$ and $\vec{H}_\mu$ have either TE or TM superscripts. Thus, we obtain six equations for determination of the expansion coefficients in (3.2). Substitution of the latter equations in (3.17) and using (3.14) to (3.16) along with the fact that

$$\nabla\times \vec{e}_\mu = 0\,, \quad \nabla\times \vec{h}_\mu = 0 \qquad in\ V$$

also

$$\hat{n}\times \left\{ \begin{array}{c} \vec{E}_\mu^{TE} \\ \vec{E}_\mu^{TM} \end{array} \right\} = 0 \ \text{ and } \ \hat{n}\times \vec{e}_\mu = 0 \qquad on\ S$$

yields after solving the system of linear equations the following results:

$$A_\nu^e = \frac{-\int_V \vec{J}\cdot \vec{e}_\nu\, dv}{j\omega\varepsilon\int_V |\,\vec{e}_\nu\,|^2\, dv} \tag{3.18a}$$

$$B_\nu^e = \frac{j\omega\mu\int_V \vec{J}\cdot \vec{E}_\nu^{TE} dv + k_\nu^{TE}\int_V \vec{M}\cdot \vec{H}_\nu^{TE} dv + k_\nu^{TE}\int_S (\hat{n}\times \vec{E})\cdot \vec{H}_\nu^{TE} ds}{[k^2 - (k_\nu^{TE})^2]\int_V |\,\vec{E}_\nu^{TE}\,|^2\, dv} \tag{3.18b}$$

$$A_\nu^h = \frac{\int_V \vec{M}\cdot \vec{h}_\nu dv + \int_S (\hat{n}\times \vec{E})\cdot \vec{h}_\nu\, ds}{-j\omega\mu\int_V |\,\vec{h}_\nu\,|^2\, dv} \tag{3.18c}$$

$$B_\nu^h = \frac{j\omega\varepsilon\int_V \vec{M}\cdot \vec{H}_\nu^{TE} dv - k_\nu^{TE}\int_V \vec{J}\cdot \vec{E}_\nu^{TE} dv + j\omega\varepsilon\int_S (\hat{n}\times \vec{E})\cdot \vec{H}_\nu^{TE} ds}{[k^2 - (k_\nu^{TE})^2]\int_V |\,\vec{H}_\nu^{TE}\,|^2\, dv} \tag{3.18d}$$

The equations for C_ν^e and C_ν^h may be obtained from those for B_ν^e and B_ν^h, respectively, through a change of superscript from TE to TM. Substituting the above results in (3.2) and re-arranging the terms we obtain the following equations for the fields:

$$\vec{E}(\vec{r}) = -j\omega\mu\int_V \vec{J}(\vec{r}')\cdot \overleftrightarrow{G}_e(\vec{r}'\,|\,\vec{r})\, dv' - \int_V \vec{M}(\vec{r}')\cdot \nabla'\times \overleftrightarrow{G}_e(\vec{r}'\,|\,\vec{r})\, dv' - \int_S \hat{n}\times \vec{E}(\vec{r}')\cdot \nabla'\times \overleftrightarrow{G}_e(\vec{r}'\,|\,\vec{r})\, ds' \tag{3.19}$$

where $\overleftrightarrow{G}_e(\vec{r}' \mid \vec{r})$ is the electric-type dyadic Green's function defined by

$$\overleftrightarrow{G}_e(\vec{r}' \mid \vec{r}) = \sum_\nu \frac{-\vec{e}_\nu(\vec{r}')\,\vec{e}_\nu(\vec{r})}{k^2 \int_V |\vec{e}_\nu|^2 dv'} + \sum_\nu \frac{\vec{E}_\nu^{TE}(\vec{r}')\;\vec{E}_\nu^{TE}(\vec{r})}{[(k_\nu^{TE})^2 - k^2]\int_V |\vec{E}_\nu^{TE}|^2 dv'}$$

$$+ \sum_\nu \frac{\vec{E}_\nu^{TM}(\vec{r}')\,\vec{E}_\nu^{TM}(\vec{r})}{[(k_\nu^{TM})^2 - k^2]\int_V |\vec{E}_\nu^{TM}|^2 dv'} \tag{3.20}$$

and

$$\nabla' \times \overleftrightarrow{G}_e(\vec{r}' \mid \vec{r}) = \sum_\nu \frac{k_\nu^{TE}\;\vec{H}_\nu^{TE}(\vec{r}')\,\vec{E}_\nu^{TE}(\vec{r})}{[(k_\nu^{TE})^2 - k^2]\int_V |\vec{E}_\nu^{TE}|^2 dv'} + \sum_\nu \frac{k_\nu^{TM}\;\vec{H}_\nu^{TM}(\vec{r}')\,\vec{E}_\nu^{TM}(\vec{r})}{[(k_\nu^{TM})^2 - k^2]\int_V |\vec{E}_\nu^{TM}|^2 dv'}$$

The integral expression for the magnetic field is obtained as

$$\vec{H}(\vec{r}) = \int_V \vec{J}(\vec{r}') \cdot \nabla' \times \overleftrightarrow{G}_m(\vec{r}' \mid \vec{r})\, dv' - j\omega\varepsilon \int_V \vec{M}(\vec{r}') \cdot \overleftrightarrow{G}_m(\vec{r}' \mid \vec{r})\, dv'$$

$$- j\omega\varepsilon \int_S \hat{n} \times \vec{E}(\vec{r}') \cdot \overleftrightarrow{G}_m(\vec{r}' \mid \vec{r})\, ds' \tag{3.21}$$

where $\overleftrightarrow{G}_m(\vec{r}' \mid \vec{r})$ is the magnetic-type dyadic Green's function defined by

$$\overleftrightarrow{G}_m(\vec{r}' \mid \vec{r}) = \sum_\nu \frac{-\vec{h}_\nu(\vec{r}')\,\vec{h}_\nu(\vec{r})}{k^2 \int_V |\vec{h}_\nu|^2 dv'} + \sum_\nu \frac{\vec{H}_\nu^{TE}(\vec{r}')\;\vec{H}_\nu^{TE}(\vec{r})}{[(k_\nu^{TE})^2 - k^2]\int_V |\vec{H}_\nu^{TE}|^2 dv'}$$

$$+ \sum_\nu \frac{\vec{H}_\nu^{TM}(\vec{r}')\;\vec{H}_\nu^{TM}(\vec{r})}{[(k_\nu^{TM})^2 - k^2]\int_V |\vec{H}_\nu^{TM}|^2 dv'} \tag{3.22}$$

and

$$\nabla' \times \overleftrightarrow{G}_m(\vec{r}' \mid \vec{r}) = \sum_\nu \frac{k_\nu^{TE}\;\vec{E}_\nu^{TE}(\vec{r}')\,\vec{H}_\nu^{TE}(\vec{r})}{[(k_\nu^{TE})^2 - k^2]\int_V |\vec{H}_\nu^{TE}|^2 dv'} + \sum_\nu \frac{k_\nu^{TM}\;\vec{E}_\nu^{TM}(\vec{r}')\,\vec{H}_\nu^{TM}(\vec{r})}{[(k_\nu^{TM})^2 - k^2]\int_V |\vec{H}_\nu^{TM}|^2 dv'}$$

3.2- Dyadic Green's functions for a rectangular cavity

In this section we specialize the general results obtained in (3.20) and (3.22) for the case of a rectangular cavity with dimensions a, b and c. The previously defined scalar potentials for this problem are given by

$$\phi_\nu^e = \sin(k_m x)\, \sin(k_n y)\, \sin(k_p z) \tag{3.23a}$$

$$\phi_\nu^h = -\cos(k_m x)\, \cos(k_n y)\, \cos(k_p z) \tag{3.23b}$$

$$\psi_\nu^{TE} = \cos(k_m x)\, \cos(k_n y)\, \sin(k_p z) \tag{3.23c}$$

$$\psi_\nu^{TM} = \sin(k_m x)\, \sin(k_n y)\, \cos(k_p z) \tag{3.23d}$$

where m, n and p are integers and

$$k_m = \frac{m\pi}{a}\,, \quad k_n = \frac{n\pi}{b}\,, \quad k_p = \frac{p\pi}{c} \tag{3.24}$$

Since there is no preferred axis in the rectangular cavity, the constant vector $\vec{c}$ in the transverse eigenvectors defined in Sec. 3.1 can be any of the unit vectors $\hat{x}$, $\hat{y}$ or $\hat{z}$. With the choice of $\vec{c} = \hat{z}$, the irrotational and the two independent solenoidal electric-field eigenvectors are given by

$$\begin{aligned}\vec{e}_\nu = {} & k_m \cos(k_m x)\, \sin(k_n y)\, \sin(k_p z)\, \hat{x} \\ & + k_n \sin(k_m x)\, \cos(k_n y)\, \sin(k_p z)\, \hat{y} \\ & + k_p \sin(k_m x)\, \sin(k_n y)\, \cos(k_p z)\, \hat{z}\end{aligned} \tag{3.25a}$$

$$\begin{aligned}\vec{E}_\nu^{TE} = {} & -k_n \cos(k_m x)\, \sin(k_n y)\, \sin(k_p z)\, \hat{x} \\ & + k_m \sin(k_m x)\, \cos(k_n y)\, \sin(k_p z)\, \hat{y}\end{aligned} \tag{3.25b}$$

$$\begin{aligned}\vec{E}_\nu^{TM} = \frac{1}{k_\nu^{TM}} \Big[{} & -k_m k_p \cos(k_m x)\, \sin(k_n y)\, \sin(k_p z)\, \hat{x} \\ & - k_n k_p \sin(k_m x)\, \cos(k_n y)\, \sin(k_p z)\, \hat{y} \\ & + k_{mn}^2 \sin(k_m x)\, \sin(k_n y)\, \cos(k_p z)\, \hat{z} \Big]\end{aligned} \tag{3.25c}$$

Similarly the irrotational and the two independent solenoidal magnetic-field eigenvectors are given by

$$\vec{h}_\nu = k_m \sin(k_m x)\cos(k_n y)\cos(k_p z)\,\hat{x} + k_n \cos(k_m x)\sin(k_n y)\cos(k_p z)\,\hat{y} + k_p \cos(k_m x)\cos(k_n y)\sin(k_p z)\,\hat{z} \tag{3.26a}$$

$$\vec{H}_\nu^{TM} = k_n \sin(k_m x)\cos(k_n y)\cos(k_p z)\,\hat{x} - k_m \cos(k_m x)\sin(k_n y)\cos(k_p z)\,\hat{y} \tag{3.26b}$$

$$\vec{H}_\nu^{TE} = \frac{1}{k_\nu^{TE}}\left[- k_m k_p \sin(k_m x)\cos(k_n y)\cos(k_p z)\,\hat{x} - k_n k_p \cos(k_m x)\sin(k_n y)\cos(k_p z)\,\hat{y} + k_{mn}^2 \cos(k_m x)\cos(k_n y)\sin(k_p z)\,\hat{z}\right] \tag{3.26c}$$

In these equations

$$k_\nu^{TE} = k_\nu^{TM} = k_\nu = (k_{mn}^2 + k_p^2)^{1/2} \tag{3.27}$$

$$k_{mn}^2 = k_m^2 + k_n^2 \tag{3.28}$$

The squares of normalization factors of the above functions are obtained as

$$\int_V |\vec{e}_\nu|^2\, dv = \int_V |\vec{h}_\nu|^2\, dv = \frac{abc\, k_\nu^2}{\varepsilon_m \varepsilon_n \varepsilon_p} \tag{3.29a}$$

$$\int_V |\vec{E}_\nu|^2\, dv = \int_V |\vec{H}_\nu|^2\, dv = \frac{abc\, k_{mn}^2}{\varepsilon_m \varepsilon_n \varepsilon_p} \qquad (TE \text{ or } TM) \tag{3.29b}$$

where ε_i, $i = m, n, p$, is the Neumann number defined by

$$\varepsilon_i = \begin{cases} 1, & i = 0 \\ 2, & i > 0 \end{cases} \tag{3.30}$$

Substitution of the above eigenvectors along with their normalization factors into (3.20) and (3.22) yields the electric and magnetic-type dyadic Green's functions for a rectangular

cavity in terms of an infinite triple series over the indices m, n and p, i.e.

$$\overleftrightarrow{G}_e(\vec{r}' \mid \vec{r}) = \sum_{\nu} \frac{\varepsilon_m \varepsilon_n \varepsilon_p}{abck_{mn}^2} \left[\frac{1}{k_\nu^2 - k^2} \left(\vec{E}_\nu'^{TE} \vec{E}_\nu^{TE} + \vec{E}_\nu'^{TM} \vec{E}_\nu^{TM} \right) - \frac{k_{mn}^2}{k^2 k_\nu^2} \vec{e}_\nu' \vec{e}_\nu \right] \tag{3.31}$$

$$\overleftrightarrow{G}_m(\vec{r}' \mid \vec{r}) = \sum_{\nu} \frac{\varepsilon_m \varepsilon_n \varepsilon_p}{abck_{mn}^2} \left[\frac{1}{k_\nu^2 - k^2} \left(\vec{H}_\nu'^{TE} \vec{H}_\nu^{TE} + \vec{H}_\nu'^{TM} \vec{H}_\nu^{TM} \right) - \frac{k_{mn}^2}{k^2 k_\nu^2} \vec{h}_\nu' \vec{h}_\nu \right] \tag{3.32}$$

which are the same as those obtained from the Ohm-Rayleigh method [52].

For computational purposes it is desirable to reduce the triple series in (3.31) and (3.32) into a double summation if possible. Fortunately in the cases of rectangular and cylindrical cavities, the summation over the index p can be written in closed form and therefore the reduction is possible. First, we consider the electric-type dyadic Green's function. In an attempt to single out the z dependence in the electric-field eigenvectors (3.25) in order to simplify the process of reducing the triple series, we define the following auxiliary vector functions:

$$\vec{u}_{mn}^{e}(x, y) = k_m \cos(k_m x) \sin(k_n y) \hat{x} + k_n \sin(k_m x) \cos(k_n y) \hat{y} \tag{3.33a}$$

$$\vec{v}_{mn}^{e}(x, y) = \sin(k_m x) \sin(k_n y) \hat{z} \tag{3.33b}$$

$$\vec{w}_{mn}^{e}(x, y) = -k_n \cos(k_m x) \sin(k_n y) \hat{x} + k_m \sin(k_m x) \cos(k_n y) \hat{y} \tag{3.33c}$$

Thus, the electric-field eigenvectors may be written as

$$\vec{e}_\nu = \vec{u}^e \sin(k_p z) + k_p \vec{v}^e \cos(k_p z) \tag{3.34a}$$

$$\vec{E}_\nu^{TE} = \vec{w}^e \sin(k_p z) \tag{3.34b}$$

$$\vec{E}_\nu^{TM} = \frac{1}{k_\nu^{TM}} \left[-k_p \vec{u}^e \sin(k_p z) + k_{mn}^2 \vec{v}^e \cos(k_p z) \right] \tag{3.34c}$$

where the subscript mn of the auxiliary vector functions is omitted for convenience. Substitution of the above quantities into (3.31) yields

$$\overleftrightarrow{G}_e(\vec{r}' \mid \vec{r}) = \frac{2}{abck^2} \sum_{m,\,n} \varepsilon_m\, \varepsilon_n \left\{ \vec{u}'^e\, \vec{u}^e \frac{K_{mn}^2}{k_{mn}^2} \sum_{p=1}^{\infty} \frac{\sin(k_p z')\sin(k_p z)}{k_p^2 - K_{mn}^2} \right.$$

$$- \vec{u}'^e\, \vec{v}^e \sum_{p=1}^{\infty} \frac{k_p \sin(k_p z') \cos(k_p z)}{k_p^2 - K_{mn}^2} - \vec{v}'^e\, \vec{u}^e \sum_{p=1}^{\infty} \frac{k_p \cos(k_p z') \sin(k_p z)}{k_p^2 - K_{mn}^2}$$

$$+ \vec{v}'^e\, \vec{v}^e \left[k^2 \sum_{p=0}^{\infty} \frac{(\varepsilon_p/2)\cos(k_p z') \cos(k_p z)}{k_p^2 - K_{mn}^2} - \sum_{p=1}^{\infty} \frac{k_p^2 \cos(k_p z') \cos(k_p z)}{k_p^2 - K_{mn}^2} \right]$$

$$\left. + \vec{w}'^e\, \vec{w}^e \frac{k^2}{k_{mn}^2} \sum_{p=1}^{\infty} \frac{\sin(k_p z') \sin(k_p z)}{k_p^2 - K_{mn}^2} \right\} \tag{3.35}$$

where

$$K_{mn}^2 = k^2 - k_{mn}^2 \tag{3.36}$$

and the primed vector functions are defined with respect to the primed variables x', y'. The infinite summations over the index p can be written in closed form by using the contour integration method explained in Appendix B and the results are summarized here

$$\sum_{p=1}^{\infty} \frac{\sin(k_p z') \sin(k_p z)}{k_p^2 - K_{mn}^2} = A_{mn}\, f_{mn}(z, z') \tag{3.37a}$$

$$\sum_{p=0}^{\infty} \frac{(\varepsilon_p/2) \cos(k_p z') \cos(k_p z)}{k_p^2 - K_{mn}^2} = -A_{mn}\, g_{mn}(z, z') \tag{3.37b}$$

$$\sum_{p=1}^{\infty} \frac{k_p \cos(k_p z') \sin(k_p z)}{k_p^2 - K_{mn}^2} = A_{mn} \frac{\partial g_{mn}}{\partial z} \tag{3.37c}$$

$$\sum_{p=1}^{\infty} \frac{k_p \sin(k_p z') \cos(k_p z)}{k_p^2 - K_{mn}^2} = A_{mn} \frac{\partial f_{mn}}{\partial z} \tag{3.37d}$$

$$\sum_{p=1}^{\infty} \frac{k_p^2 \cos(k_p z') \cos(k_p z)}{k_p^2 - K_{mn}^2} = A_{mn} \frac{\partial^2 g_{mn}}{\partial z^2} \tag{3.37e}$$

$$\sum_{p=1}^{\infty} \frac{k_p^2 \sin(k_p z') \sin(k_p z)}{k_p^2 - K_{mn}^2} = - A_{mn} \frac{\partial^2 f_{mn}}{\partial z^2} \tag{3.37f}$$

where

$$A_{mn} = \frac{c}{2 K_{mn} \sin(K_{mn} c)} \tag{3.38}$$

$$f_{mn}(z, z') = \begin{cases} \sin[K_{mn}(c - z')] \sin(K_{mn} z), & z < z' \\ \sin(K_{mn} z') \sin[K_{mn}(c - z)], & z > z' \end{cases} \tag{3.39}$$

$$g_{mn}(z, z') = \begin{cases} \cos[K_{mn}(c - z')] \cos(K_{mn} z), & z < z' \\ \cos(K_{mn} z') \cos[K_{mn}(c - z)], & z > z' \end{cases} \tag{3.40}$$

In calculating the second derivative of g_{mn} in (3.37e) one should note that although $g_{mn}(z, z')$ is continuous at $z = z'$, its derivative

$$\frac{\partial g_{mn}}{\partial z} = K_{mn} \begin{cases} - \cos[K_{mn}(c - z')] \sin(K_{mn} z), & z < z' \\ \cos(K_{mn} z') \sin[K_{mn}(c - z)], & z > z' \end{cases}$$

has a discontinuity equal to $K_{mn} \sin(K_{mn} c)$ at $z = z'$. Thus

$$\frac{\partial^2 g_{mn}}{\partial z^2} = - K_{mn}^2 g_{mn}(z, z') + K_{mn} \sin(K_{mn} c) \delta(z - z') \tag{3.41}$$

Applying the series (3.37a–d) in (3.35) and after some manipulations we obtain the reduced form of the electric-type dyadic Green's function for a rectangular cavity as

$$\overleftrightarrow{G}_e(\vec{r}' \mid \vec{r}) = \frac{1}{abk^2} \sum_{m=0}^{\infty} \sum_{n=0}^{\infty} \frac{\varepsilon_m \varepsilon_n}{K_{mn} \sin(K_{mn} c)} \left[\frac{1}{k_{mn}^2} (K_{mn}^2 \vec{u}'^e \vec{u}^e + k^2 \vec{w}'^e \vec{w}^e) f_{mn} \right.$$

$$\left. - \vec{u}'^e \vec{v}^e \frac{\partial f_{mn}}{\partial z} - \vec{v}'^e \vec{u}^e \frac{\partial g_{mn}}{\partial z} - k_{mn}^2 \vec{v}'^e \vec{v}^e g_{mn} \right]$$

$$- \frac{1}{k^2} \delta(\vec{r}' - \vec{r}) \hat{z}\hat{z} \tag{3.42}$$

where we have used the following relations to simplify the singular term

$$\delta(\hat{r} - \hat{r}') = \delta(x - x') \delta(y - y') \delta(z - z') \tag{3.43}$$

$$\delta(x-x') = \frac{2}{a} \sum_m \sin(k_m x)\, \sin(k_m x') \tag{3.44a}$$

$$\delta(y-y') = \frac{2}{b} \sum_n \sin(k_n y)\, \sin(k_n y') \tag{3.44b}$$

Following a similar procedure we can reduce the triple series of the magnetic-type dyadic Green's function in (3.32). To this end we define the following auxiliary vector functions:

$$\vec{u}^h_{mn}(x, y) = k_m \sin(k_m x)\, \cos(k_n y)\, \hat{x} + k_n \cos(k_m x)\, \sin(k_n y)\, \hat{y} \tag{3.45a}$$

$$\vec{v}^h_{mn}(x, y) = \cos(k_m x)\, \cos(k_n y)\, \hat{z} \tag{3.45b}$$

$$\vec{w}^h_{mn}(x, y) = k_n \sin(k_m x)\, \cos(k_n y)\, \hat{x} - k_m \cos(k_m x)\, \sin(k_n y)\, \hat{y} \tag{3.45c}$$

Thus the irrotational and solenoidal magnetic-field eigenvectors can be written in the form

$$\vec{h}_\nu = \vec{u}^h \cos(k_p z) + k_p \vec{v}^h \sin(k_p z) \tag{3.46a}$$

$$\vec{H}^{TE}_\nu = \frac{1}{k^{TE}_\nu} \left[- k_p \vec{u}^h \cos(k_p z) + k^2_{mn} \vec{v}^h \sin(k_p z) \right] \tag{3.46b}$$

$$\vec{H}^{TM}_\nu = \vec{w}^h \cos(k_p z) \tag{3.46c}$$

where again the subscript mn of the vector functions is omitted. Substitution of these into (3.32) and using relations (3.37) for the series over the index p, yields the following reduced form for the magnetic-type dyadic Green's function

$$\overleftrightarrow{G}_m(\vec{r}' \mid \vec{r}) = \frac{1}{abk^2} \sum_{m=0}^{\infty} \sum_{n=0}^{\infty} \frac{\varepsilon_m\, \varepsilon_n}{K_{mn} \sin(K_{mn} c)} \left[- \frac{1}{k^2_{mn}} (K^2_{mn}\, \vec{u}'^h\, \vec{u}^h + k^2\, \vec{w}'^h\, \vec{w}^h)\, g_{mn} \right.$$

$$\left. - \vec{u}'^h\, \vec{v}^h\, \frac{\partial g_{mn}}{\partial z} - \vec{v}'^h\, \vec{u}^h\, \frac{\partial f_{mn}}{\partial z} + k^2_{mn}\, \vec{v}'^h\, \vec{v}^h\, f_{mn} \right]$$

$$- \frac{1}{k^2}\, \delta(\vec{r}' - \vec{r})\, \hat{z}\hat{z} \tag{3.47}$$

3.3- Discussion of the resonant modes

From the field expansion coefficients in (3.18) it is seen that the terms associated with the solenoidal eigenvectors have resonant behavior. In other words, as the wavenumber $k = 2\pi/\lambda$ approaches either the eigenvalues k_ν^{TE} or k_ν^{TM}, the amplitude of the corresponding mode and thus the fields inside the cavity tend to infinity. However, in the physical reality there always exist losses, whatever small, that limit the field amplitude. For this reason, the effect of losses cannot be ignored for the resonant modes and will be taken into account in the following calculations.

To calculate the amplitude of the resonant modes we assume that when $k \to k_\nu^{TE}$ or k_ν^{TM}, the corresponding mode is dominant. Thus, in the general case where k_ν^{TE} and k_ν^{TM} are different, for example in a cylindrical cavity, one can write

$$\vec{E}(\vec{r}) \simeq B_\nu^e \; \vec{E}_\nu^{TE}(\vec{r}) \tag{3.48a}$$

$$\vec{H}(\vec{r}) \simeq B_\nu^h \; \vec{H}_\nu^{TE}(\vec{r}) \tag{3.48b}$$

for $k \to k_\nu^{TE}$ and

$$\vec{E}(\vec{r}) \simeq C_\nu^e \; \vec{E}_\nu^{TM}(\vec{r}) \tag{3.49a}$$

$$\vec{H}(\vec{r}) \simeq C_\nu^h \; \vec{H}_\nu^{TM}(\vec{r}) \tag{3.49b}$$

for $k \to k_\nu^{TM}$. In these equations $(\vec{E}_\nu\,,\ \vec{H}_\nu)$ are the solenoidal eigenvectors of the TE or TM modes and the coefficients B_ν and C_ν are given by (3.18).

In calculating the fields from (3.2), we single out the dominant resonant mode ν_r and obtain the contribution of all the other modes by performing the summation over $\nu \neq \nu_r$. In terms of the integral expressions for the fields in (3.19) and (3.21), the above procedure is equivalent to isolating the terms where $k = k_\nu$ (TE or TM) in the summations of the appropriate dyadic Green's functions. Next, the relations in (3.48) or (3.49) can be used to obtain the amplitude of the appropriate resonant mode and thus its contribution to the total field. In the following we calculate the amplitude B_ν^h of the magnetic field due to the resonant TE mode. Other coefficients may be obtained in a similar fashion.

Let $S = S_0 + A$ where S is the boundary surface of the closed region in the form of a cavity, A is the area of a possible opening (aperture) in the cavity wall and S_0 denotes the metallic surface of the wall which has a finite conductivity. The electric field at the points of the non-perfectly conducting wall is given by [53]

$$\vec{E} \mid_{S_0} = - Z_s \, \hat{n} \times \vec{H} \mid_{S_0} \tag{3.50}$$

where $\hat{n}$ is the unit normal pointing outwards and Z_s is the surface impedance of the wall

$$Z_s = \sqrt{\frac{\omega \mu_0}{2\sigma}} \, (1 + j)$$

From (3.18d) we have

$$B_v^h = \frac{1}{A_1} \left[\Omega + j\omega \varepsilon \int_{S_0} \hat{n} \times \vec{E}(\vec{r}') \cdot \vec{H}_v^{TE}(\vec{r}') \, ds' \right] \tag{3.51}$$

where

$$\Omega = j\omega \varepsilon \int_V \vec{M}(\vec{r}') \cdot \vec{H}_v^{TE}(\vec{r}') \, dv' - k_v^{TE} \int_V \vec{J}(\vec{r}') \cdot \vec{E}_v^{TE}(\vec{r}') \, dv'$$

$$+ j\omega \varepsilon \int_A \hat{n} \times \vec{E}(\vec{r}') \cdot \vec{H}_v^{TE}(\vec{r}') \, ds' \tag{3.52}$$

and

$$A_1 = [k^2 - (k_v^{TE})^2] \int_V \mid \vec{H}_v^{TE} \mid^2 dv' \tag{3.53}$$

From (3.50) and with the assumption that at resonance (i.e. $k \rightarrow k_v^{TE}$) $\vec{H} \simeq B_v^h \, \vec{H}_v^{TE}$, the integral over S_0 in (3.51) can be written as

$$\int_{S_0} \hat{n} \times \vec{E}(\vec{r}') \cdot \vec{H}_v^{TE}(\vec{r}') \, ds' = B_v^h \, Z_s \int_{S_0} \mid \hat{n} \times \vec{H}_v^{TE} \mid^2 ds'$$

Thus

$$B_\nu^h = \Omega \left[A_1 - j\omega \varepsilon Z_s \int_{S_0} | \hat{n} \times \vec{H}_\nu^{TE} |^2 \, ds' \right]^{-1} \tag{3.54}$$

At resonance, $A_1 \rightarrow 0$ and assuming $\vec{M} = 0$ in (3.52), we have

$$B_\nu^h = \frac{-k_\nu^{TE} \int_V \vec{J}(\vec{r}') \cdot \vec{E}_\nu^{TE}(\vec{r}') dv' + j\omega\varepsilon \int_A \hat{n} \times \vec{E}(\vec{r}') \cdot \vec{H}_\nu^{TE}(\vec{r}') ds'}{- j\omega \varepsilon Z_s \int_{S_0} | \hat{n} \times \vec{H}_\nu^{TE} |^2 \, ds'} \tag{3.55}$$

This is the amplitude of the resonant TE mode contributing to the magnetic field in the cavity and shows the significance of the finite surface impedance of the cavity wall.

In the special case where $k_\nu^{TE} = k_\nu^{TM} = k_\nu$, for example in a rectangular cavity, there are two resonant terms in the field expressions. These terms which correspond to the TE and TM modes are both dominant at the same frequency and cannot be treated separately in the way discussed above. For this case as $k \rightarrow k_\nu$, one may write the resonant field as

$$\vec{E} \simeq B_\nu^e \, \vec{E}_\nu^{TE} + C_\nu^e \, \vec{E}_\nu^{TM} \tag{3.56a}$$

$$\vec{H} \simeq B_\nu^h \, \vec{H}_\nu^{TE} + C_\nu^h \, \vec{H}_\nu^{TM} \tag{3.56b}$$

In the following we present the calculation of B_ν^h and C_ν^h. An expression for B_ν^h is given in (3.51). A similar expression may be written for C_ν^h, namely

$$C_\nu^h = \frac{1}{A_2} \left[\Pi + j\omega \varepsilon \int_{S_0} \hat{n} \times \vec{E}(\vec{r}') \cdot \vec{H}_\nu^{TM}(\vec{r}') \, ds' \right] \tag{3.57}$$

where

$$\Pi = j\omega \varepsilon \int_V \vec{M}(\vec{r}') \cdot \vec{H}_\nu^{TM}(\vec{r}') \, dv' - k_\nu^{TM} \int_V \vec{J}(\vec{r}') \cdot \vec{E}_\nu^{TM}(\vec{r}') \, dv'$$

$$+ j\omega \varepsilon \int_A \hat{n} \times \vec{E}(\vec{r}') \cdot \vec{H}_\nu^{TM}(\vec{r}') \, ds' \tag{3.58}$$

and

$$A_2 = [k^2 - (k_\nu^{TM})^2] \int_V | \vec{H}_\nu^{TM} |^2 \, dv' \tag{3.59}$$

For this case the integrals over S_0 in (3.51) and (3.57) are given by

$$\int_{S_0} \hat{n} \times \vec{E}(\vec{r}') \cdot \vec{H}_\nu^{TE}(\vec{r}') \, ds' = (B_\nu^h \, I_1 + C_\nu^h \, I) \, Z_s \tag{3.60}$$

$$\int_{S_0} \hat{n} \times \vec{E}(\vec{r}') \cdot \vec{H}_\nu^{TM}(\vec{r}') \, ds' = (B_\nu^h \, I + C_\nu^h \, I_2) \, Z_s \tag{3.61}$$

where

$$I = \int_{S_0} \hat{n} \times \vec{H}_\nu^{TE}(\vec{r}') \cdot \hat{n} \times \vec{H}_\nu^{TM}(\vec{r}') \, ds' \tag{3.62}$$

$$I_1 = \int_{S_0} | \hat{n} \times \vec{H}_\nu^{TE}(\vec{r}') |^2 \, ds' \tag{3.63}$$

$$I_2 = \int_{S_0} | \hat{n} \times \vec{H}_\nu^{TM}(\vec{r}') |^2 \, ds' \tag{3.64}$$

Substituting (3.60) and (3.61) into (3.51) and (3.57) and solving the resulting system of equations for B_ν^h and C_ν^h yields

$$B_\nu^h = \frac{\Omega + j\omega\varepsilon Z_s I C_\nu^h}{A_1 - j\omega\varepsilon Z_s I_1}$$

$$C_\nu^h = \frac{j\omega\varepsilon \, Z_s I \, \Omega + (A_1 - j\omega\varepsilon \, Z_s \, I_1) \, \Pi}{A_1 A_2 - j\omega\varepsilon Z_s (A_2 I_1 + A_1 I_2) + \omega^2 \varepsilon^2 Z_s{}^2 (I^2 - I_1 I_2)}$$

As $k \to k_\nu$, we have $A_1 \to 0$ and $A_2 \to 0$ and thus the above relations reduce to

$$B_\nu^h = \Gamma \, (I_2 \, \Omega - I \, \Pi) \tag{3.65}$$

$$C_\nu^h = - \Gamma \, (I \, \Omega - I_1 \, \Pi) \tag{3.66}$$

where

$$\Gamma = -j \left[\omega \varepsilon (I^2 - I_1 I_2) Z_s \right]^{-1} \tag{3.67}$$

Substituting these coefficients in (3.56b) and using the expressions for Ω and Π, one may obtain a relation similar to (3.21) for the contribution of the resonant modes to the magnetic field in the cavity. For $\vec{M} = 0$, we have

$$\vec{H}_r = \int_V \vec{J}(\vec{r}') \cdot \nabla' \times \overleftrightarrow{G}_m^r(\vec{r}' \mid \vec{r})\, dv'$$

$$- j\omega \varepsilon \int_A \hat{n} \times \vec{E}(\vec{r}') \cdot \overleftrightarrow{G}_m^r(\vec{r}' \mid \vec{r})\, ds' \tag{3.68}$$

where $\overleftrightarrow{G}_m^r(\vec{r}' \mid \vec{r})$ is the magnetic-type dyadic Green's function for the resonant modes in the cavity given by

$$\overleftrightarrow{G}_m^r = \Gamma \left[(I\vec{H}_\nu'^{TE} - I_1 \vec{H}_\nu'^{TM})\, \vec{H}_\nu^{TM} + (I\vec{H}_\nu'^{TM} - I_2 \vec{H}_\nu'^{TE})\, \vec{H}_\nu^{TE} \right] \tag{3.69}$$

and

$$\nabla' \times \overleftrightarrow{G}_m^r = \Gamma\, k_\nu \left[(I\vec{E}_\nu'^{TE} - I_1 \vec{E}_\nu'^{TM})\, \vec{H}_\nu^{TM} + (I\vec{E}_\nu'^{TM} - I_2 \vec{E}_\nu'^{TE})\, \vec{H}_\nu^{TE} \right] \tag{3.70}$$

CHAPTER 4

CAVITY-BACKED APERTURE RADIATORS

In practical applications of the slot antennas, the slot is normally backed by a conducting enclosure (cavity) forcing it to radiate into a half-space. The resulting cavity-backed slot (CBS) radiator, which has the capability of dielectric and ferrite loading, may be flush mounted and therefore is suitable for airborne and missile applications. Furthermore, if used in an array, the CBS produces small mutual effects which make it desirable as an element of large antenna array systems.

In this Chapter the general problem of a cavity-backed aperture radiator is formulated for the tangential electric field in the aperture. The result is used to obtain an integro-differential equation for the special case of a narrow slot backed by a rectangular cavity resonator. This equation is then solved numerically by the method of moments with the proper choice of piecewise sinusoidal basis and testing functions to remove the differential operator in the integrand. The method based on the Fourier transform presented in Chapter 2 is not applicable to this problem due to the fact that elements of the moment matrix are not in the form of convolution integral as will be shown later.

4.1- General formulation

The general problem of cavity-backed aperture is shown in Fig. 4.1 where an aperture in a perfectly conducting screen located in the $x-y$ plane is backed by a conducting cavity of arbitrary shape. The two regions separated by the aperture are homogeneous and may have different characteristic parameters. It is assumed that the structure is excited in general by known volume electric and magnetic current densities $\vec{J}$ and $\vec{M}$ inside the cavity and possible electric surface current density $\vec{J}_s^a$ on the aperture. The cases where the aperture is excited by an incident plane wave or by current sources outside the cavity can be handled in a similar fashion and are not considered here.

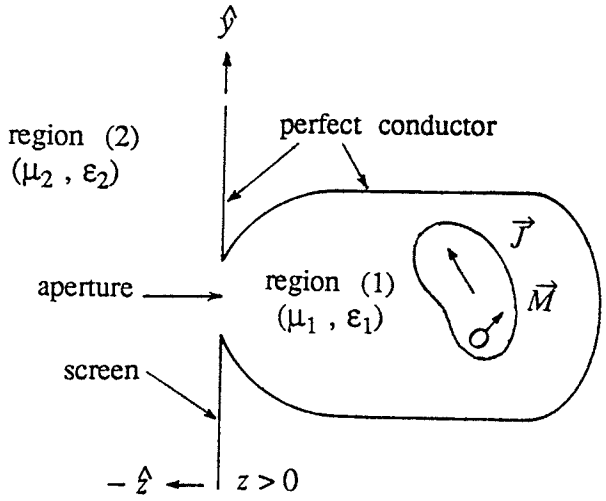

Fig. 4.1- Geometry of the general cavity-backed aperture problem.

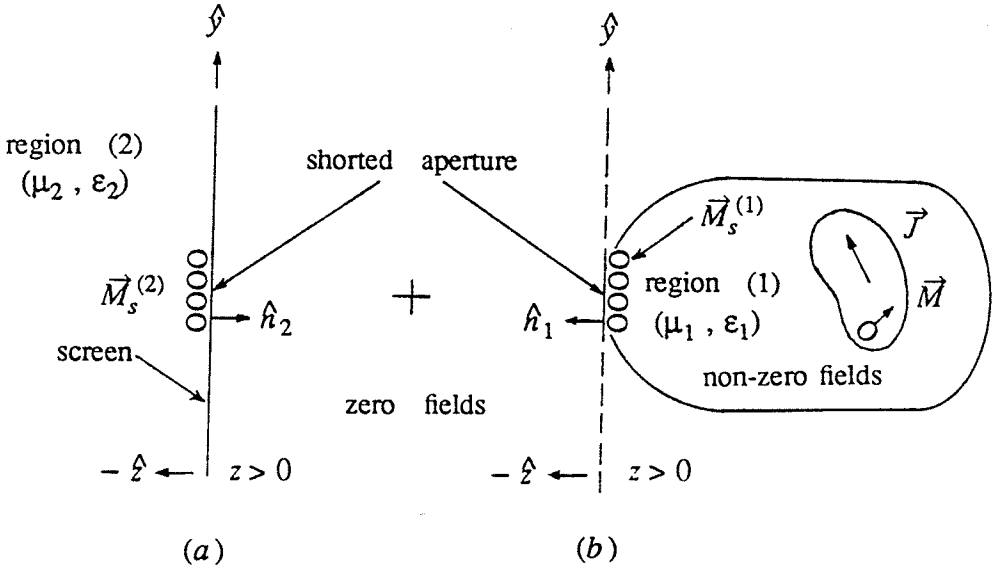

Fig. 4.2- Equivalents of the original problem; a) valid for region (2) i.e. $z < 0$, b) valid for region (1) i.e. $z > 0$.

It is convenient to use the equivalence principle [39] to substitute the original problem with two equivalent problems. The procedure is similar to the one given in Chapter 2 for an open slot and results in the equivalent configurations shown in Fig. 4.2. In region (1) the fields are produced by the sources $\vec{J}$ and $\vec{M}$ plus the equivalent magnetic surface current density $\vec{M}_s^{(1)} = \hat{n}_1 \times \vec{E}^{(1)} \mid_A$ over the aperture surface with the aperture covered by an electric conductor and $\vec{E}^{(1)}$ is the electric field in region (1). In region (2) the fields $\vec{E}^{(2)}$ and $\vec{H}^{(2)}$ are produced by the equivalent magnetic surface current density $\vec{M}_s^{(2)} = \hat{n}_2 \times \vec{E}^{(2)} \mid_A$ over the aperture surface with the aperture covered by an electric conductor. Since in the original problem there is no magnetic surface current density in the aperture, the electric field in regions (1) and (2) are continuous in the aperture and thus $\hat{n}_1 \times [\vec{E}^{(1)} - \vec{E}^{(2)}]_A = 0$. On the other hand the unit vectors normal to the aperture are in opposite directions in regions (1) and (2). Hence $\hat{n}_1 \times \vec{E}^{(1)} \mid_A = -\hat{n}_2 \times \vec{E}^{(2)} \mid_A$ and in terms of the equivalent magnetic currents previously defined we have $\vec{M}_s^{(2)} = -\vec{M}_s^{(1)}$. The remaining boundary condition to be satisfied is that of the tangential component of the magnetic field across the aperture given by $\hat{n}_1 \times [\vec{H}^{(2)} - \vec{H}^{(1)}]_A = \vec{J}_s^a$. Thus for $\hat{n}_1 = -\hat{z}$ and the aperture in the $z = 0$ plane we have

$$\lim_{z \to 0^+} \hat{z} \times \vec{H}^{(1)}(\vec{r}) - \lim_{z \to 0^-} \hat{z} \times \vec{H}^{(2)}(\vec{r}) = \vec{J}_s^a(\vec{r}) \tag{4.1}$$

where $\vec{J}_s^a$ is a known electric surface current on the aperture. This equation can be written in the component form:

$$H_y^{(2)} - H_y^{(1)} = J_x^a , \qquad z \to 0 \tag{4.2a}$$

$$H_x^{(2)} - H_x^{(1)} = -J_y^a , \qquad z \to 0 \tag{4.2b}$$

In the following we will use the above equations to obtain a system of integral equations for the unknown tangential electric field in the aperture.

The fields in region (2), i.e. the half space $z < 0$ can be obtained from the equivalent problem shown in Fig. 4.2a. This problem has been worked out in detail in Chapter 2 and the magnetic field is given by

$$\vec{H}^{(2)}(\vec{r}) = -\frac{j\omega\varepsilon_2}{2\pi}\int_A \vec{M}_s^{(2)}(\vec{r}') \cdot \overleftrightarrow{G}_0(\vec{r}' \mid \vec{r})\, ds' \tag{4.3}$$

where the integration is over the aperture area and $\overleftrightarrow{G}_0(\vec{r}' \mid \vec{r})$ is the dyadic Green's function of free space defined in (2.3). Also $\vec{M}_s^{(2)} = \hat{n}_2 \times \vec{E}^a$ with $\hat{n}_2 = \hat{z}$ and $\vec{E}^a$ is the electric field in the aperture.

In deriving the fields in region (2) we were able to use the image theorem and thus treat $\vec{M}_s^{(2)}$ and its image as if they were in an open space. Unfortunately no such simplification can be made for the fields in region (1) where the sources reside in an arbitrarily shaped closed region. We solved this problem in Chapter 3 by expanding the fields in terms of orthogonal eigenvectors. From (3.21) the magnetic field in region (1) with a volume current density $\vec{J}$ and a magnetic surface current $\vec{M}_s^{(1)} = \hat{n}_1 \times \vec{E}^a$ on the shorted aperture is given by

$$\vec{H}^{(1)}(\vec{r}) = \int_V \vec{J}(\vec{r}') \cdot \nabla' \times \overleftrightarrow{G}_m(\vec{r}' \mid \vec{r})\, dv' - j\omega\varepsilon_1 \int_A \hat{n}_1 \times \vec{E}^a(\vec{r}') \cdot \overleftrightarrow{G}_m(\vec{r}' \mid \vec{r})\, ds' \tag{4.4}$$

where $\overleftrightarrow{G}_m(\vec{r}' \mid \vec{r})$ is the magnetic-type dyadic Green's function of the closed region and $\hat{n}_1 = -\hat{z}$. Substituting the appropriate components of (4.3) and (4.4) in (4.2), we obtain a coupled system of integral equations for the transverse components of the electric field in the aperture E_x^a and E_y^a, i.e.

$$\int_A (E_y^a F_{xx} - E_x^a F_{yx})\, ds' = f(x, y), \qquad z = 0 \tag{4.5}$$

$$\int_A (E_y^a F_{xy} - E_x^a F_{yy})\, ds' = g(x, y), \qquad z = 0 \tag{4.6}$$

where

$$F_{xx} = C_1 G_{xx}^m + C_2 (k_2^2 + \frac{\partial^2}{\partial x^2}) G_0 \tag{4.7a}$$

$$F_{xy} = C_1 G_{xy}^m + C_2 \frac{\partial^2}{\partial x \partial y} G_0 \tag{4.7b}$$

$$F_{yx} = C_1\, G^m_{yx} + C_2\, \frac{\partial^2}{\partial y\, \partial x} G_0 \tag{4.7c}$$

$$F_{yy} = C_1\, G^m_{yy} + C_2\, (k_2^2 + \frac{\partial^2}{\partial y^2}) G_0 \tag{4.7d}$$

In these equations $z = z' = 0$, $C_1 = \dfrac{4\pi k_1^2}{\mu_{r1}}$, $C_2 = \dfrac{2}{\mu_{r2}}$ and G^m_{xx}, G^m_{xy}, etc. are components of the magnetic-type dyadic Green's function of the cavity. For the general case where both a volume current $\vec{J}(\vec{r})$ in the cavity and a surface current $\vec{J}^a_s(x, y)$ on the aperture are present, the forcing functions in (4.5) and (4.6) are given by

$$f(x, y) = -j\, 4\pi\omega\mu_0 \int_V [\, J_x(x', y', z')\, (\frac{\partial G^m_{zx}}{\partial y'} - \frac{\partial G^m_{yx}}{\partial z'}) + J_y(x', y', z')\, (\frac{\partial G^m_{xx}}{\partial z'} - \frac{\partial G^m_{zx}}{\partial x'}) +$$

$$+ J_z(x', y', z')\, (\frac{\partial G^m_{yx}}{\partial x'} - \frac{\partial G^m_{xx}}{\partial y'})]\, dv' + j\, 4\pi\omega\mu_0\, J^a_y(x, y)\,, \qquad z = 0 \tag{4.8}$$

$$g(x, y) = -j\, 4\pi\omega\mu_0 \int_V [\, J_x(x', y', z')\, (\frac{\partial G^m_{zy}}{\partial y'} - \frac{\partial G^m_{yy}}{\partial z'}) + J_y(x', y', z')\, (\frac{\partial G^m_{xy}}{\partial z'} - \frac{\partial G^m_{zy}}{\partial x'}) +$$

$$+ J_z(x', y', z')\, (\frac{\partial G^m_{yy}}{\partial x'} - \frac{\partial G^m_{xy}}{\partial y'})]\, dv' - j\, 4\pi\omega\mu_0\, J^a_x(x, y)\,, \qquad z = 0 \tag{4.9}$$

The results obtained so far are quite general and before proceeding further with the calculations we need to specify some geometry of practical importance for the aperture as well as the cavity. To this end we consider a narrow slot backed by a rectangular cavity and solve the integral equation for the electric field in the slot.

4.2- Narrow slot backed by a rectangular cavity

The geometry of this problem is shown schematically in Fig. 4.3a. The narrow slot in the $x-y$ plane is of length $2L$, width $2w$ ($w \ll L$, $w \ll \lambda$) and is backed by a conducting rectangular cavity. Here we assume the structure is excited by a surface current density $\vec{J}^a_s(x, y)$ over the slot aperture and therefore the cavity can be considered as a load. The case where the excitation is through the cavity will be investigated in Chapter 5.

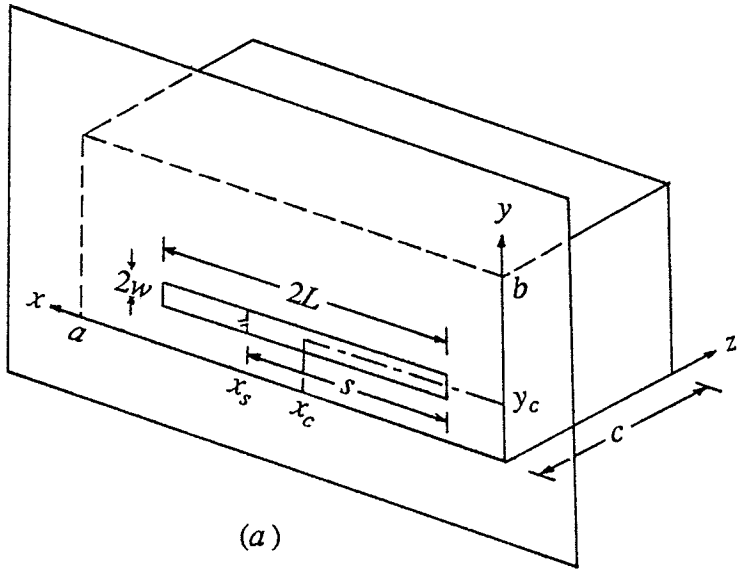

(a)

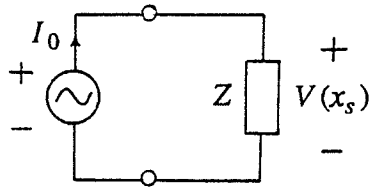

(b)

Fig. 4.3- Rectangular cavity-backed slot (CBS) antenna (a) and its equivalent circuit (b).

The components of the tangential electric field in the aperture (E_x^a and E_y^a) are the unknowns of the problem. However, for the type of excitation to be considered here the longitudinal component is negligible, i.e. $E_x^a(x, y) \simeq 0$ and the coupled integral equations in (4.5) and (4.6) reduce to a single equation for the only unknown $E_y^a(x, y)$, namely

$$\int_A E_y^a(x', y')\, F_{xx}(x', y' \mid x, y)\, ds' = f(x, y) \tag{4.10}$$

where F_{xx} is given by (4.7a) and

$$f(x, y) = j4\pi\omega\mu_0\, J_y^a(x, y) \tag{4.11}$$

In the following we assume $\varepsilon_2 = \varepsilon_0$, $\mu_2 = \mu_0$, $\varepsilon_1 = \varepsilon_r \varepsilon_0$, $\mu_1 = \mu_r \mu_0$, along with a change of notation $\mu_{r1} = \mu_r$, $k_1 = k$ and $k_2 = k_0$. Also to facilitate the computations, as will be evident shortly, we write the expression for G_{xx}^m of the rectangular cavity in the form

$$G_{xx}^m = \frac{1}{4\pi k^2}\,(k^2 + \frac{\partial^2}{\partial x^2})G_x \tag{4.12}$$

where for $z = z' = 0$ (see Appendix C)

$$G_x = -\frac{4\pi}{ab} \sum_p \sum_q \frac{\varepsilon_p \varepsilon_q}{K_{pq} \tan(K_{pq} c)} \sin(k_p x') \cos(k_q y') \sin(k_p x) \cos(k_q y) \tag{4.13}$$

with

$$K_{pq} = (k^2 - k_p^2 - k_q^2)^{1/2}, \qquad k_p = \frac{p\pi}{a}, \qquad k_q = \frac{q\pi}{b} \tag{4.14}$$

and

$$\varepsilon_p = \begin{cases} 1, & p = 0 \\ 2, & p \neq 0 \end{cases} \tag{4.15}$$

Thus (4.7a) can be written as

$$F_{xx} = \frac{1}{\mu_r}\,(k^2 + \frac{\partial^2}{\partial x^2})G_x + 2\,(k_0^2 + \frac{\partial^2}{\partial x^2})G_0, \qquad z = 0 \tag{4.16}$$

With this equation as the kernel, we proceed to solve the integral equation in (4.10) by assuming a separable solution of the form

$$E_y^a(x, y) = X(x)\, Y(y) \tag{4.17}$$

where $X(x)$ is an unknown function, while $Y(y)$ is given by

$$Y(y) = \frac{1/\pi}{\sqrt{w^2-(y-y_c)^2}} \tag{4.18}$$

which is justified by the narrow slot assumption and incorporates the proper field behavior at the edges [21]. Next we expand $X(x)$ in terms of suitable basis functions $X_n(x)$, i.e.

$$X(x) \approx \sum_{n=1}^{N} V_n\, X_n(x) \tag{4.19}$$

where V_n are unknown constants to be determined. Substituting (4.19) into (4.10) we have

$$\sum_{n=1}^{N} V_n \int_A X_n(x')\, Y(y')\, F_{xx}(x', y' \mid x, y)\, dx'\, dy' \approx f(x, y) \tag{4.20}$$

The inner product of this equation with a testing function $W_m(x, y)$ yields a system of N linear equations that can be solved for the unknowns V_n,

$$\sum_{n=1}^{N} V_n \left(\frac{1}{\mu_r}\, a_{mn} + 2\, b_{mn} \right) \approx c_m\,, \quad m=1, 2, \cdots, N \tag{4.21}$$

where

$$a_{mn} = \int_A \int_A W_m(x, y)\, X_n(x')\, Y(y') \left(k^2 + \frac{\partial^2}{\partial x^2}\right) G_x(x', y' \mid x, y)\, dx'dy'dx\, dy \tag{4.22}$$

$$b_{mn} = \int_A \int_A W_m(x, y)\, X_n(x')\, Y(y') \left(k_0^2 + \frac{\partial^2}{\partial x^2}\right) G_0(x', y' \mid x, y)\, dx'dy'dx\, dy \tag{4.23}$$

and

$$c_m = \int_A W_m(x, y)\, f(x, y)\, dx\, dy \tag{4.24}$$

Since variation of the aperture field along the y axis is known, no testing is required in this direction and thus one may choose a testing function in the form

$$W_m(x, y) = S_m(x)\ \delta(y - y_c) \tag{4.25}$$

where δ is the Dirac delta function and $S_m(x)$ is a function to be chosen properly. From (4.13) it is clear that $\frac{\partial^2 G_x}{\partial x^2} = \frac{\partial^2 G_x}{\partial x'^2}$ and therefore (4.22) can be written as

$$a_{mn} = \int_{x_c - L}^{x_c + L} X_n(x')\ (k^2 + \frac{\partial^2}{\partial x'^2}) A_m(x')\ dx' \tag{4.26}$$

where

$$A_m(x') = \int_{x_c - L}^{x_c + L} S_m(x) \left[\int_{y_c - w}^{y_c + w} Y(y')\ G_x(x', y' \mid x, y_c)\ dy' \right] dx \tag{4.27}$$

similarly (4.23) is written in the form

$$b_{mn} = \int_{x_c - L}^{x_c + L} S_m(x)\ (k_0^2 + \frac{\partial^2}{\partial x^2}) B_n(x)\ dx \tag{4.28}$$

where

$$B_n(x) = \int_{x_c - L}^{x_c + L} X_n(x') \left[\int_{y_c - w}^{y_c + w} Y(y')\ G_0(x', y' \mid x, y_c)\ dy' \right] dx' \tag{4.29}$$

Numerical computation of the integrals in (4.26) and (4.28) is hindered by the presence of derivatives in the integrands. However, choosing piecewise sinusoidal functions for $X_n(x')$ and $S_m(x)$ and integrating by parts twice, it is possible to remove the differential operators. For this purpose we choose the basis and testing functions as

$$X_n(x') = \begin{cases} \dfrac{\sin[k(\Delta - \mid x' - x_n \mid)]}{\sin(k\Delta)}, & \text{for} \quad \mid x' - x_n \mid \leq \Delta \\ 0, & \text{for} \quad \mid x' - x_n \mid > \Delta \end{cases} \tag{4.30}$$

and

$$S_m(x) = \begin{cases} \dfrac{\sin[k_0(\Delta - |\, x - x_m\,|)]}{\sin(k_0\Delta)}, & \text{for} \quad |\, x - x_m\,| \le \Delta \\ 0, & \text{for} \quad |\, x - x_m\,| > \Delta \end{cases} \tag{4.31}$$

Thus (4.26) becomes

$$a_{mn} = \frac{k}{\sin(k\Delta)} \left[A_m(x_{n-1}) - 2\cos(k\Delta)\, A_m(x_n) + A_m(x_{n+1}) \right] \tag{4.32}$$

where $A_m(x_n)$ are calculated from (4.27) and are given by (4.37). Also $x_{n-1} = x_n - \Delta$, $x_{n+1} = x_n + \Delta$, $x_n = x_c - L + n\Delta$, $n = 1, 2, \cdots, N$ and $\Delta = 2L/(N+1)$. Similarly (4.28) becomes

$$b_{mn} = \frac{k_0}{\sin(k_0\Delta)} \left[B_n(x_{m-1}) - 2\cos(k_0\Delta)\, B_n(x_m) + B_n(x_{m+1}) \right] \tag{4.33}$$

where $B_n(x_m)$ are calculated from (4.29) and are given by (4.41) with $x_{m-1} = x_m - \Delta$, $x_{m+1} = x_m + \Delta$, $x_m = x_c - L + m\Delta$ and $m = 1, 2, \cdots, N$.

Calculation of $A_m(x')$

Equation (4.27) may be written in the form

$$A_m(x') = \int_{x_c - L}^{x_c + L} S_m(x)\, P(x', x)\, dx \tag{4.34}$$

where by using (4.13) and (4.18), $P(x', x)$ is defined by

$$P(x', x) = \frac{-4}{ab} \sum_p \sum_q \frac{\varepsilon_p \varepsilon_q \cos(k_q y_c)}{K_{pq} \tan(K_{pq} c)}\, R(q)\, \sin(k_p x')\, \sin(k_p x) \tag{4.35}$$

in which

$$R(q) = \int_{y_c - w}^{y_c + w} \frac{\cos(k_q y')}{\sqrt{w^2 - (y' - y_c)^2}}\, dy' = \pi J_0(k_q w)\, \cos(k_q y_c) \tag{4.36}$$

Substituting (4.31) and (4.35) into (4.34) and performing the integration we obtain

$$A_m(x') = \frac{-4\pi}{ab} \sum_p \sum_q \frac{\varepsilon_p \varepsilon_q \cos^2(k_q y_c)}{K_{pq} \tan(K_{pq} c)} J_0(k_q w)\, T_m(p)\, \sin(k_p x') \qquad (4.37)$$

where

$$T_m(p) = \frac{4k_0 \sin(k_p x_m)}{(k_0^2 - k_p^2)\sin(k_0 \Delta)} \sin[(k_0 - k_p)\frac{\Delta}{2}] \sin[(k_0 + k_p)\frac{\Delta}{2}] \qquad (4.38)$$

Calculation of $B_n(x)$

Equation (4.29) may be written in the form

$$B_n(x) = \int_{x_c - L}^{x_c + L} X_n(x')\, Q(x' - x)\, dx' \qquad (4.39)$$

where

$$Q(x', x) = \int_{y_c - w}^{y_c + w} Y(y')\, G_0(x', y' \mid x, y_c)\, dy' \qquad (4.40)$$

Substituting $X_n(x')$ from (4.30) and with a change of variable $x' = x_n + t$, we have

$$B_n(x_m) = \frac{1}{\sin(k\Delta)} \int_{-\Delta}^{+\Delta} \sin[k(\Delta - |t|)]\, Q[(m-n)\Delta - t]\, dt \qquad (4.41)$$

where from (4.40), (4.18) and (2.4)

$$Q(\xi) = \frac{2}{\pi} \int_0^{\pi/2} \frac{e^{-jk_0[\,\xi^2 + (w\sin\theta)^2\,]^{1/2}}}{[\,\xi^2 + (w\sin\theta)^2\,]^{1/2}}\, d\theta \approx \frac{e^{-jk_0[\,\xi^2 + (w/2)^2\,]^{1/2}}}{[\,\xi^2 + (w/2)^2\,]^{1/2}} \qquad (4.42)$$

In the computations, the integral in (4.41) is evaluated numerically by using a 20 points Gaussian quadrature.

4.3- Excitation of the slot

The system of N linear equations in (4.21) may be written in the matrix form

$$[\, y_{mn} \,]\, [\, V_n \,] = [\, c_m \,] \qquad (4.43)$$

Up to this point we have obtained expressions from which the matrix elements y_{mn} can be evaluated. However, to solve for the unknowns V_n and thus the field distribution in the slot, we need the source vector elements c_m as well. From (4.24) and (4.25) these elements are given by

$$c_m = \int_{x_c - L}^{x_c + L} S_m(x)\, f(x, y_c)\, dx \tag{4.44}$$

In the following we calculate c_m for the case where the excitation source can be modeled by a uniform current distribution of amplitude I_0 given by $J_y^a(x) = I_0\, \delta(x - x_s)$ on the slot aperture. Practical examples of such a model include feeding the slot by a two-wire transmission line or a coaxial cable. It is assumed that the feed extends across the slot and thus the current distribution can be considered uniform along that portion of the line which lies in the slot. The position of the feed-point along the slot x_s is arbitrary and provides a convenient means for matching the antenna to the source as will be shown later. For the above current distribution and with $f(x, y_c) = j4\pi\omega\mu_0\, J_y^a(x)$, we have from (4.44)

$$c_m = \begin{cases} \dfrac{j4\pi\omega\mu_0 I_0}{\sin(k_0\Delta)} \sin[k_0(\Delta - |x_s - x_m|)], & \text{for} \quad |x_s - x_m| \le \Delta \\ 0, & \text{for} \quad |x_s - x_m| > \Delta \end{cases} \tag{4.45}$$

In exciting the slot by a strip-line, one may include the finite width $2d$ of the line by taking a step function model for the current distribution, namely

$$J_y^a(x) = \begin{cases} \dfrac{I_0}{2d}, & \text{for} \quad |x - x_s| \le d \\ 0, & \text{for} \quad |x - x_s| > d \end{cases} \tag{4.46}$$

which for $d \to 0$ reduces to the δ function model. However, a wide strip-line would perturb the radiated field and for actual excitations the width should be kept to a minimum. The above model may also be used for the case of feeding by a probe to take into account its finite radius r_0 by substituting $d = 2\, r_0$.

4.4- Voltage distribution and input impedance

The voltage distribution along the slot is given by

$$V(x) = -\int_{y_c - w}^{y_c + w} E_y^a(x, y)\, dy \tag{4.47}$$

From (4.17)-(4.19) it is easy to show that

$$V(x) \simeq \sum_{n=1}^{N} V_n\, X_n(x) \tag{4.48}$$

where $X_n(x)$ are given by (4.30) and for which a typical set is shown in Fig. 2.5c. The value of k in (4.30) does not affect the behavior of $X_n(x)$ and only changes its slope. It is important to note that the voltage distribution in (4.48) has riples in the intervals (x_i, x_{i+1}), $i = 1, 2, \cdots, N-1$ and does not represent the correct value of the voltage at the points in these intervals. However, at the points x_j, $j = 1, 2, \cdots, N$ which correspond to the maxima of $X_j(x)$, only one of the two overlapping basis functions contributes to the value of the voltage. Thus the complex values of V_n obtained from (4.43) give the actual amplitude and phase of the voltage at points x_j. This data can then be used to find the voltage at other points along the slot by interpolation.

In calculating the voltage distribution along the slot we assumed the excitation was through a uniform current distribution of a total current I_0 set up by the generator. To study the circuit parameters, one may replace the antenna structure by an equivalent impedance given by $Z = V(x_s) / I_0$ where $V(x_s)$ is the voltage across the feed point (see Fig. 4.3b). Thus for $I_0 = 1\ Amp$, the value of $V(x_s)$ in volts directly determines the input impedance of the antenna in Ohms.

4.5- Bandwidth

For a CBS antenna the bandwidth is rather limited in general due to the resonant behavior of its structure. However, for the case of rectangular CBS a number of parameters such as cavity width and depth, slot width and material in the cavity have considerable

effect on the bandwidth as will be shown in Sec. 4.7 and therefore it is possible to maximize the bandwidth while maintaining an acceptable radiation resistance and efficiency.

To achieve a wide bandwidth, in addition to the proper choice of physical dimensions, there are special feed configurations that have proven useful. One such method is exciting the cavity by a T-bar feed. In an experimental parametric study by Newman and Thiele [54], T-bars of cylindrical and thin rectangular cross section were used as the feed leading to noticeable improvement in the bandwidth of the antenna. In another experimental study Crews and Thiele [55] optimized the shape, size and position of a flat T-bar and achieved a *VSWR* less than 2:1 over the frequency range 500-2000 *MHz*, although at some frequencies they had to use tuning stubs to maintain the gain. Figures 4.4 and 4.5 show the T-bar feed of cylindrical cross-section and optimized shape of the flat T-bar feed, respectively. For the case where the CBS is excited by a microstrip line, attachment of a monopole to the strip-line at the point where it crosses the slot is another method that has been used to obtain a broad-band operation [56]. The concept in developing this configuration, which is shown in Fig. 4.6, has been to combine on the same feed line two radiating structures with impedances which have dual properties when normalized to the feed-line impedance. While the above techniques are applicable to single antenna elements, it is always possible to obtain a wider bandwidth by using the narrow-band elements in a log-periodic array. Roederer [57] has tested such an array and reported *VSWR* below 2.5:1 over the 2.8-5.9 *GHz* frequency range.

4.6- Resonant modes

In the preceding calculations we implicitly assumed that frequency of the excitation source is different from the natural resonance frequencies of the cavity and thus $k \neq k_v$, with k_v for the rectangular cavity given by

$$k_v = \left[(p\pi/a)^2 + (q\pi/b)^2 + (l\pi/c)^2 \right]^{1/2} \tag{4.49}$$

From (4.13) it is clear that when $k = k_v$ the dyadic Green's function and therefore the field

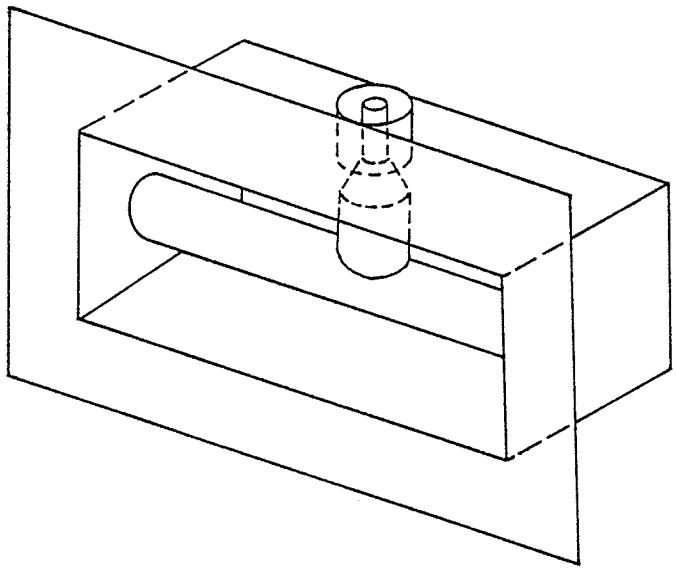

Fig. 4.4- CBS antenna fed by a T-bar of cylindrical cross-section.

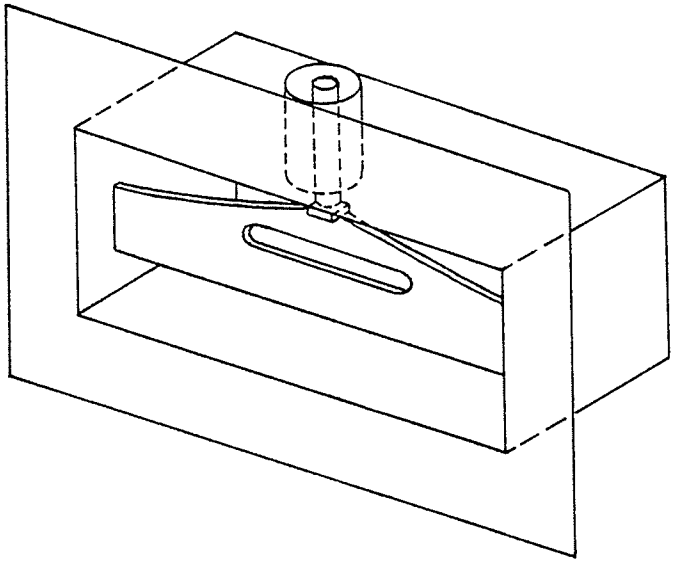

Fig. 4.5- The optimized shape of the flat T-bar feed.

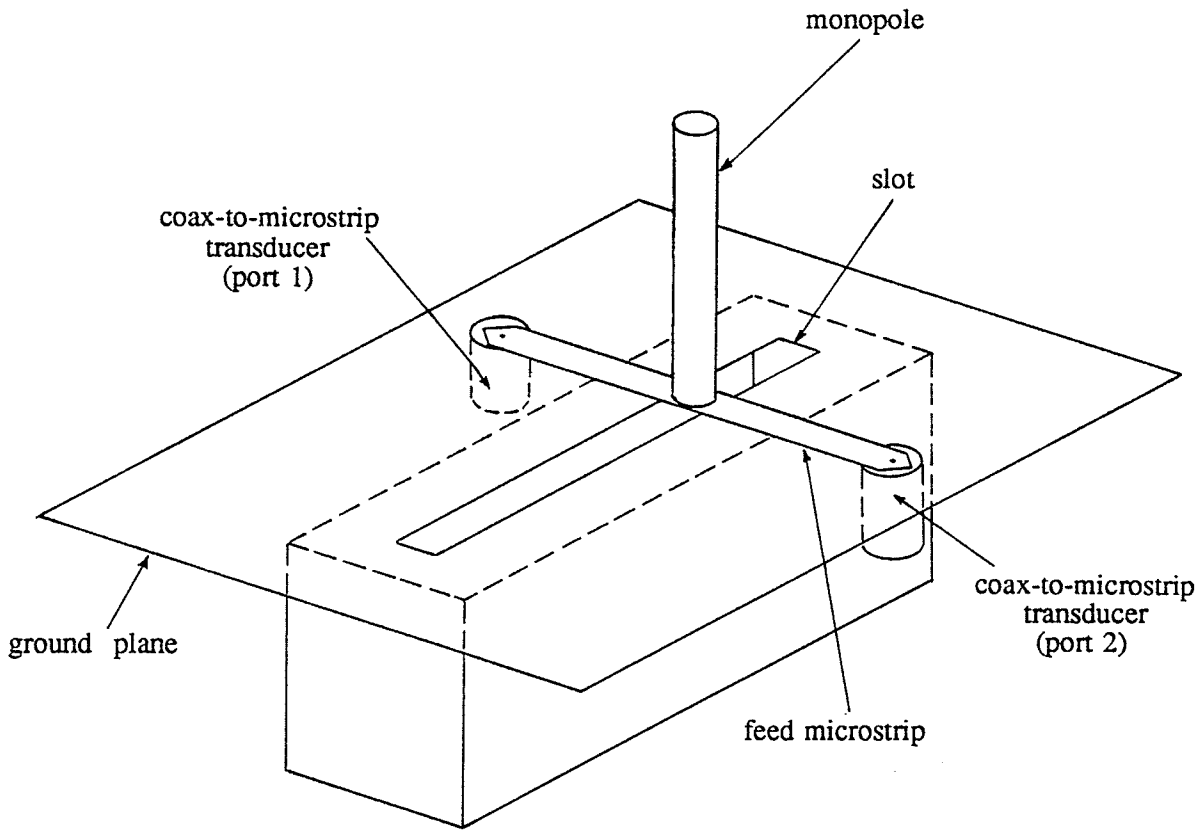

Fig. 4.6- Feed configuration for increasing the bandwidth of a CBS antenna.

amplitude tend to infinity. However, in the physical reality the field amplitude is limited due to the losses in the structure and thus for such a case one cannot ignore the finite conductivity of the cavity walls, whatever small it might be.

It is well-known that for a rectangular cavity the eigenvalues of the TE and TM modes are equal and hence the resonance of these modes occurs concurrently at the same frequency. To calculate the contribution of these resonant modes to the total field, we assumed in Sec. 3.3 that the resonant modes are dominant and derived the corresponding magnetic-type dyadic Green's function at resonance $\overleftrightarrow{G}_m^r$ which is given by (3.69). Of course the contribution from the non-resonant modes can be calculated in the usual way after removing the resonant term from (4.13). The magnetic field in the cavity region due to the resonant modes can be obtained in general from (4.4) by replacing $\overleftrightarrow{G}_m$ with the appropriate dyadic Green's function at resonance. In the following calculations we will need only the xx component of this function which from (3.69) and for $z = z' = 0$ is given by

$$G_{xx}^{mr} = C_r \sin(k_p x') \cos(k_q y') \sin(k_p x) \cos(k_q y) \tag{4.50}$$

where

$$C_r = \frac{j(I_1 k_v^2 k_q^2 + 2 I k_v k_p k_q k_l + I_2 k_p^2 k_l^2)}{\omega \varepsilon k_v^2 Z_s (I^2 - I_1 I_2)} \tag{4.51}$$

and

$$k_p = \frac{p\pi}{a}, \quad k_q = \frac{q\pi}{b}, \quad k_l = \frac{l\pi}{c}, \quad p, q, l = 1, 2, \cdots$$

In (4.51) Z_s is the surface impedance of the cavity wall given by

$$Z_s = \sqrt{\frac{\omega\mu_0}{2\sigma}}(1 + j) \tag{4.52}$$

and the quantities I, I_1 and I_2 are defined by (3.62) to (3.64). For the rectangular CBS problem considered in this Chapter we have

$$I = \frac{k_p k_q k_l}{2\, k_v} \left[(b-a)c + 4(BL - Aw) \right] \tag{4.53}$$

$$I_1 = \frac{1}{2k_v^2} \Big[k_{pq}^2\, k_l^2\, ab + (k_{pq}^4 + k_q^2\, k_l^2)\, bc + (k_{pq}^4 + k_p^2\, k_l^2)\, ac - \\ - 2\, k_p^2\, k_l^2\, (L-A)(w+B) - 2\, k_q^2\, k_l^2\, (L+A)(w-B) \Big] \tag{4.54}$$

$$I_2 = \frac{1}{2}k_{pq}^2 ab + \frac{1}{2}k_p^2 bc + \frac{1}{2}k_q^2 ac - k_p^2(L+A)(w-B) - k_q^2(L-A)(w+B) \tag{4.55}$$

where

$$k_{pq}^2 = k_p^2 + k_q^2 \tag{4.56}$$

$$A = \frac{1}{2k_p} \sin(2k_p L)\cos(2k_p x_c) \tag{4.57}$$

$$B = \frac{1}{2k_q} \sin(2k_q w)\cos(2k_q y_c) \tag{4.58}$$

Now we can calculate the contribution from the resonant modes to the electric field in the slot by solving the integral equation (4.10) with the kernel given by

$$F_{xx}(x', y' \mid x, y) = \frac{4\pi k^2}{\mu_r} G_{xx}^{m^r} + 2\,(k_0^2 + \frac{\partial^2}{\partial x^2}) G_0 \tag{4.59}$$

Doing so, the result for b_{mn} in (4.33) still holds and, with no volume current source inside the cavity, i.e. $\vec{J} = 0$ in (4.8), the source vector elements c_m do not change either. However for the resonant modes we have

$$a_{mn} = 4\pi k^2 C_r\; T_m(k_0)\; T_n(k)\; J_0(k_q w)\cos^2(k_q y_c) \tag{4.60}$$

where $T_m(k_0)$ is the same as $T_m(p)$ in (4.38) and $T_n(k)$ is defined similarly.

4.7- Numerical results

Before presenting the numerical results, it is worthwhile to mention a number of computational notes. The admittance matrix [y_{mn}] in (4.43) is composed of two parts, namely [a_{mn}] due to the cavity region and [b_{mn}] due to the half space, as indicated in (4.21).

The elements $a_{mn} = a(m, n)$ have the properties $a(m, n) = a(m-1, n-1)$ for $m, n = 2, 3, \cdots, N$ and also $a(m, n) = a(n, m)$. Thus, for $[\, a_{mn} \,]$ we need to evaluate only N elements of one row or column and the other entries of the matrix are just repetitions of these values. On the other hand the matrix $[\, b_{mn} \,]$ can be written as the sum of two matrices with elements b'_{mn} and b''_{mn}, where b'_{mn} have properties similar to a_{mn} while for b''_{mn} we have $b''(m, n) = b''(m-1, n+1)$, $m = 2, 3, \cdots, N$ and $n = 1, 2, \cdots, N-1$. Hence to find N^2 entries of $[\, b_{mn} \,]$ we only need to evaluate N elements of $[\, b'_{mn} \,]$ and $2N-1$ elements of $[\, b''_{mn} \,]$. The above considerations reduce the computation time for evaluating the matrix elements by a factor of $N^2/(3N-1)$. To ensure the convergence of the moment solution in the numerical computations, the slot is divided into 50 equal segments, although in many cases fewer segments were sufficient for this purpose. Also we have used 100 terms in each of the series in (4.37) while in most cases as low as 50 terms proved to give two digits of accuracy.

In a slot radiator, the voltage distribution along the slot is the most important quantity that is essential in determining both the radiation properties and circuit parameters of the antenna. The moment method used is able to provide an accurate solution to the integral equation for the voltage distribution. Obviously any of the numerous parameters of the CBS problem such as the cavity dimensions (a, b, and c), slot dimensions ($2L$ and $2w$), positions of the slot center (x_c and y_c) and the feed point (x_s or s), material in the cavity (μ_r and ε_r), etc. may affect the voltage distribution and therefore change the radiation pattern and more significantly the circuit quantities such as input impedance, resonance frequency and bandwidth of the antenna. However, we have to be selective in presenting the results and only those that seem to be more useful from the practical design point of view are given here. A typical rectangular CBS radiator excited by a delta current source with $a/\lambda = 0.7$, $b/\lambda = 0.2$, $c/\lambda = 0.3$, $2L/\lambda = 0.5$, $w/L = 0.04$, $x_c = a/2$, $y_c = b/2$, $s = L$ and operating at $f = 3\ GHz$ is used in most cases, while alterations to these values are mentioned explicitly.

Fig. 4.7 shows the amplitude and phase of the voltage distribution along a slot of length $2L/\lambda = 0.6$ for feed point locations $s/L = 0.2\ (1.0)\ 0.2$. The corresponding impedance values for each case are also given in Table 4.1. These results which should be compared with Fig. 2.8 and Table 2.1 for an open slot in Chapter 2, clearly show the important role of the parameter s on the slot voltage and input impedance. Fig. 4.8 compares the voltage distribution along slots of lengths $2L/\lambda = 0.5$, 0.6 and 0.7 and shows that the field is maximum for $2L = \lambda/2$, as expected. In these figures the dashed lines represent the phase variation along the slot.

Table 4.1

s/L	$R\ (\Omega)$	$X\ (\Omega)$
0.2	26.5	77.3
0.4	77.0	15.8
0.6	134.0	− 82.4
0.8	179.0	− 168.0
1.0	195.0	− 202.0

The methods available in the literature for analysis of the rectangular CBS antenna, namely the variational method [25] and the method using the complex Poynting theorem [27], are basically applied in calculating the input admittance. However, the assumption of sinusoidal voltage distribution in these methods is not accurate, especially at the excitation point where voltage determines the input admittance. Furthermore, a number of important parameters such as positions of the slot center and feed point do not appear in those formulations. With these points in mind, Fig. 4.9 compares the resistance R and reactance X versus frequency, obtained from various methods as well as experimental data [28] for a CBS with $a = 35\ cm$, $b = 10\ cm$, $c = 17.86\ cm$, $2L = 25\ cm$, $w/L = 0.04$, $x_c = a/2$, $y_c = b/2$ and $s = L$. This figure indicates that the results obtained from the moment method

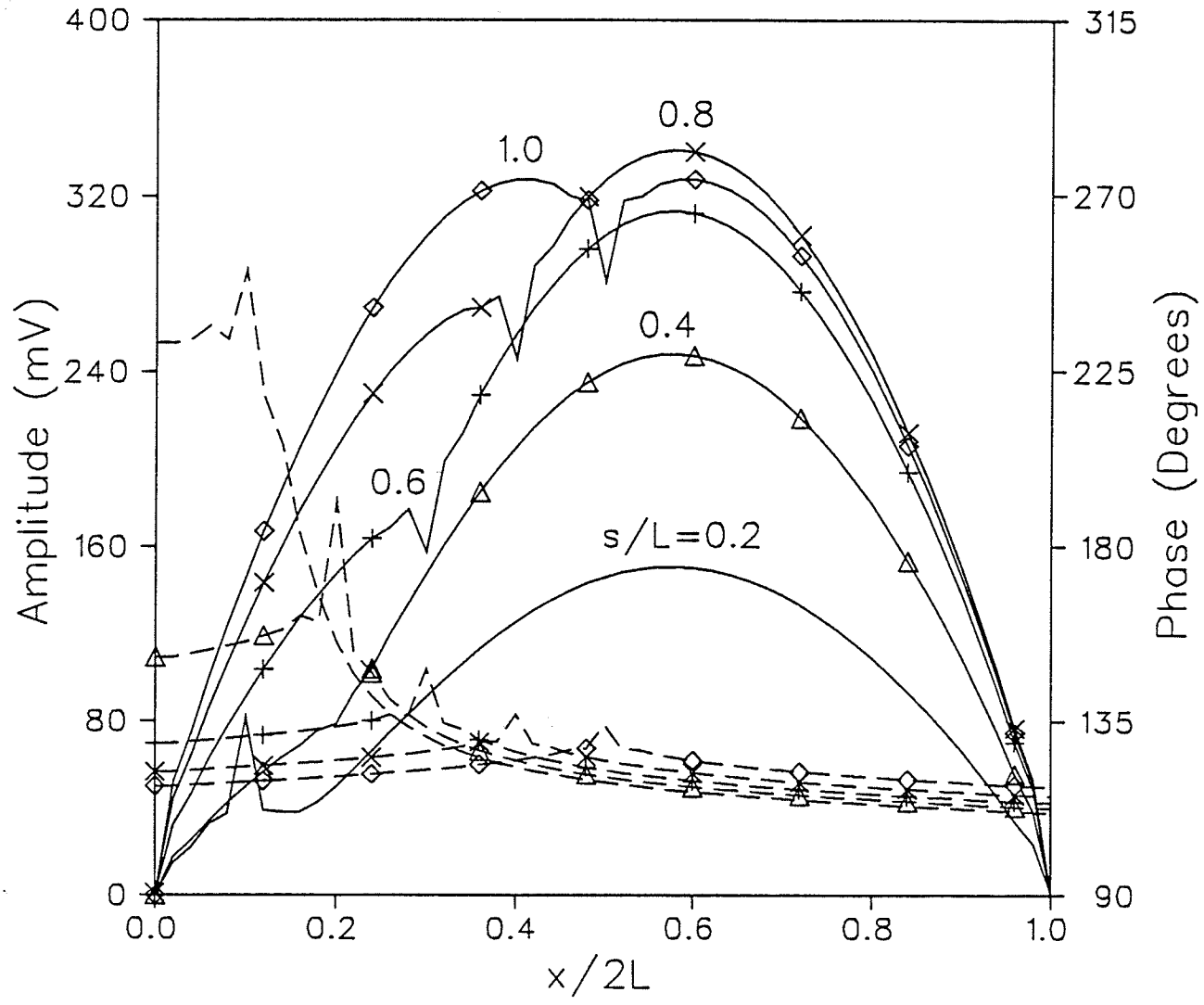

Fig. 4.7- Amplitude and phase (dashed lines) of voltage distribution along the slot of a CBS antenna with $2L/\lambda = 0.6$ and feed-point locations $s/L = 0.2$ (1.0) 0.2.

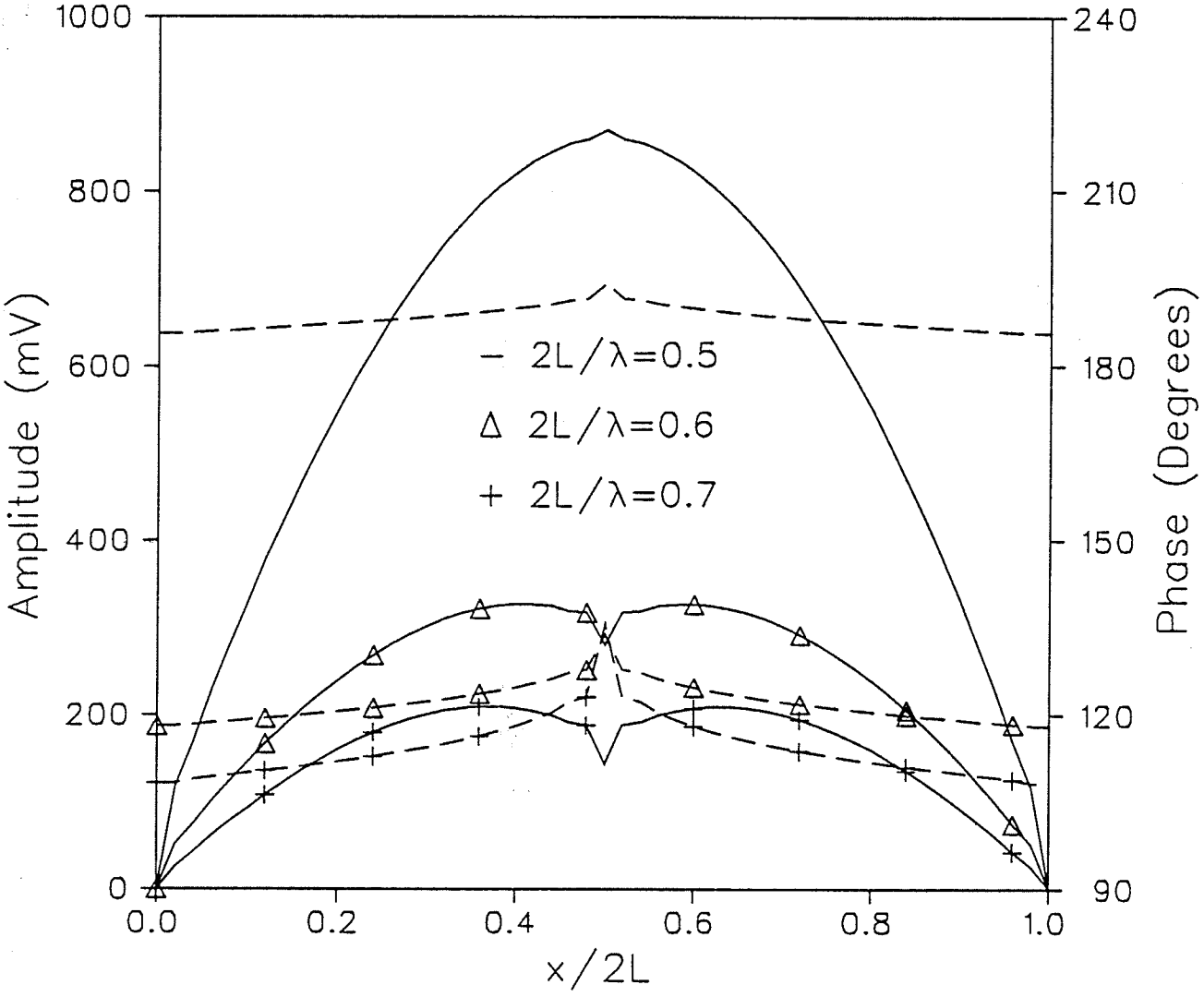

Fig. 4.8- Amplitude and phase (dashed lines) of voltage distribution along the slot of a CBS antenna with slot lengths $2L/\lambda$ = 0.5, 0.6 and 0.7.

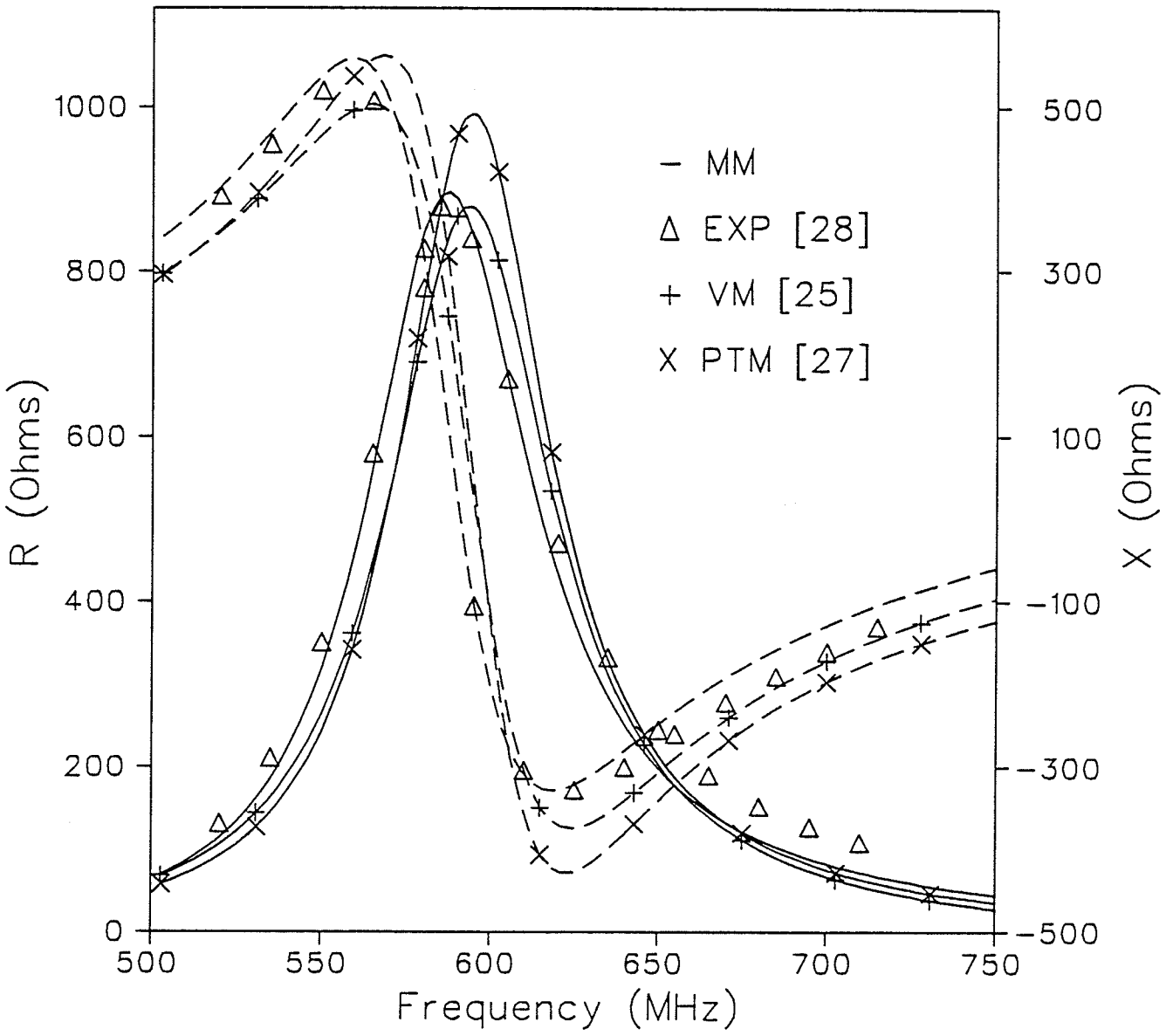

Fig. 4.9- Comparison of the resistance R and reactance X (dashed lines) versus frequency obtained from Moments Method (MM), Poynting Theorem Method (PTM), Variational Method (VM) and experimental measurements (EXP) for a CBS antenna.

are closer to experiment while the other two methods suffer a considerable shift in the resonance frequency defined by $X(f_r) = 0$. The discrepancy between our results and the experimental data is mainly due to the fact that in the experiments, the slot was cut in a finite conducting plane with a noticeable thickness of $1/4''$ and with finite conductivity, while in our formulation the slot is located in an infinite perfectly conducting ground plane of vanishing thickness.

Fig. 4.10 shows the resistance and reactance versus cavity depth for a CBS with $a/\lambda = 0.7$, $b/\lambda = 0.2$, $w/L = 0.04$, $x_c = a/2$, $y_c = b/2$, $s = L$ and slot lengths $2L/\lambda = 0.5$, 0.6, 0.7. In this and the rest of the figures, a dashed line is used to denote the reactance. The effect of cavity width on the impedance is shown in Fig. 4.11 which indicates that a larger b corresponds to a smaller resonant depth c_r defined as the cavity depth at which resonance occurs. Fig. 4.12 gives the impedance as a function of frequency for various cavity depths and shows that one should expect a wider bandwidth for a shallower cavity. In Fig. 4.13 we present the effect of the feed-point location on the values of resistance and reactance. This data is very useful for the purpose of matching the antenna to a generator and in this respect it corresponds to Fig. 2.10 for the case of an open slot. However, in comparing the results of this Chapter with those of Chapter 2, one should remember that in a CBS the number of physical dimensions that affect the circuit and radiation parameters of the antenna are far more than those of an open slot. Therefore any comparison between these two radiators (with similar excitation and slot size) has only a qualitative value to show the effect of the cavity backing on the open slot.

The slot position has some effects on the impedance which become more marked as the slot length increases. This is shown in Fig. 4.14 for a slot length $2L = 0.7\lambda$ and various vertical positions $y_c = w$, $b/4$ and $b/2$. Fig. 4.15 shows the voltage standing wave ratio as a function of frequency for different cavity depths. Such data may be used to obtain the bandwidth, defined as the range of frequencies over which the *VSWR* remains below 2:1.

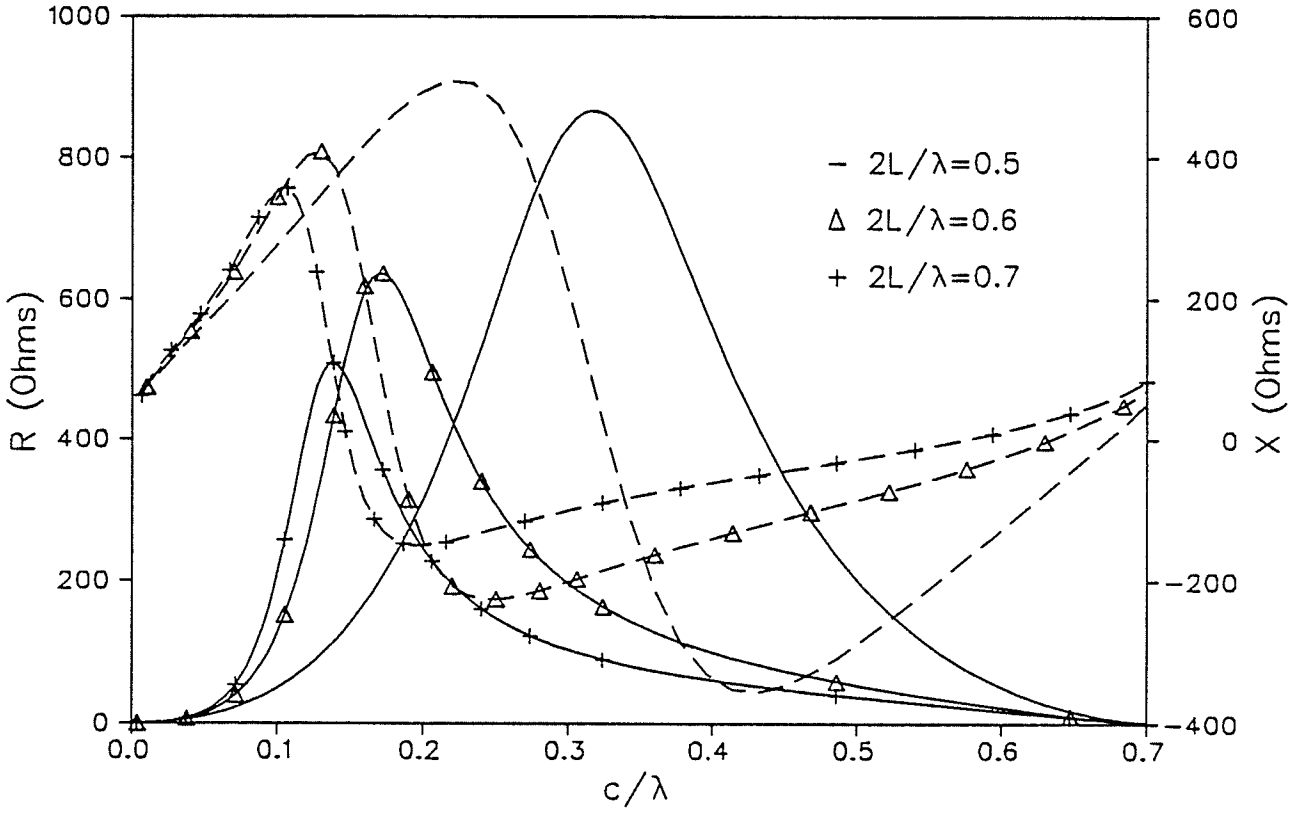

Fig. 4.10- Resistance R and reactance X (dashed lines) versus cavity depth c/λ for a CBS antenna with slot lengths $2L/\lambda = 0.5$, 0.6 and 0.7.

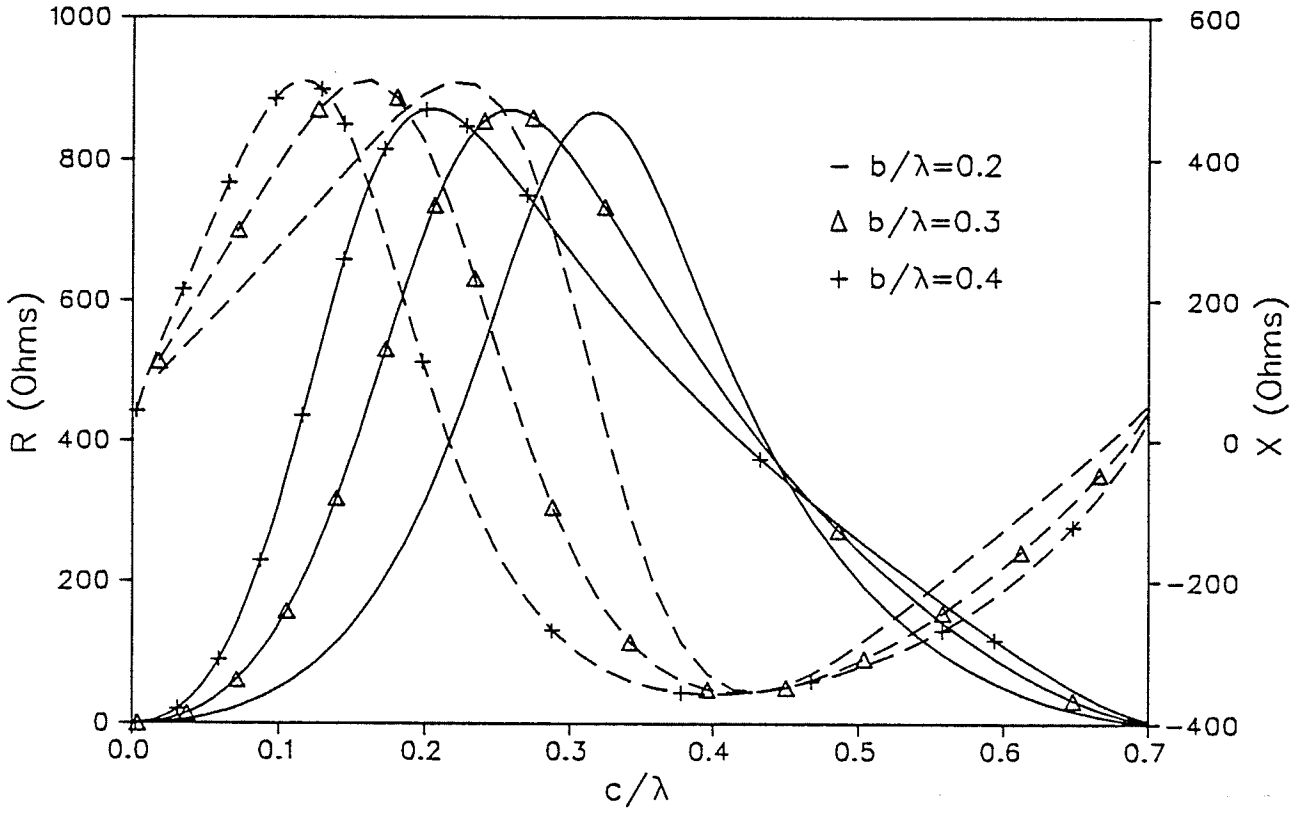

Fig. 4.11- Resistance R and reactance X (dashed lines) versus cavity depth c/λ for a CBS antenna with cavity widths b/λ = 0.2, 0.3 and 0.4.

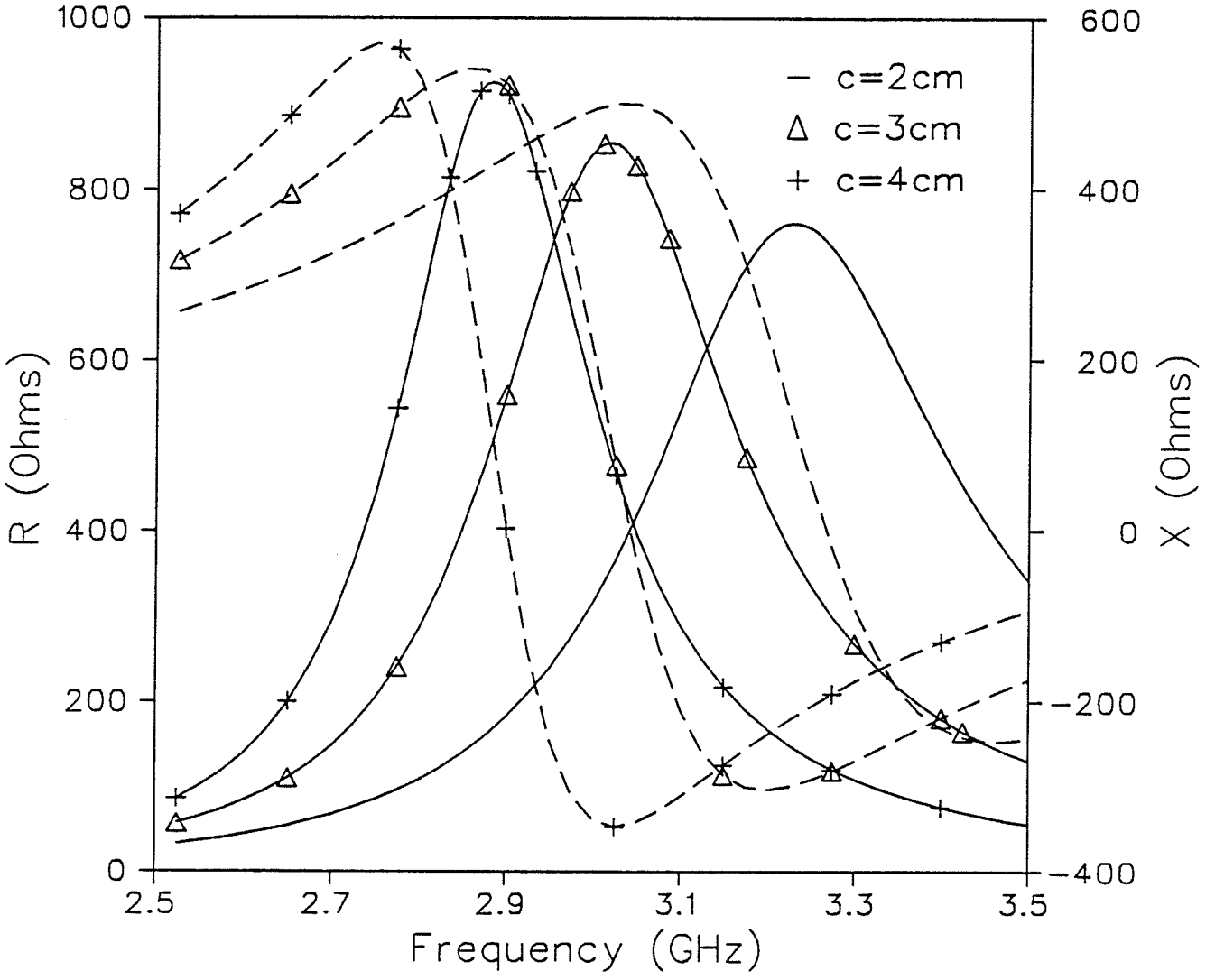

Fig. 4.12- Resistance R and reactance X (dashed lines) versus frequency for a CBS antenna with cavity depths $c = 2$, 3 and 4 cm.

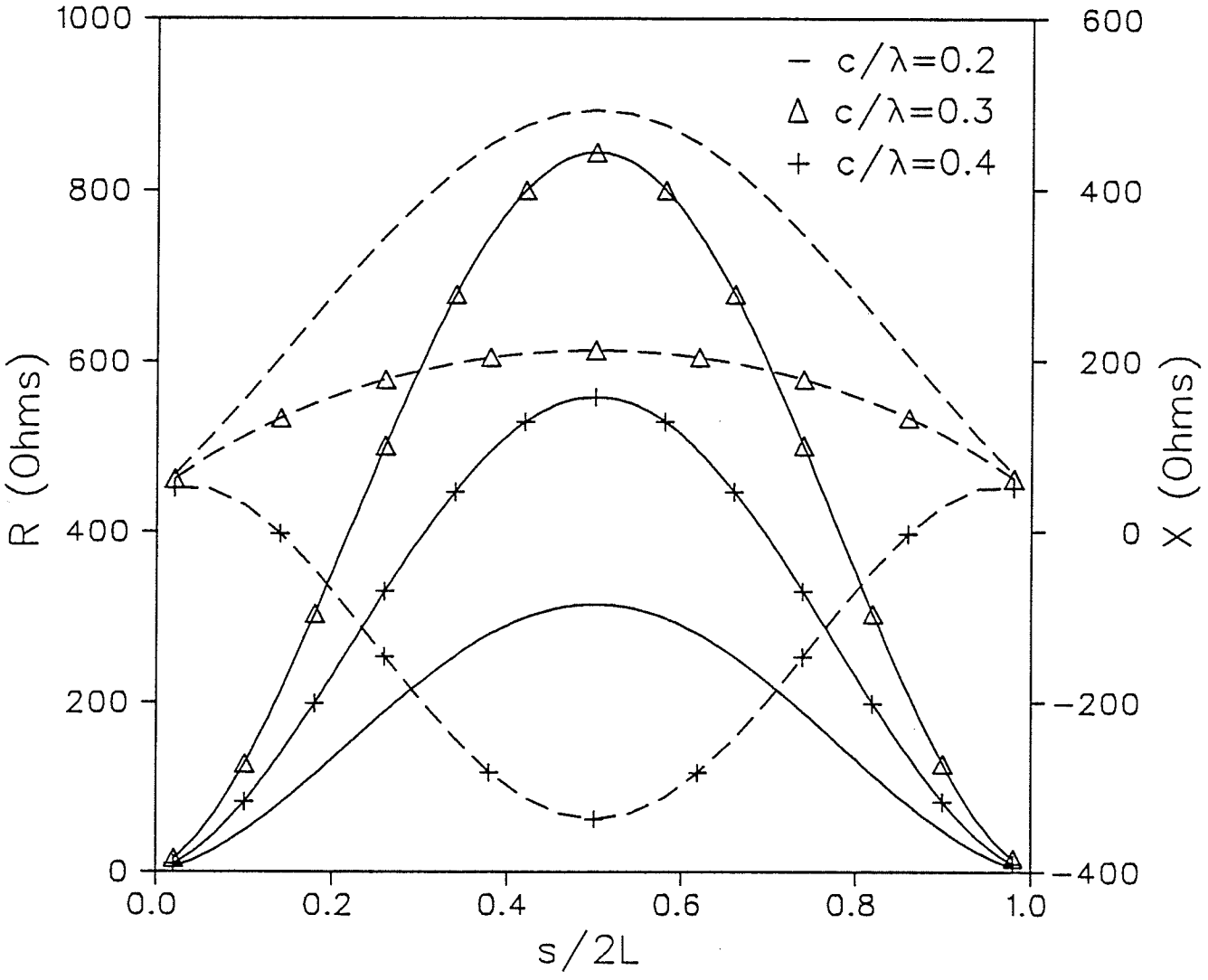

Fig. 4.13- Resistance R and reactance X (dashed lines) versus feed-point locations $s/2L$ for a CBS antenna with cavity depths c/λ = 0.2, 0.3 and 0.4.

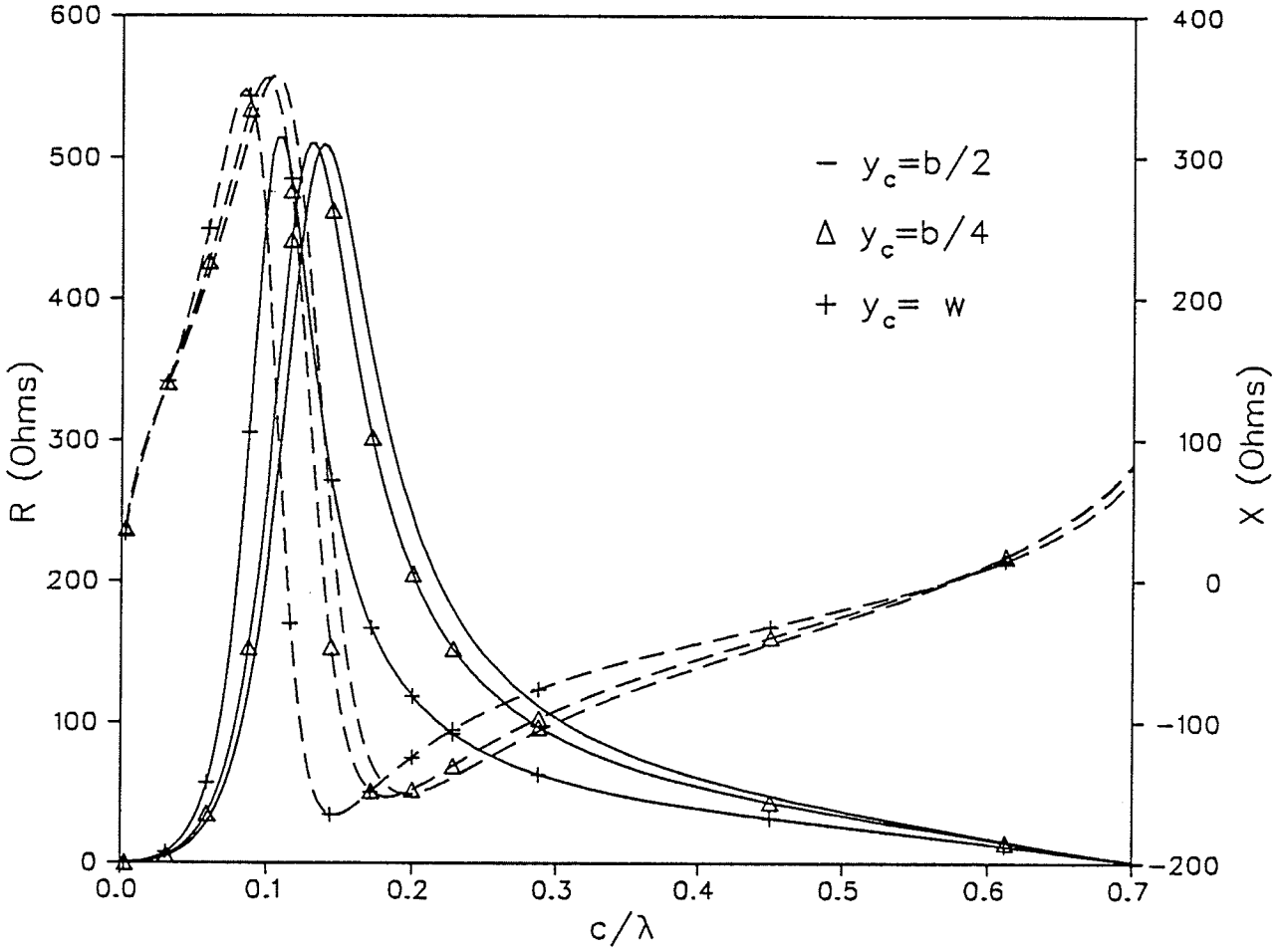

Fig. 4.14- Resistance R and reactance X (dashed lines) versus cavity depths c/λ for a CBS antenna with $2L/\lambda = 0.7$ and slot locations $y_c = w$, $b/4$ and $b/2$.

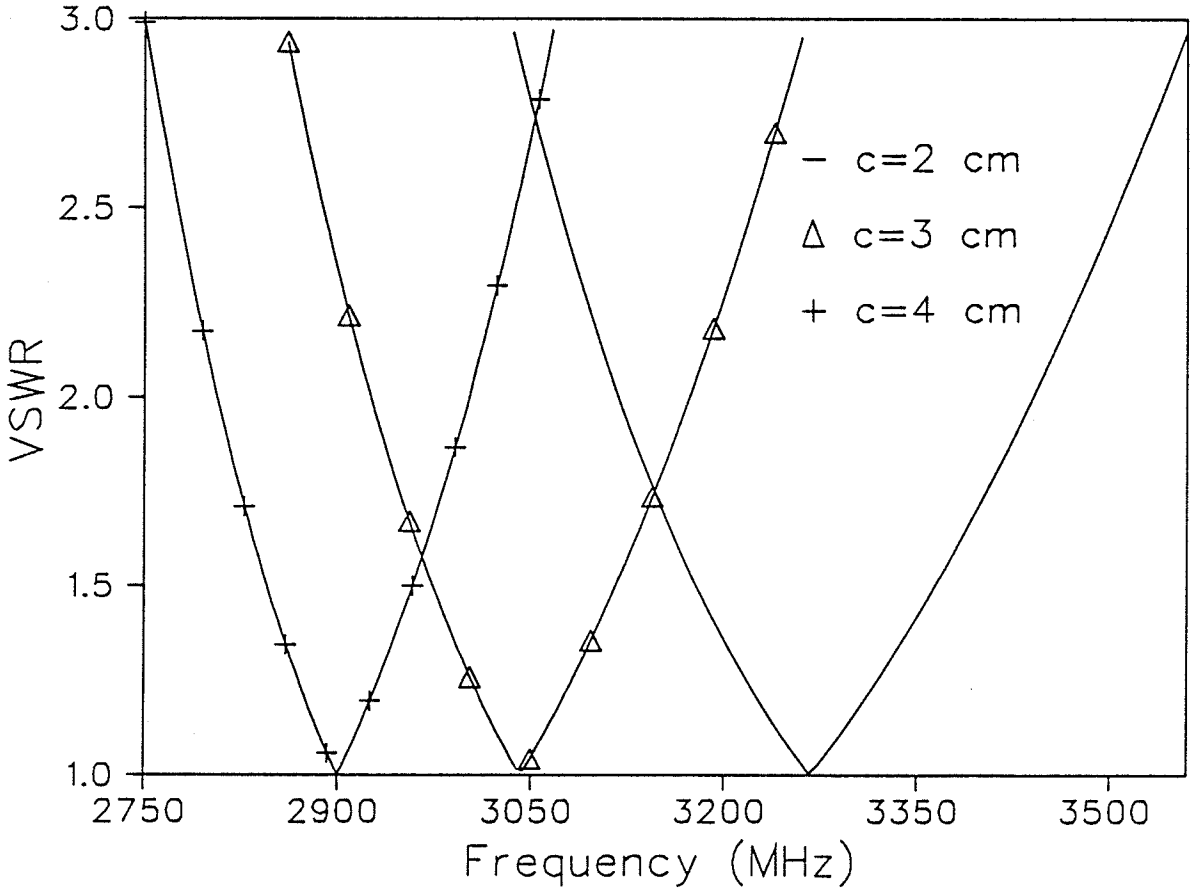

Fig. 4.15- *VSWR* vs frequency for a CBS antenna with cavity depths $c = 2$, 3 and 4 *cm*.

Tables 4.2 to 4.4 present typical numerical results for the resonance frequency f_r, bandwidth Δf as defined above, radiation resistance R_r and radiation quality factor $Q_r = f_r / \Delta f$. From Table 4.2 and Figs. 4.16 and 4.17 it is seen that for a fixed cavity width b, a smaller cavity depth results in higher resonance frequency and bandwidth but a lower R_r and Q_r. On the other hand for a fixed cavity depth it is possible to obtain higher f_r and Δf by decreasing b provided that the cavity depth is less than a certain value as shown in the figures. Table 4.3 contains data from an investigation of the effect of the slot width on the circuit parameters of the antenna. From this table and Fig. 4.19 it is observed that in general a wider slot results in a higher bandwidth especially for smaller cavity depths. However, the trade off is a lower radiation efficiency as evident from the values of R_r and Q_r. The slot width can have appreciable effect on the resonance frequency for very shallow cavities as shown in Fig. 4.18. From Table 4.4, the location of the feed-point appears to have little effect on the resonance frequency and bandwidth but can drastically change the radiation resistance. It is also seen that a change in the slot length may have noticeable effect on f_r but has a small effect on Δf; facts which held true for the corresponding case of an open slot as were shown in Figs. 2.13 and 2.15, respectively.

Finally for the case where the cavity is loaded by a dielectric material, the resistance and reactance versus frequency are shown in Fig. 4.20 for various dielectric constants $\varepsilon_r = 2, 3, 4$ and compared with the unloaded case. The resonance frequency, bandwidth and radiation resistance for each case are also given in Table 4.5. It is seen that dielectric loading in general has the effect of increasing the electrical dimensions of the unloaded antenna resulting in a lower resonance frequency. On the other hand the radiation resistance (and thus efficiency) is considerably enhanced by dielectric loading. These properties can be used to advantage to reduce the physical size of the antenna at lower frequency ranges or in applications where a high efficiency is required. However, these are achieved only at the expense of an immense drop in bandwidth.

Table 4.2

	$c\,(cm)$	$f_r\,(MHz)$	$\Delta f\,(MHz)$	$R_r\,(\Omega)$	Q_r
$b = 2\ cm$	1	3822	490	557	7.8
	2	3267	320	739	10.2
	3	3042	248	837	12.3
	4	2900	195	911	14.9
	5	2794	152	974	18.4
$b = 3\ cm$	1	3465	383	665	9.0
	2	3110	292	808	10.6
	3	2963	246	880	12.0
	4	2867	208	933	13.8
	5	2791	174	978	16.0
$b = 4\ cm$	1	3267	322	739	10.1
	2	3020	270	853	11.2
	3	2914	237	909	12.3
	4	2843	210	950	13.5
	5	2785	181	985	15.4

$a = 7\ cm$, $2L = 5\ cm$, $w/L = 0.04$, $s = L$ and $b = 2,\ 3,\ 4\ cm$

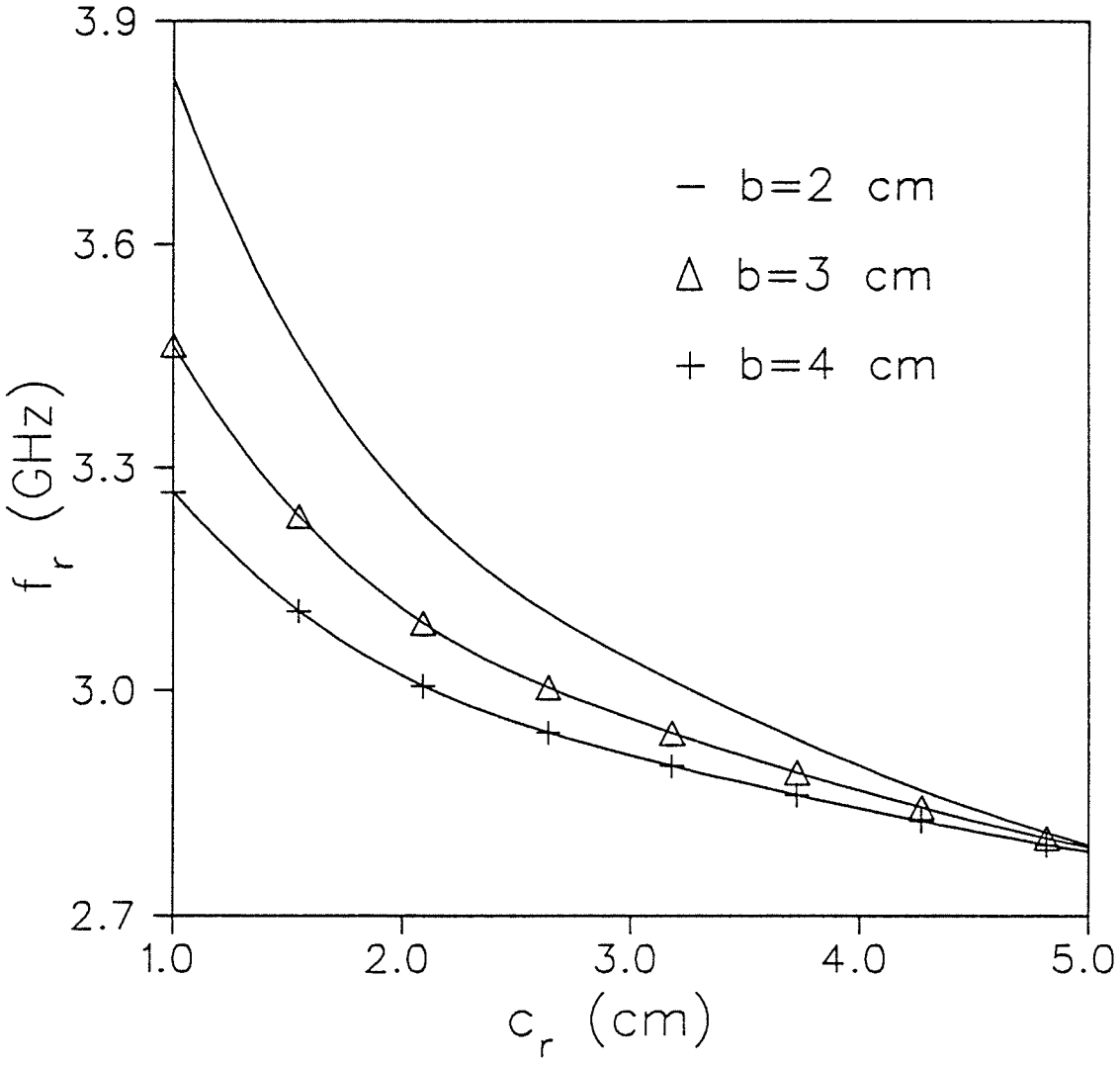

Fig. 4.16- Resonant depth c_r for a CBS antenna with cavity widths $b = 2$, 3 and 4 cm.

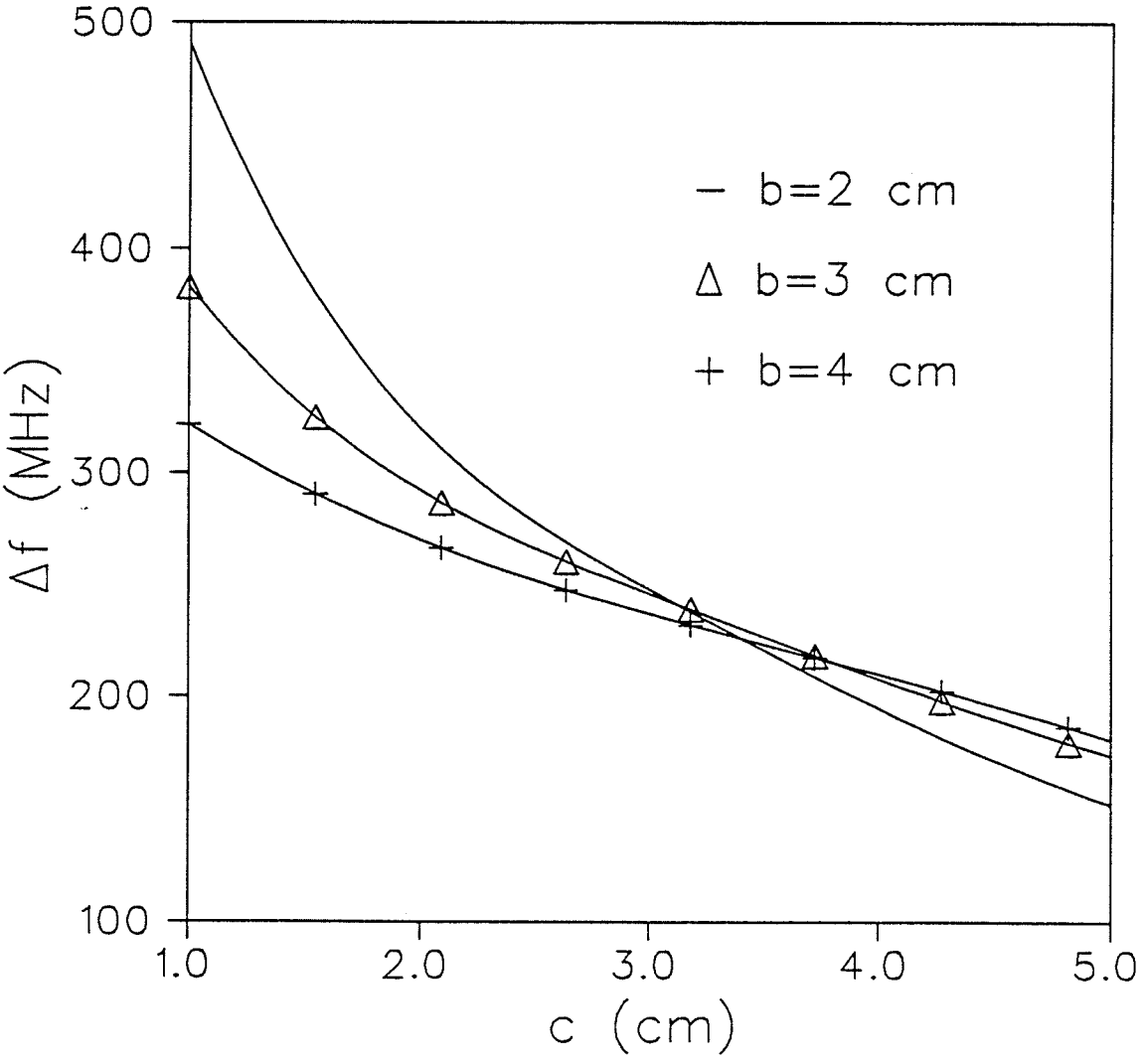

Fig. 4.17- Bandwidth Δf versus cavity depth c for a CBS antenna with cavity widths $b = 2$, 3 and 4 cm.

Table 4.3

	$c\,(cm)$	$f_r\,(MHz)$	$\Delta f\,(MHz)$	$R_r\,(\Omega)$	Q_r
$w/L = 0.02$	1	3647	350	629	10.4
	2	3213	252	786	12.7
	3	3032	204	868	14.9
	4	2914	166	931	17.5
	5	2821	132	984	21.4
$w/L = 0.04$	1	3822	490	557	7.8
	2	3267	320	739	10.2
	3	3042	248	837	12.3
	4	2900	195	911	14.9
	5	2794	152	974	18.4
$w/L = 0.06$	1	4019	661	475	6.1
	2	3324	390	692	8.5
	3	3055	285	806	10.7
	4	2894	218	889	13.3
	5	2778	167	956	16.6

$a = 7\ cm$, $b = 2\ cm$, $2L = 5\ cm$, $s = L$ and $w/L = 0.02, 0.04, 0.06$

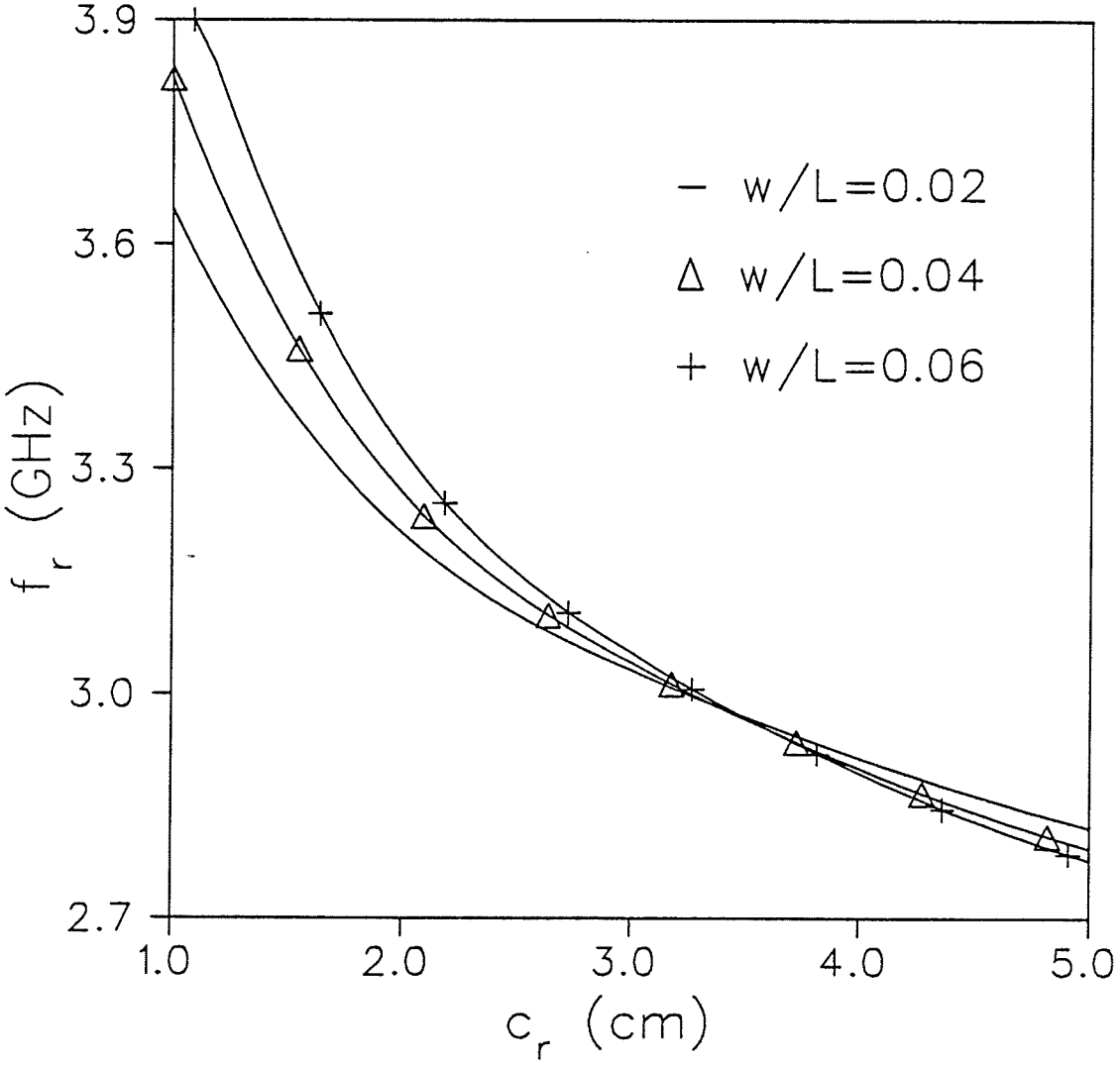

Fig. 4.18- Resonant depth c_r for a CBS with slot widths $w/L = 0.02$, 0.04 and 0.06.

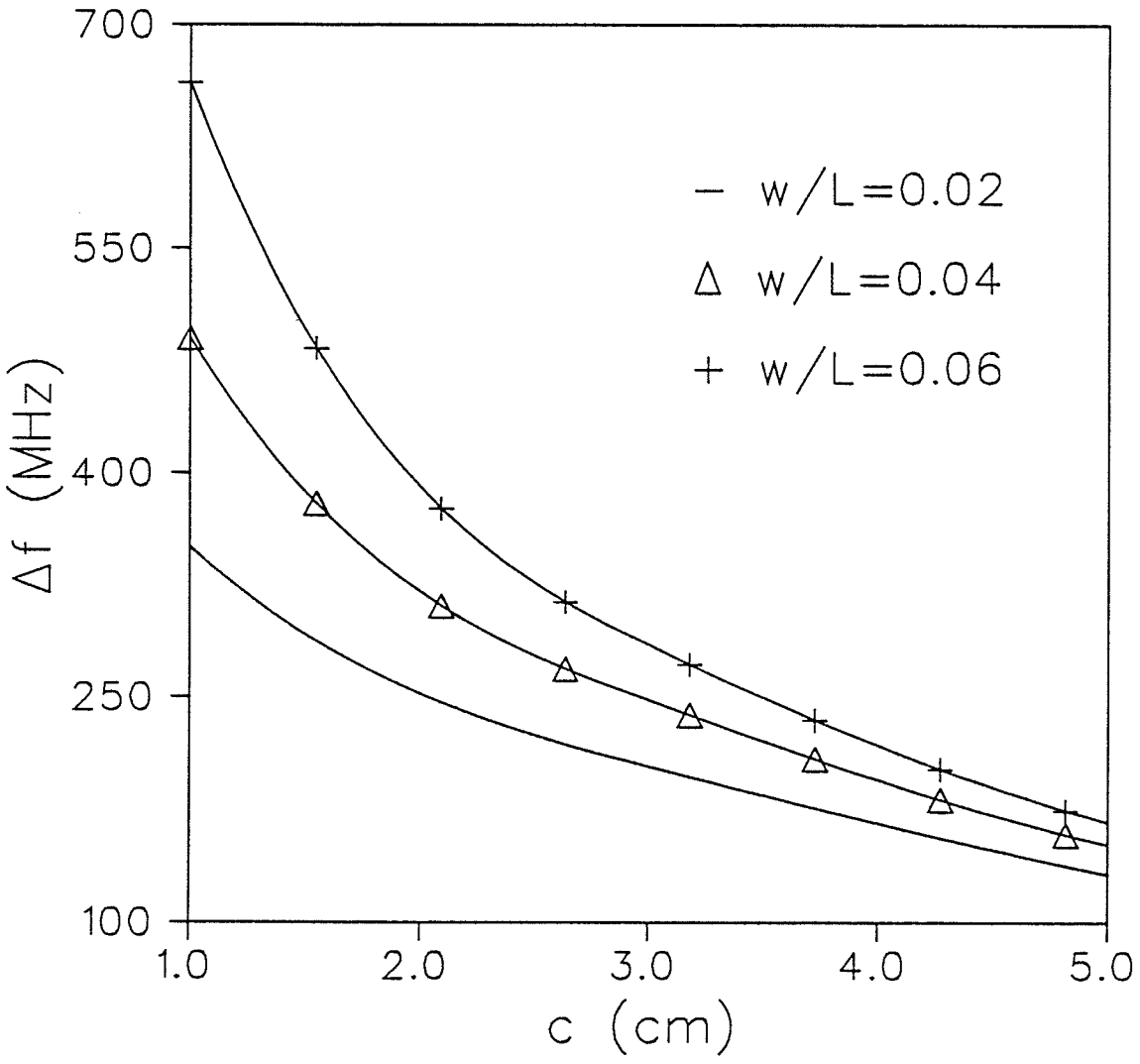

Fig. 4.19- Bandwidth Δf versus cavity depth c for a CBS antenna with normalized slot widths $w/L = 0.02$, 0.04 and 0.06.

Table 4.4

	s/L	$f_r\,(MHz)$	$\Delta f\,(MHz)$	$R_r\,(\Omega)$	Q_r
$2L = 5\ cm$	0.4	3177	312	276	10.2
	0.6	3128	299	546	10.5
	0.8	3114	294	738	10.6
	1.0	3110	292	808	10.6
$2L = 6\ cm$	0.4	2835	289	211	9.8
	0.6	2755	288	490	9.6
	0.8	2739	282	670	9.7
	1.0	2734	281	738	9.7
$2L = 7\ cm$	0.4	2623	301	146	8.7
	0.6	2552	293	425	8.7
	0.8	2529	283	607	8.9
	1.0	2524	281	673	9.0

$a = 7\ cm$, $b = 3\ cm$, $c = 2\ cm$, $w/L = 0.04$, and $2L = 5, 6, 7\ cm$

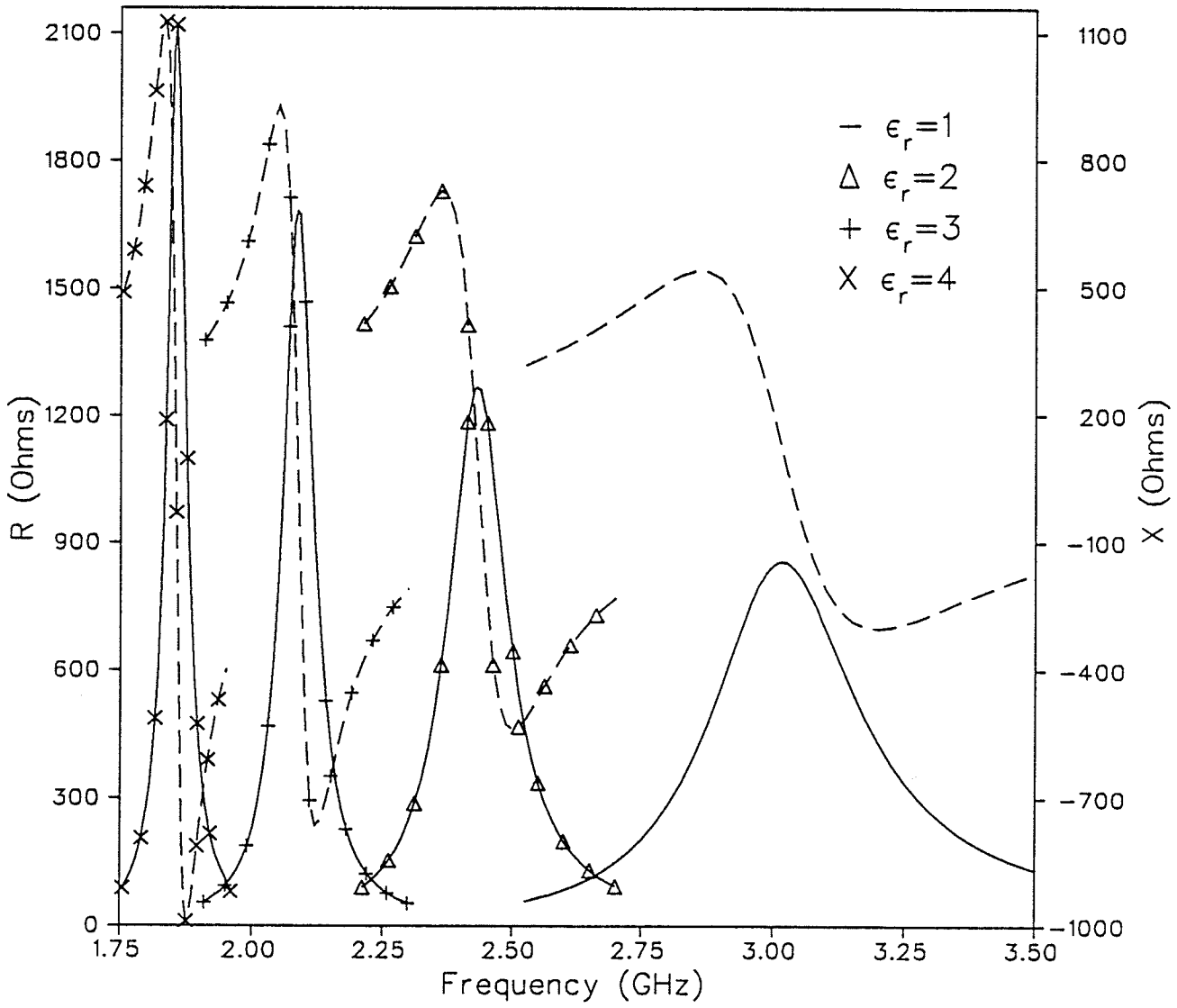

Fig. 4.20- Resistance R and reactance X (dashed lines) versus frequency for a dielectric loaded CBS antenna with dielectric constants ε_r = 2, 3 and 4.

Table 4.5

ε_r	$f_r\,(MHz)$	$\Delta f\,(MHz)$	$R_r\,(\Omega)$	Q_r
1	3042	248	837	12.3
2	2436	98	1264	24.9
3	2088	50	1692	41.8
4	1855	30	2120	61.8

$a = 7\ cm,\ b = 2\ cm,\ c = 3\ cm,\ 2L = 5\ cm,\ w/L = 0.04,\ s = L$

CHAPTER 5

PROBE EXCITATION OF RECTANGULAR CAVITY-BACKED SLOTS

In formulating the cavity-backed aperture problem in Chapter 4 we presented a general expression for the forcing function which included both a surface current distribution on the aperture and a volume current distribution in the cavity. This expression was then specialized to the case of a rectangular cavity-backed slot radiator fed by a current source on the slot aperture. In this Chapter we investigate the case of excitation by a coaxial-line probe inside the cavity. The voltage distribution along the narrow slot is obtained and used in calculating the input impedance of the antenna. The procedure for calculating the impedance is based on the Poynting theorem and requires that the effect of diffraction from the slot aperture be taken into account.

5.1- Voltage distribution in the slot aperture

The geometry of the rectangular cavity-backed slot fed by a coaxial-line probe is shown in Fig. 5.1a. The coaxial-line of outer radius r_1 is terminated at the $x-z$ plane. The inner conductor (probe) of radius $r_0 \ll \lambda$ with its center at the point $(x_0\ ,\ z_0)$ is parallel to the y axis and extends a distance d into the cavity. The integral equation for the voltage distribution along the slot in this problem is similar to the one derived in Sec. 4.2 except for the forcing function which is different. Thus in solving this equation by the method of moments, the matrix elements remain unchanged and only the source vector elements should be calculated accordingly.

The current distribution on a thin probe may be assumed to flow in the axial direction, namely $\vec{J}(\vec{r}) = J_y(\vec{r})\ \hat{y}$. Thus the forcing function in (4.8) reduces to

$$f(x, y) = -j\,4\pi\omega\mu_0 \int_V J_y(x', y', z') \left(\frac{\partial G_{xx}^m}{\partial z'} - \frac{\partial G_{zx}^m}{\partial x'}\right) dx'dy'dz', \qquad z = 0 \tag{5.1}$$

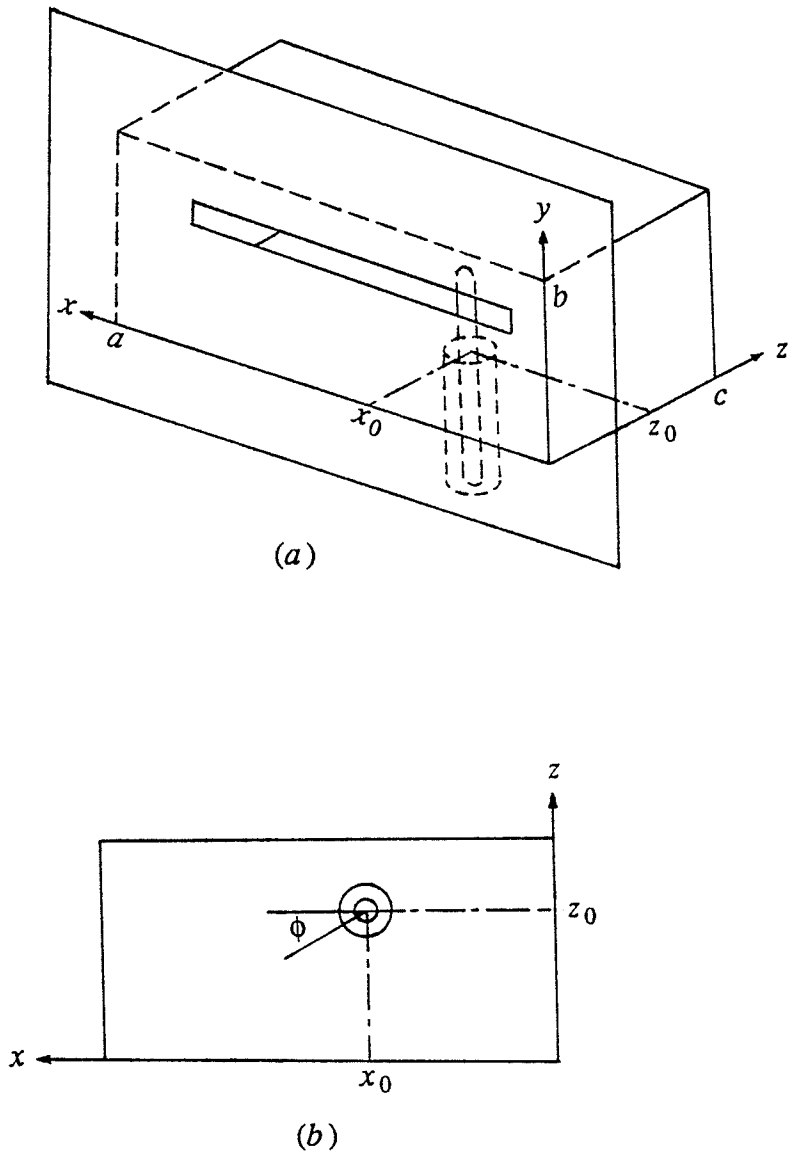

Fig. 5.1- Geometry of the probe-fed cavity-backed slot antenna (a) and the probe position in polar coordinates (b).

where with the assumption of a filamentary sinusoidal current distribution, J_y is given by

$$J_y(x, y, z) = \begin{cases} \dfrac{I_0}{\sin(kd)} \sin[k(d-y)]\ \delta(x-x_0)\ \delta(z-z_0)\ , & 0 \le y \le d \\ 0\ , & otherwise \end{cases} \tag{5.2}$$

The quantities G_{xx}^m and G_{zx}^m are components of the magnetic-type dyadic Green's function $\overleftrightarrow{G}_m$ $(z < z')$ and are given for a rectangular cavity by the expressions (see Appendix C)

$$G_{xx}^m = \sum_{p,q} C_{pq}(k_p^2 - k^2) \sin k_p x' \cos k_q y' \sin k_p x \cos k_q y \cos K_{pq}(c - z') \cos K_{pq} z \tag{5.3a}$$

$$G_{zx}^m = -\sum_{p,q} C_{pq} k_p K_{pq} \cos k_p x' \cos k_q y' \sin k_p x \cos k_q y \sin K_{pq}(c - z') \cos K_{pq} z \tag{5.3b}$$

with

$$C_{pq} = \varepsilon_p \varepsilon_q \left[abk^2 K_{pq} \sin(K_{pq} c) \right]^{-1/2} \tag{5.4}$$

Substituting (5.2) and (5.3) into (5.1) yields,

$$f(x, y) = \frac{j16\pi k \omega\mu_0 I_0}{ab \sin(kd)} \sum_{p=1}^{\infty} \sum_{q=0}^{\infty} \frac{\varepsilon_q \sin(k_p x_0) \sin[K_{pq}(c - z_0)]}{(k_q^2 - k^2) \sin(K_{pq} c)}$$

$$\sin[(k_q - k)\frac{d}{2}] \sin[(k_q + k)\frac{d}{2}] \sin(k_p x) \cos(k_q y) \tag{5.5}$$

On the other hand, from (4.44) the source vector elements are given by

$$c_m = \int_{x_c - L}^{x_c + L} S_m(x) f(x, y_c)\, dx \tag{5.6}$$

where (x_c, y_c) is the coordinate of the slot center and $S_m(x)$ are the piecewise sinusoidal testing functions defined by (4.31). Thus

$$c_m = C_0 \sum_{p=1}^{\infty} G(p) \sin(k_p x_m) \tag{5.7a}$$

where

$$C_0 = \frac{j64\pi\omega\mu_0 I_0 k k_0}{ab\sin(k_0\Delta)\sin(kd)} \tag{5.7b}$$

$$G(p) = A(p) \sum_{q=0}^{\infty} \varepsilon_q B(q) \frac{sin[K_{pq}(c - z_0)]}{\sin(K_{pq} c)} \tag{5.7c}$$

$$A(p) = \frac{\sin(k_p x_0)}{(k_p^2 - k_0^2)} \sin[(k_p - k_0)\frac{\Delta}{2}] \sin[(k_p + k_0)\frac{\Delta}{2}] \tag{5.7d}$$

$$B(q) = \frac{\cos(k_q y_c)}{(k_q^2 - k^2)} \sin[(k_q - k)\frac{d}{2}] sin[(k_q + k)\frac{d}{2}] \tag{5.7e}$$

$$K_{pq} = [k^2 - k_p^2 - k_q^2]^{1/2} \tag{5.7f}$$

Upon calculating the source vector elements in (5.7), the voltage distribution along the slot can be obtained from (4.48) and (4.43).

5.2- Electric field in the cavity

The electric field produced by electric and magnetic current sources in a bounded region of arbitrary shape was derived in Chapter 3 and given by (3.19). From this equation and for $\vec{M} = 0$, we have

$$\vec{E}(x, y, z) = -j\omega\mu \int_V \vec{J}(\vec{r}') \cdot \overleftrightarrow{G}_e(\vec{r}' \mid \vec{r})\, dv' - \int_A \hat{n} \times \vec{E}^a(\vec{r}') \cdot \nabla' \times \overleftrightarrow{G}_e(\vec{r}' \mid \vec{r})\, ds' \tag{5.8}$$

where $\vec{J}(\vec{r})$ is the excitation source in the form of a volume electric current density and $\overleftrightarrow{G}_e$ is the electric-type dyadic Green's function of an enclosure with perfectly conducting walls given by (3.42). The volume integral in (5.8) is due to the field in the cavity with no apertures, while the surface integral can be considered as the contribution of the field diffracted by the apertures in the cavity wall.

For the specified orientation of the feeding probe, the longitudinal component of the electric field in the slot $E_x^a(x, y)$ is negligible in comparison with the transverse component $E_y^a(x, y)$. On the other hand, in calculating the input impedance we only need the y component of the electric field in the cavity as will be shown in the next section. Thus from

(5.8) we have,

$$E_y(x, y, z) = -j\omega\mu \int_V J_y(\vec{r}') \, G^e_{yy}(\vec{r}' \mid \vec{r}) \, dv'$$

$$- \int_A E^a_y(x', y') \left(\frac{\partial G^e_{zy}}{\partial y'} - \frac{\partial G^e_{yy}}{\partial z'}\right)_{z'=0} dx' \, dy' \qquad (5.9)$$

where G^e_{yy} and G^e_{zy} are components of $\overleftrightarrow{G}_e$ $(z > z')$ given by (see Appendix C)

$$G^e_{yy} = -\sum_{p,q} C_{pq}(k_q^2 - k^2) \sin k_p x' \cos k_q y' \sin k_p x \cos k_q y \sin K_{pq} z' \sin K_{pq}(c - z) \qquad (5.10a)$$

$$G^e_{zy} = -\sum_{p,q} C_{pq} k_q K_{pq} \sin k_p x' \sin k_q y' \sin k_p x \cos k_q y \cos K_{pq} z' \sin K_{pq}(c - z) \qquad (5.10b)$$

Substituting (5.2) and (5.10) into (5.9), we obtain the y component of the electric field in the cavity as the sum of two terms, namely

$$E_y(\vec{r}) = E^c_y(\vec{r}) + E^d_y(\vec{r}) \qquad (5.11)$$

where E^c_y is the field in the closed cavity with no apertures and E^d_y is the field diffracted by the slot aperture. The expressions for these fields are given by

$$E^c_y(x, y, z) = \frac{j4\omega\mu I_0}{abk \sin(kd)} \sum_{p=1}^{\infty} \sum_{q=0}^{\infty} \frac{\varepsilon_q \sin(k_p x_0)}{K_{pq} \sin(K_{pq} c)}$$

$$\sin\left[(k_q - k)\frac{d}{2}\right] \sin\left[(k_q + k)\frac{d}{2}\right] \sin(k_p x) \cos(k_q y) \, h_{pq}(z, z_0) \qquad (5.12)$$

where

$$h_{pq}(z, z_0) = \begin{cases} \sin[K_{pq}(c - z_0)] \sin(K_{pq} z), & z < z_0 \\ \sin(K_{pq} z_0) \sin[K_{pq}(c - z)], & z > z_0 \end{cases} \qquad (5.13)$$

and

$$E^d_y(x, y, z) = \frac{2}{ab} \sum_{p=1}^{\infty} \sum_{q=0}^{\infty} \frac{\varepsilon_q \, I(p)}{\sin(K_{pq} c)} J_0(k_q w)$$

$$\cos(k_q y_c) \sin(k_p x) \cos(k_q y) \sin[K_{pq}(c - z)] \qquad (5.14)$$

where

$$I(p) = \int_{x_c - L}^{x_c + L} X(x') \sin(k_p x')\, dx' \tag{5.15}$$

In deriving (5.14) we have used the usual expression for the electric field in the slot aperture given by (4.17) and (4.18) with

$$X(x) = \sum_{l=1}^{N} V_l\, X_l(x) \tag{5.16}$$

where the expansion coefficients V_l should be obtained from Sec. 5.1 by using the piecewise sinusoidal functions for $X_l(x)$. Note that due to the piecewise nature of these functions, the values of $X(x)$ in (5.16) are correct only at the points x_j, $j = 1, 2, \cdots, N$ and one should resort to interpolation to obtain values of the function at other points before attempting the numerical evaluation of the integral in (5.15). However, an alternative and simple approximation is to assume that the function is constant in each interval as it would be for the case of a rectangular pulse expansion, i.e.

$$X_l(x) = \begin{cases} 1, & \text{for} \quad |x - x_l| \le \dfrac{\Delta}{2} \\ 0, & \text{for} \quad |x - x_l| > \dfrac{\Delta}{2} \end{cases} \tag{5.17}$$

Thus, the integral in (5.15) reduces to

$$I(p) = \frac{2}{k_p} \sin(k_p \frac{\Delta}{2}) \sum_{l=1}^{N} V_l \sin(k_p x_l) \tag{5.18}$$

where $x_l = x_c - L + l\Delta$, $l = 1, 2, \cdots, N$ and $\Delta = 2L/(N+1)$.

5.3- Calculation of the input impedance

For the case where the slot is fed by a current source on the aperture, the input impedance can be obtained directly from a knowledge of the voltage distribution along the slot aperture as was discussed in Chapter 4. However, when the structure is excited by a probe inside the cavity, though still requiring the voltage distribution in the slot, the calculation of the input impedance is much more involved. For a small coaxial-line opening, one

may to a first approximation assume that the higher-order coaxial-line modes are negligible. The fields in the opening will then be those associated with the incident and reflected *TEM* modes in the coaxial line. If both the total voltage V and the total probe current at the aperture plane I_0 were known, there would be no difficulty in determining the input impedance and the fields in the feed opening are given by

$$\vec{E}_0 = \frac{V}{r \ln \frac{r_1}{r_0}} \hat{\rho}, \qquad \vec{H}_0 = \frac{-I_0}{2\pi r} \hat{\theta}$$

However, assuming I_0 is given, the total voltage wave V is in general unknown. It is possible to use the equivalence principle and consider the effect of the coaxial-line by means of an equivalent electric current density on the feed opening. This current which is related to the electric field in the cavity through an integral relation can then be taken as the primary source of the fields. The induced electric current on the conducting probe as well as the voltage distribution along the narrow slot are the unknown quantities for which one can obtain two coupled integral equations by satisfying the appropriate boundary conditions, namely zero tangential electric field on the probe and continuity of the tangential magnetic field in the slot aperture. To simplify the calculations, we assume a known sinusoidal current distribution on the probe. Note that the assumption of an infinitesimally thin probe which was used to calculate the aperture field in Sec. 5.1 results in an infinite value for the input reactance and therefore one should take into account the finite thickness of the probe in the impedance calculation.

We use the Poynting theorem to calculate the input impedance. The opening of the coaxial-line probe provides the power flow into the cavity region such that integration of the complex Poynting vector over the opening area yields

$$P = \frac{1}{2} Z_{in} I_0^2 \tag{5.19}$$

which is equal to

$$P = P_s + 2j\omega\,(W_m - W_e)$$

In this equation P_s is the radiated power from the slot aperture (assuming no metal and dielectric losses) and the imaginary part is the time-average net reactive energy in the cavity. On the other hand, with the assumption of small coaxial-line opening, we have

$$P = -\frac{1}{2}\int_S \vec{E}(\vec{r}) \cdot \vec{J}_s^p(\vec{r})\, ds \tag{5.20}$$

where $\vec{E}(\vec{r})$ is the electric field in the cavity produced by the filamentary current distribution in (5.2) and $\vec{J}_s^p = J_y^p(y)\,\hat{y}$ is the assumed current distribution on the probe surface S with its component

$$J_y^p(y) = \frac{I_0}{2\pi r_0}\,\frac{\sin[k(d-y)]}{\sin(kd)} \tag{5.21}$$

From (5.19) to (5.21), the input impedance of the antenna may be written as

$$Z_{in} = \frac{-1}{I_0^2}\int_S E_y(\vec{r})\, J_y^p(y)\, ds \tag{5.22}$$

where $E_y(\vec{r})$ is given by (5.11) and the integral is over the probe surface.

The expression for $E_y(\vec{r})$ in (5.11) shows that the input impedance is composed of two parts. The part corresponding to the stored energy in the closed cavity Z_{in}^c is reactive in the absence of ohmic losses, while the part corresponding to the radiation from the slot aperture, i.e. Z_{in}^s, has a resistive component due to the radiation loss.

To perform the integration in (5.22), we use polar coordinates for the probe shown in Fig. 5.1b where $x = x_0 + r_0 \cos\phi$ and $z = z_0 + r_0 \sin\phi$. The results are

$$Z_{in} = Z_{in}^c + Z_{in}^s \tag{5.23}$$

$$Z_{in}^c = C_1 \sum_{p=1}^{\infty}\sum_{q=0}^{\infty} \frac{\varepsilon_q \sin(k_p x_0)}{K_{pq}\sin(K_{pq} c)}\, \bar{B}(q)\, R(p, q) \tag{5.24}$$

where

$$C_1 = \frac{-j4\omega\mu}{\pi ab \sin^2(kd)} \tag{5.25}$$

$$\bar{B}(q) = \frac{1}{(k_q^2 - k^2)} \sin^2[(k_q - k)\frac{d}{2}] \sin^2[(k_q + k)\frac{d}{2}] \tag{5.26}$$

$$R(p, q) = \int_0^{2\pi} \sin(k_p x)\, h_{pq}(z, z_0)\, d\phi \tag{5.27}$$

$$\approx \pi \sin(k_p x_0) \left[\sin(K_{pq} z_0) \sin[K_{pq}(c - z_0 - r_0)] + \sin[K_{pq}(c - z_0)] \sin[K_{pq}(z_0 - r_0)]\right]$$

and

$$Z_{in}^s = C_2 \sum_{p=1}^{\infty} \sum_{q=0}^{\infty} \frac{\varepsilon_q J_0(k_q w)}{\sin(K_{pq} c)} I(p)\, B(q)\, T(p, q) \tag{5.28}$$

where $I(p)$ and $B(q)$ are defined by (5.18) and (5.7e), respectively, and

$$C_2 = \frac{-2k}{\pi ab I_0 \sin(kd)} \tag{5.29}$$

$$T(p, q) = \int_0^{2\pi} \sin(k_p x) \sin[K_{pq}(c - z)]\, d\phi \tag{5.30}$$

$$\approx 2\pi \sin(k_p x_0) \sin[K_{pq}(c - z_0 - r_0)]$$

Note that in (5.27) and (5.30) with the assumption of $r_0 \ll x_0$, $r_0 \ll z_0$ and $r_0 \ll c - z_0$, the integrands are essentially independent of ϕ and we have chosen $\phi = \frac{\pi}{2}$ ($\frac{3\pi}{2}$ for $\pi \le \phi \le 2\pi$ in (5.27)) to obtain the approximate expressions. It is important to retain the finite value of r_0 in these expressions to guarantee the exponential convergence of the series in (5.24) and (5.28). This can be verified by noting that as the parameters p and q increase, the quantity $K_{pq} = (k^2 - k_p^2 - k_q^2)^{1/2}$ becomes imaginary and the resulting hyperbolic functions have exponential asymptotic behavior.

5.4- Numerical results

We have performed computations for a typical probe-fed CBS radiator which, unless otherwise stated, operates at $f = 3\ GHz$ with cavity dimensions $a/\lambda = 0.7$, $b/\lambda = 0.3$, and $c/\lambda = 0.3$; slot dimensions $2L/\lambda = 0.5$ and $w/L = 0.04$ with slot center at $x_c = a/2$ and $y_c = b/2$; probe location at $x_0 = a/2$ and $z_0 = c/2$ with its length $d/\lambda = 0.25$, radius $r_0/\lambda = 0.01$ and input current $I_0 = 1\ mA$. Also in the figures, we have used dashed lines to denote either of the phase function or reactance.

The amplitude and phase of the voltage distribution along the slot is shown in Fig. 5.2 for slot lengths $2L/\lambda = 0.5$, 0.6 and 0.7. Fig. 5.3 shows the effect of probe location on the voltage amplitude at the slot center $|V_c|$. The data shown in Fig. 5.4 for the input impedance of the antenna indicates that as the probe is moved closer to the wall containing the slot, the value of R increases as expected. The effect of the probe length on $|V_c|$ is shown in Fig. 5.5 for various cavity depths $c/\lambda = 0.2$, 0.3 and 0.4. From this figure it is seen that a longer probe induces a larger voltage in the slot. Similar behavior can be observed from Fig. 5.6 for the input impedance of an antenna with $c/\lambda = 0.3$. The reactance X_c of the closed cavity (without slot) is also shown in this figure for comparison. In a closed cavity, the reactance is capacitive for small probe lengths and, as the length is increased, resonance occurs at a certain point, i.e. $X_c = 0$. Further increase in probe length results in inductive reactance as can be seen from the figure. This property suggests a convenient means for adjusting the input impedance by varying the probe length. The cavity depth may also affect the input impedance for which a typical example is shown in Fig. 5.7.

To investigate the input impedance as a function of frequency, we have used an antenna with $a = 7\ cm$, $b = c = 3\ cm$, $2L = 5\ cm$, $w/L = 0.04$ fed by a probe of length $d = 2.5\ cm$ and radius $r_0 = 1\ mm$ located at $x_0 = a/2$, $z_0 = 1\ cm$. The impedance characteristic of the antenna as well as the reactance of the closed cavity versus frequency are shown in Fig. 5.8. In general, the resonance frequencies of the open slot and the closed cavity are different and the value of X_c, which is mainly determined by the probe length, can significantly affect the resonance behavior of the antenna as a whole. Figs. 5.9 and 5.10

show the resistance and reactance of the antenna versus frequency for various cavity depths and slot lengths, respectively. It is observed that a deeper cavity results in a higher radiation resistance and narrower bandwidth as well as lower resonance frequency. On the other hand, the slot length has major role in determining the resonance frequency of the antenna and an increase in length beyond $\lambda/2$ results in a decrease in the radiation resistance as expected. The numerical results presented in this Chapter could not be compared due to the lack of experimental data or other theoretical methods in the literature.

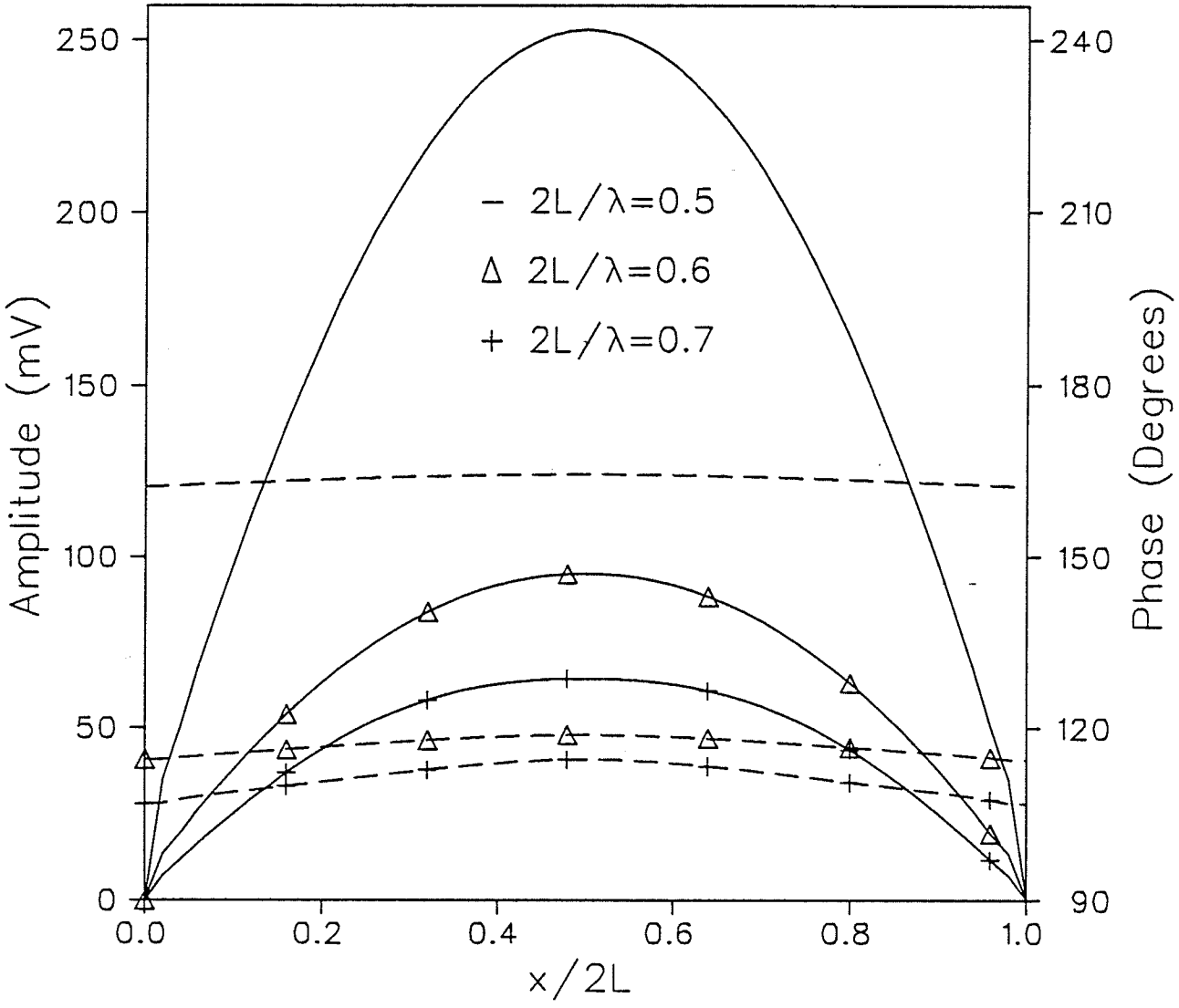

Fig. 5.2- Amplitude and phase (dashed lines) of voltage distribution along the slot of a probe-fed CBS antenna with slot lengths $2L/\lambda = 0.5$, 0.6 and 0.7.

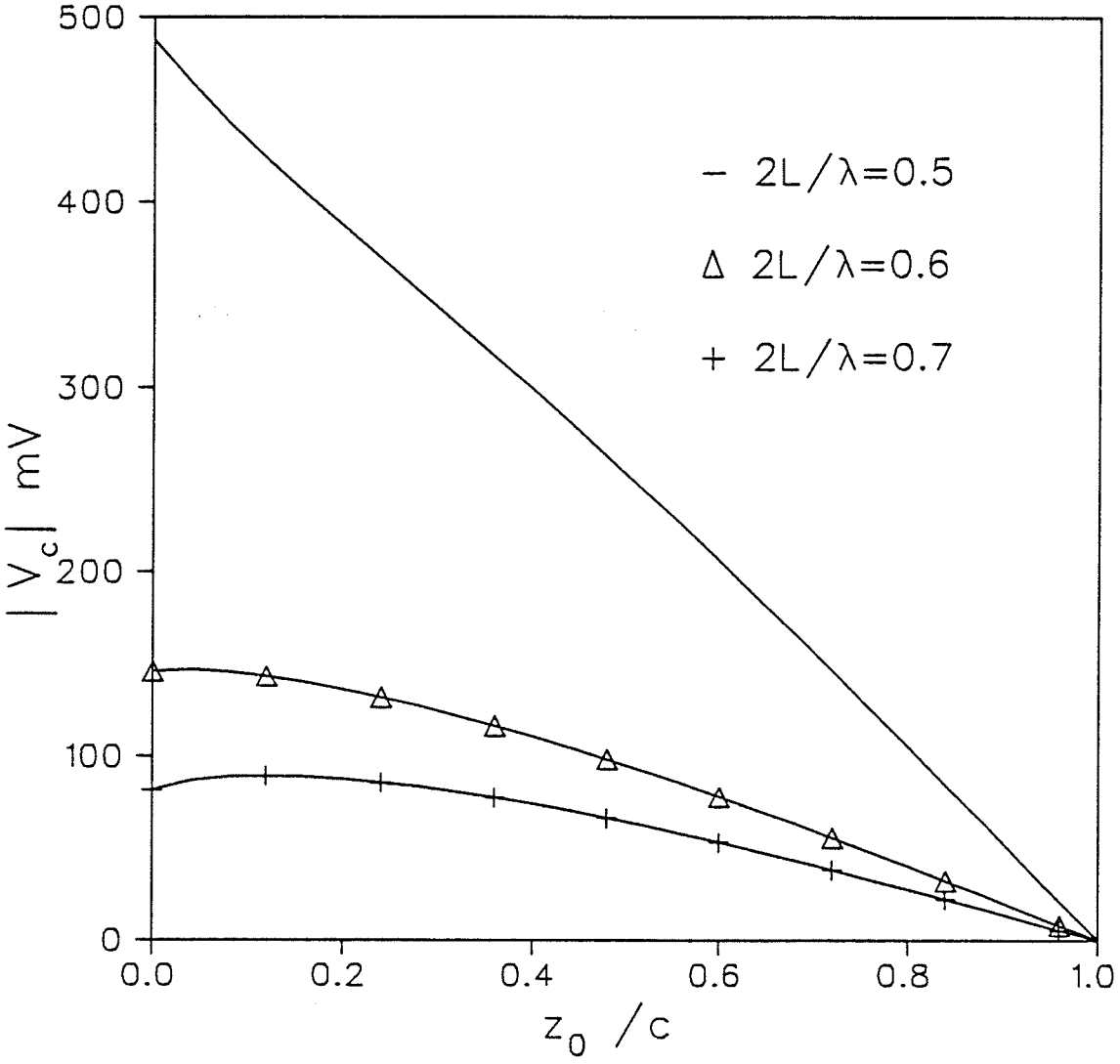

Fig. 5.3- Amplitude of voltage at the slot center versus normalized probe location z_0/c for slot lengths $2L/\lambda$ = 0.5, 0.6 and 0.7.

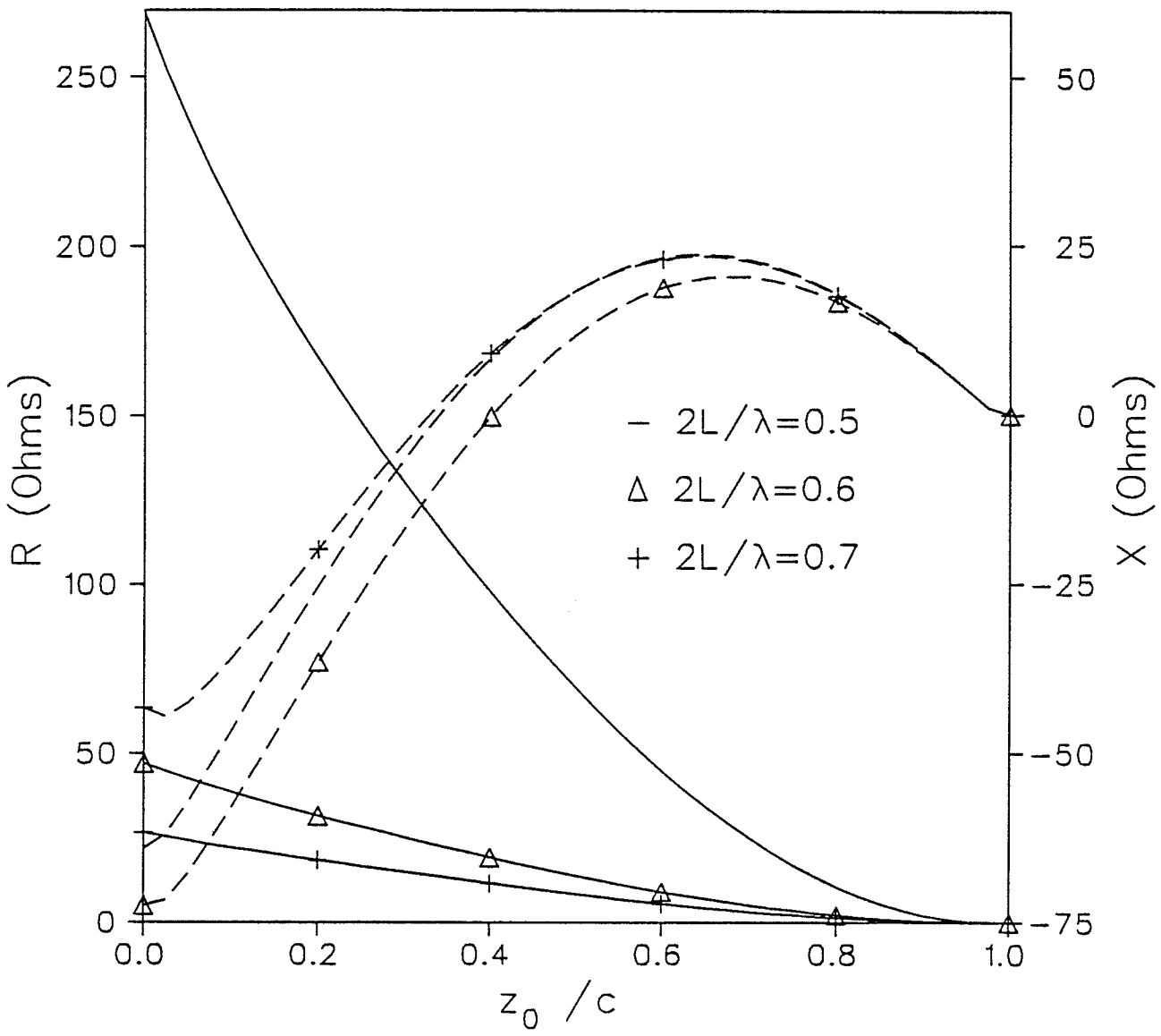

Fig. 5.4- Resistance R and reactance X (dashed lines) versus normalized probe location z_0/c for slot lengths $2L/\lambda = 0.5$, 0.6 and 0.7.

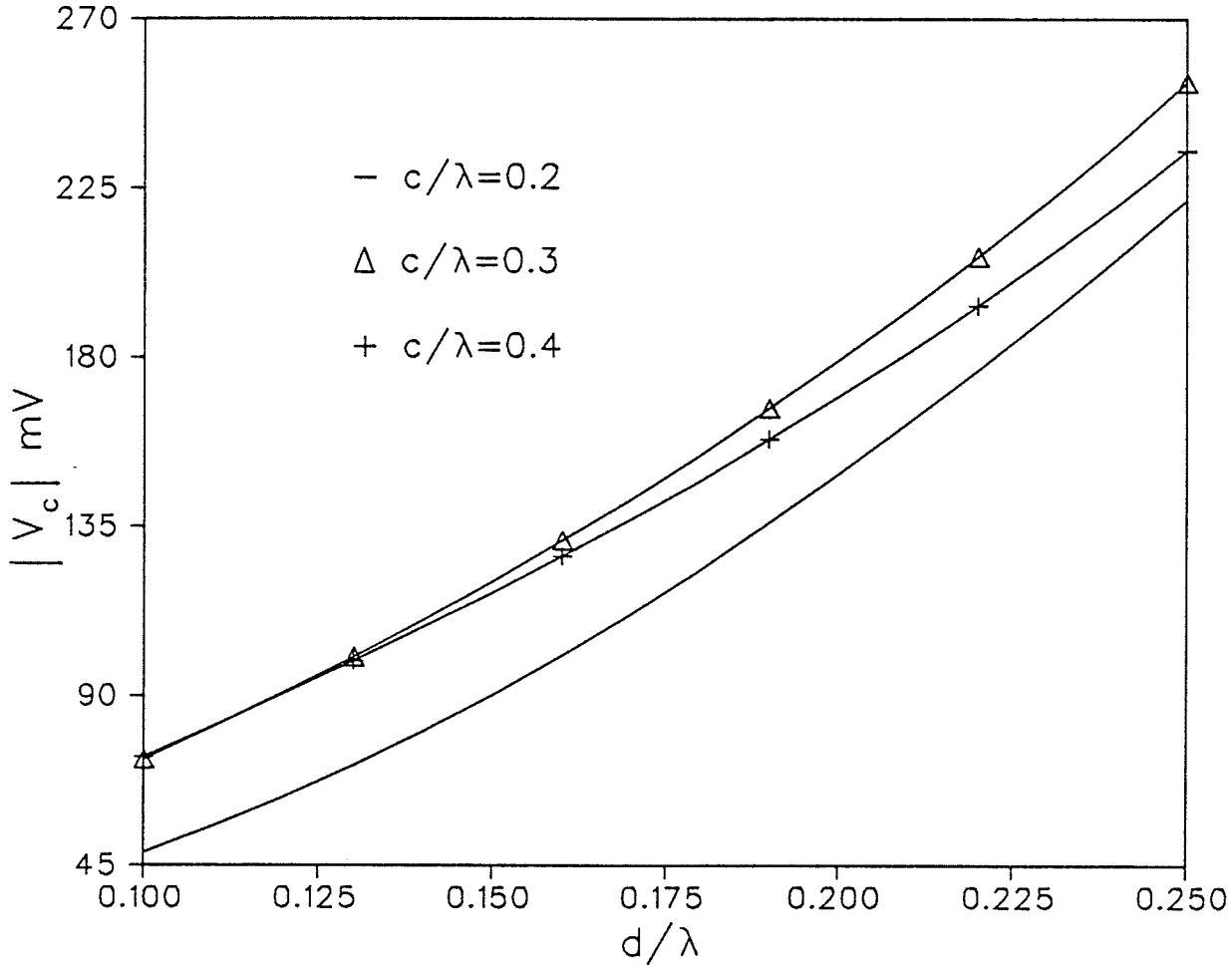

Fig. 5.5- Amplitude of voltage at the slot center versus probe length d/λ for cavity depths c/λ = 0.2, 0.3 and 0.4.

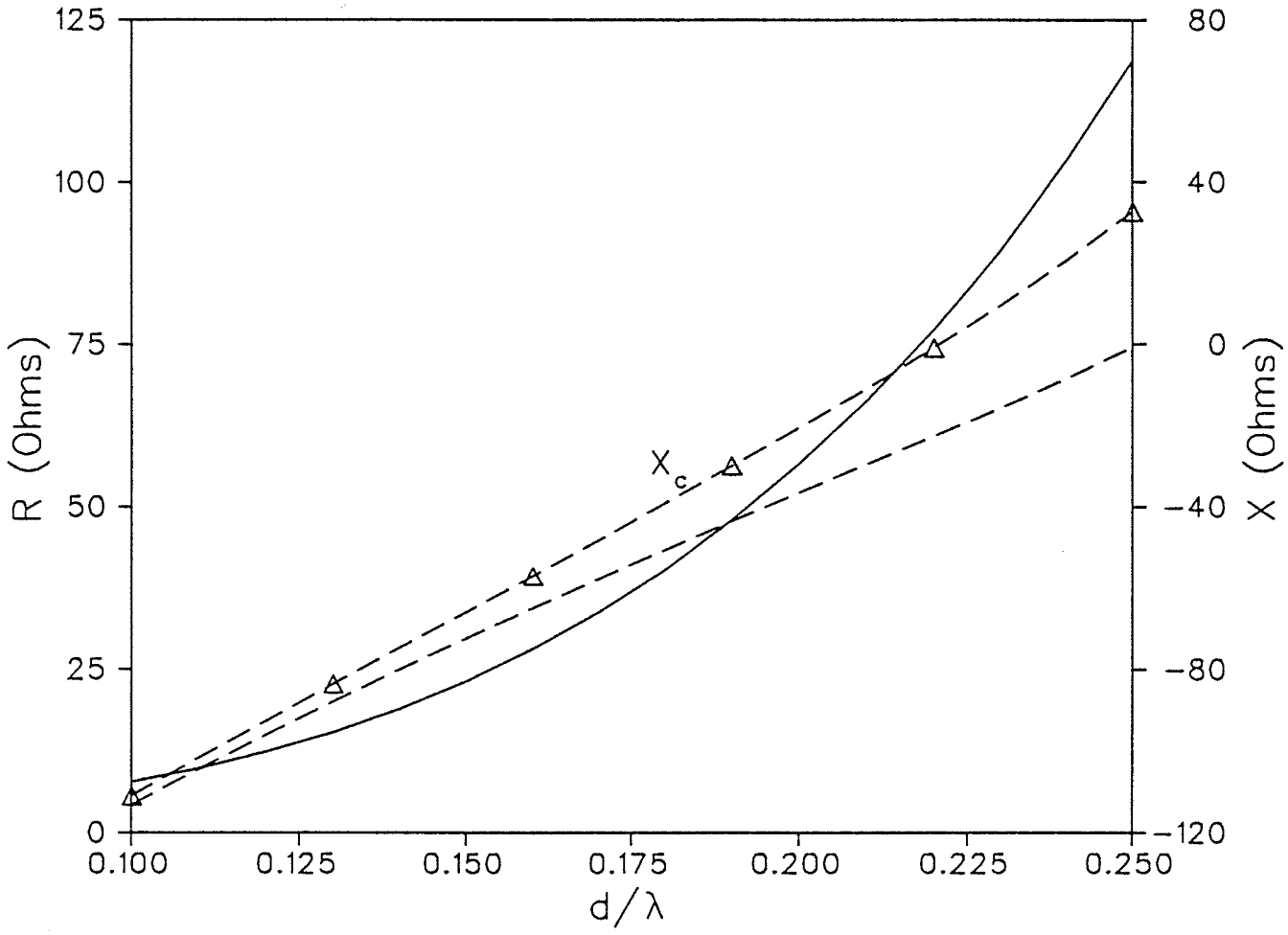

Fig. 5.6- Resistance R and reactance X (dashed lines) of probe-fed CBS antenna and reactance of closed cavity X_c versus probe length d/λ.

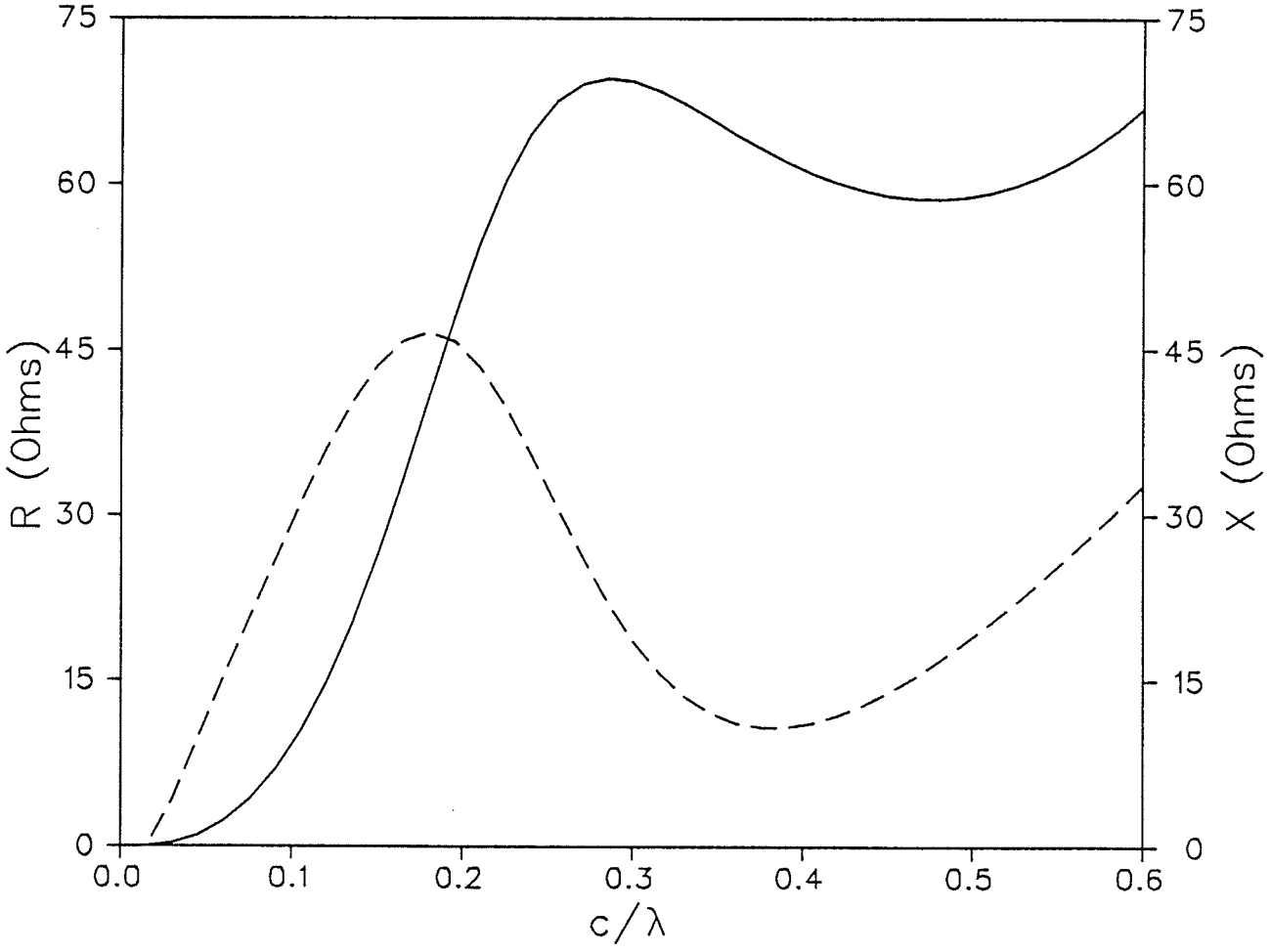

Fig. 5.7- Resistance R and reactance X (dashed line) versus cavity depth c/λ for a probe-fed CBS.

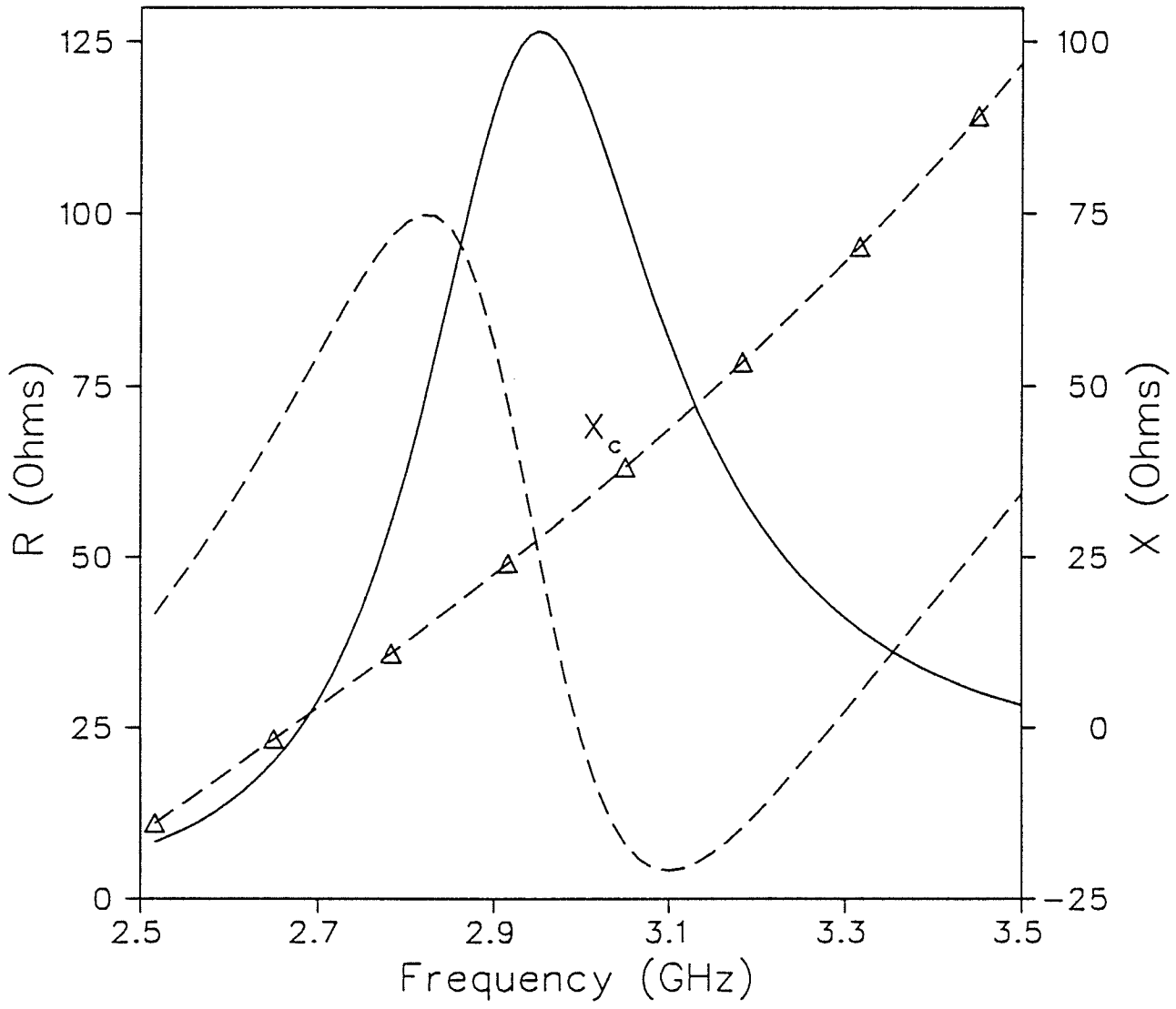

Fig. 5.8- Resistance R and reactance X (dashed lines) of probe-fed CBS antenna and reactance of closed cavity X_c versus frequency.

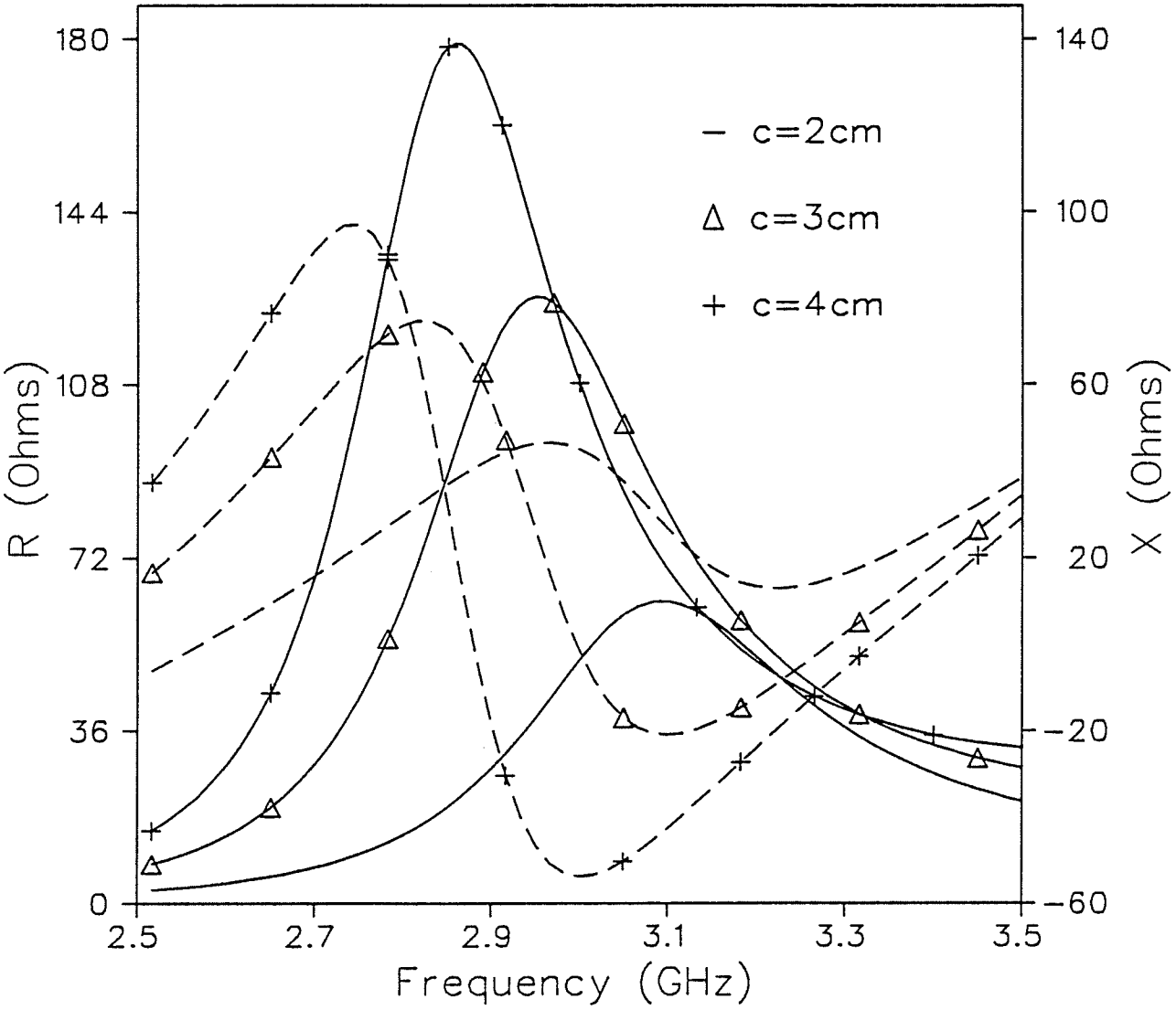

Fig. 5.9- Resistance R and reactance X (dashed lines) as a function of frequency for a probe-fed CBS antenna with cavity depths $c = 2$, 3 and 4 cm.

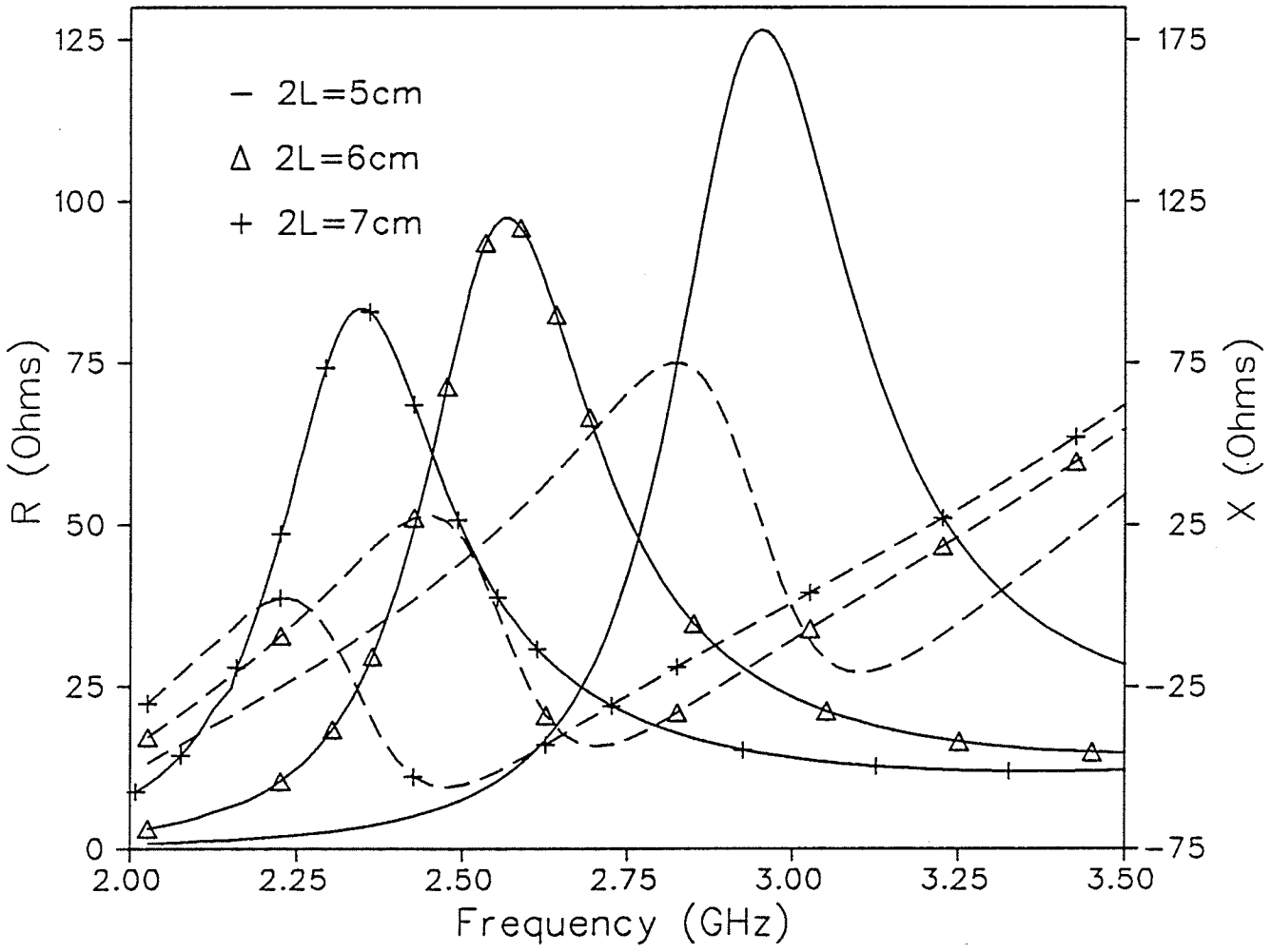

Fig. 5.10- Resistance R and reactance X (dashed lines) as a function of frequency for a probe-fed CBS antenna with slot lengths $2L = 5$, 6 and 7 cm.

CHAPTER 6

GAUSSIAN CAVITY-BACKED SLOT RADIATORS

To extend the scope of the slot radiator applications to specialized fields such as monopulse radar and tracking, it is essential to minimize or if possible suppress the side-lobes in the radiation pattern of the antenna. This can be achieved in principle if the voltage distribution along the slot aperture is in the form of a Gaussian function which in turn can be realized by introducing a cavity of suitable shape to back the slot. The so-called Gaussian cavity should support electromagnetic fields that decay exponentially in a certain direction and is constructed from a Gaussian beam-waveguide by placing reflecting surfaces at two suitable constant-phase planes. The dyadic Green's functions of such a cavity are not known beforehand and therefore to obtain the fields inside the cavity, one cannot directly use the field expressions derived in Chapter 3.

In this Chapter we first present a general solution for the fields between two parallel conducting plates in terms of a continuous spectrum of elementary plane waves. The wave beam condition is then used to obtain an approximate solution for the waves which are confined to a small solid angle about the principal axis of the antenna. The equation for the surface of the cavity back-wall is obtained and solved numerically. The restrictions imposed on the cavity dimensions by the wave beam assumption are also discussed. The fields in the cavity are expanded in terms of Gauss-Hermite functions whose orthogonality property is used to obtain the expansion coefficients. The slot cut in the front wall of the cavity is excited by a current source on the aperture and an integral equation is derived for the tangential electric field in the slot. The moments method with entire-domain basis and testing functions is used in the numerical solution of the integral equation for the voltage distribution along the slot aperture.

6.1- Electromagnetic fields between two conducting parallel plates

In this section we present the appropriate solution of Maxwell's equations for the fields between two conducting parallel plates located at $y = \pm b$. In a source free region of space the electromagnetic fields can be expressed in terms of two scalar potentials u and v as follows [51]

$$\vec{E} = \nabla \times \nabla \times (u\ \vec{c}) - jk\ \nabla \times (v\ \vec{c}) \tag{6.1}$$

$$\vec{H} = \sqrt{\varepsilon/\mu}\ \left[\ jk\ \nabla \times (u\ \vec{c}) + \nabla \times \nabla \times (v\ \vec{c})\ \right] \tag{6.2}$$

where $\vec{c}$ is an arbitrary constant vector and the potential functions satisfy the scalar Helmholtz equation,

$$\nabla^2 \psi + k^2\ \psi = 0 \tag{6.3}$$

An elementary solution of (6.3) in rectangular coordinates which is suitable for our problem is given by

$$\psi_{k_x k_y k_z}(x, y, z) = f(k_x)\ h(k_y y)\ e^{-j(k_x x + k_z z)} \tag{6.4}$$

where $f(k_x)$ is an arbitrary analytic function, $h(k_y y)$ is a harmonic function and k_x, k_y and k_z are separation parameters which satisfy the relation

$$k_x^2 + k_y^2 + k_z^2 = k^2 \tag{6.5}$$

From this equation it is clear that only two of these parameters, say k_x and k_y, can be specified independently. For the geometry in question which extends to infinity in the x direction, the corresponding parameter k_x forms a continuous spectrum of eigenvalues while in the y direction the structure is finite and therefore the eigenvalues k_y are discrete quantities to be determined from the appropriate boundary conditions. Thus the general solution of (6.3) which is obtained by superimposing the elementary solutions over the independent eigenvalues, can be written in the form

$$\psi(x, y, z) = \sum_{k_y} h(k_y y) \int_{k_x} f(k_x)\ e^{-j(k_x x + k_z z)}\ dk_x \tag{6.6}$$

where the summation is over the discrete eigenvalues k_y and the integration is performed over the continuous values of k_x.

From (6.1) and (6.2) and for $\vec{c} = \hat{z}$, the field components are given by

$$E_x = \frac{\partial^2 u}{\partial z \partial x} - jk \frac{\partial v}{\partial y} \tag{6.7a}$$

$$E_y = \frac{\partial^2 u}{\partial z \partial y} + jk \frac{\partial v}{\partial x} \tag{6.7b}$$

$$E_z = -\frac{\partial^2 u}{\partial x^2} - \frac{\partial^2 u}{\partial y^2} \tag{6.7c}$$

$$H_x = \sqrt{\varepsilon/\mu} \left(\frac{\partial^2 v}{\partial z \partial x} + jk \frac{\partial u}{\partial y} \right) \tag{6.8a}$$

$$H_y = \sqrt{\varepsilon/\mu} \left(\frac{\partial^2 v}{\partial z \partial y} - jk \frac{\partial u}{\partial x} \right) \tag{6.8b}$$

$$H_z = -\sqrt{\varepsilon/\mu} \left(\frac{\partial^2 v}{\partial x^2} + \frac{\partial^2 v}{\partial y^2} \right) \tag{6.8c}$$

where u and v satisfy expressions similar to (6.6).

To determine the proper form of the harmonic functions and their eigenvalues, we use the boundary condition which requires that the tangential electric field vanish on the conducting surfaces at $y = \pm b$. Thus

$$u(x, y, z) = \sum_q \bar{A}_q \sin\left(\frac{q\pi}{b} y\right) \int_{-\infty}^{+\infty} \bar{f}_1(k_x)\, e^{-j(k_x x + k_z z)}\, dk_x \tag{6.9}$$

$$v(x, y, z) = \sum_q \bar{B}_q \cos\left(\frac{q\pi}{b} y\right) \int_{-\infty}^{+\infty} \bar{f}_2(k_x)\, e^{-j(k_x x + k_z z)}\, dk_x \tag{6.10}$$

where the discrete eigenvalues $k_y = q\pi/b$, $q = 0, 1, 2, \cdots$ are substituted. In these equations $\bar{f}_1(k_x)$ and $\bar{f}_2(k_x)$, i.e. the amplitude spectrum of the elementary waves are arbitrary functions with the only restriction being that the integrands and their first and second derivatives with respect to x, y, and z must be integrable for all field points. From (6.7) to (6.10), the field components are given by

$$E_x = \sum_q A_q \sin(k_y y) \int_{-\infty}^{+\infty} [- k_x k_z f_1(k_x) + jkk_y f_2(k_x)] \, e^{-j(k_x x + k_z z)} dk_x \tag{6.11a}$$

$$E_y = \sum_q B_q \cos(k_y y) \int_{-\infty}^{+\infty} [- jk_y k_z f_1(k_x) + kk_x f_2(k_x)] \, e^{-j(k_x x + k_z z)} dk_x \tag{6.11b}$$

$$E_z = \sum_q A_q \sin(k_y y) \int_{-\infty}^{+\infty} (k_x^2 + k_y^2) \, f_1(k_x) \, e^{-j(k_x x + k_z z)} dk_x \tag{6.11c}$$

$$H_x = \sqrt{\varepsilon/\mu} \sum_q B_q \cos(k_y y) \int_{-\infty}^{+\infty} [jkk_y f_1(k_x) - k_x k_z f_2(k_x)] \, e^{-j(k_x x + k_z z)} dk_x \tag{6.12a}$$

$$H_y = \sqrt{\varepsilon/\mu} \sum_q A_q \sin(k_y y) \int_{-\infty}^{+\infty} [- kk_x f_1(k_x) + jk_y k_z f_2(k_x)] \, e^{-j(k_x x + k_z z)} dk_x \tag{6.12b}$$

$$H_z = \sqrt{\varepsilon/\mu} \sum_q B_q \cos(k_y y) \int_{-\infty}^{+\infty} (k_x^2 + k_y^2) \, f_2(k_x) \, e^{-j(k_x x + k_z z)} dk_x \tag{6.12c}$$

where

$$k_z = \begin{cases} (k^2 - k_x^2 - k_y^2)^{1/2}, & k \geq (k_x^2 + k_y^2)^{1/2} \\ -j(k_x^2 + k_y^2 - k^2)^{1/2}, & k < (k_x^2 + k_y^2)^{1/2} \end{cases} \tag{6.13}$$

Thus the above fields, which constitute an exact solution of Maxwell's equations in the specified region, are the superposition of propagating and evanescent plane waves.

6.2- Wave beams

To obtain the wave beams, i.e. waves whose direction of propagation lie within a small solid angle about the z axis, we require that $k_x \ll k_z$ and $k_y \ll k_z$. With these assumptions and from (6.13), one can use a first order approximation $k_z \simeq k$ for the amplitude terms and a second order approximation $k_z \simeq k - (k_x^2 + k_y^2) / 2k$ for the phase terms of the components in (6.11) and (6.12). This results in the following approximate fields

$$E_x = k\ e^{-jkz} \sum_q A_q\ e^{j\frac{z}{2k}k_y^2} \sin(k_y y) \int_{-\infty}^{+\infty} f(k_x)\ e^{-jk_x x} e^{j\frac{z}{2k}k_x^2} dk_x \tag{6.14a}$$

$$E_y = k\ e^{-jkz} \sum_q B_q\ e^{j\frac{z}{2k}k_y^2} \cos(k_y y) \int_{-\infty}^{+\infty} g(k_x)\ e^{-jk_x x} e^{j\frac{z}{2k}k_x^2} dk_x \tag{6.14b}$$

$$E_z = k\ e^{-jkz} \sum_q A_q\ e^{j\frac{z}{2k}k_y^2} \sin(k_y y) \int_{-\infty}^{+\infty} [-k_x f(k_x) + jk_y g(k_x)] e^{-jk_x x} e^{j\frac{z}{2k}k_x^2} dk_x \tag{6.14c}$$

$$H_x = -k\sqrt{\varepsilon/\mu}\ e^{-jkz} \sum_q B_q\ e^{j\frac{z}{2k}k_y^2} \cos(k_y y) \int_{-\infty}^{+\infty} g(k_x)\ e^{-jk_x x} e^{j\frac{z}{2k}k_x^2} dk_x \tag{6.15a}$$

$$H_y = k\ \sqrt{\varepsilon/\mu}\ e^{-jkz} \sum_q A_q\ e^{j\frac{z}{2k}k_y^2} \sin(k_y y) \int_{-\infty}^{+\infty} f(k_x)\ e^{-jk_x x} e^{j\frac{z}{2k}k_x^2} dk_x \tag{6.15b}$$

$$H_z = k\sqrt{\varepsilon/\mu} e^{-jkz} \sum_q B_q e^{j\frac{z}{2k}k_y^2} \cos(k_y y) \int_{-\infty}^{+\infty} [-jk_y f(k_x) + k_x g(k_x)] e^{-jk_x x} e^{j\frac{z}{2k}k_x^2} dk_x \tag{6.15c}$$

Note that according to the wave beam assumption, we should have $k_x \ll k$ and therefore the integrations over k_x should actually be limited to $|k_x| \le K_x$ with $K_x \ll k$. However, if the amplitude functions $f(k_x)$ and $g(k_x)$ rapidly tend to zero outside this range, the integration can be carried out over the entire k_x values without significant error. We will shortly elaborate on this point which greatly facilitates the analytical calculations. Also note that the approximation used for the phase terms is valid only in a restricted range of z values such that

$$[\ K_x^2 + (q\pi/b)^2\ ]\ z\ /\ 2k < 2\pi \tag{6.16}$$

The implications of the above conditions are further developed in Sec. 6.5.

Examination of (6.14) and (6.15) reveals that the transverse field components may be written as

$$E_x = F\ e^{-j\,k\,z}\ , \qquad H_y = \sqrt{\varepsilon/\mu}\ E_x \tag{6.17}$$

where

$$F = k \sum_q A_q \; e^{j\frac{z}{2k}k_y^2} \sin(k_y y) \int_{-\infty}^{+\infty} f(k_x) \; e^{-jk_x x} e^{j\frac{z}{2k}k_x^2} dk_x \tag{6.18}$$

and

$$E_y = G \; e^{-j\,k\,z} \;, \qquad H_x = -\sqrt{\varepsilon/\mu}\; E_y \tag{6.19}$$

where

$$G = k \sum_q B_q \; e^{j\frac{z}{2k}k_y^2} \cos(k_y y) \int_{-\infty}^{+\infty} g(k_x) \; e^{-jk_x x} e^{j\frac{z}{2k}k_x^2} dk_x \tag{6.20}$$

Thus, the wave beam approximation results in simple relations between the transverse electric and magnetic fields which are similar to those of a *TEM* wave. The z components of the fields can be obtained from the transverse components through Maxwell's equations.

To comply with the requirements on behavior of the amplitude function as mentioned above, we expand $f(k_x)$ and $g(k_x)$ in terms of Gauss-Hermite functions in the form $\exp\left[-\frac{1}{4}(k_x/\rho)^2\right] He_p(k_x/\rho)$. Here ρ is a parameter which determines the energy concentration in the wave beam to be discussed in the next section and He_p is the Hermite polynomial of degree p defined by the Rodrigues' formula,

$$He_p(x) = (-1)^p \; e^{x^2/2} \frac{d^p}{dx^p} e^{-x^2/2} \tag{6.21}$$

These are even functions for even p, odd functions for odd p and satisfy the following recurrence formula [42]:

$$He_{p+1}(x) = x \; He_p(x) - p \; He_{p-1}(x)$$

with $He_0(x) = 1$ and $He_1(x) = x$. Hermite polynomial defined in (6.21) is orthogonal in the interval $-\infty \le x \le +\infty$ with respect to the weighting function $\exp(-\frac{1}{2}x^2)$ such that

$$\int_{-\infty}^{+\infty} e^{-\frac{1}{2}x^2} \; He_p(x) \; He_r(x) \; dx = (2\pi)^{1/2} \, p! \; \delta_{pr} \tag{6.22}$$

where

$$\delta_{pr} = \begin{cases} 1, & p = r \\ 0, & p \neq r \end{cases} \tag{6.23}$$

Upon expanding the amplitude functions, (6.18) and (6.20) may be written in the form

$$F = k \sum_{p,\,q} A_{pq}\; e^{\,j(\frac{q\pi}{b})^2 \frac{z}{2k}}\; H_p(x,\,z)\; \sin(\frac{q\pi}{b} y) \tag{6.24}$$

$$G = k \sum_{p,\,q} B_{pq}\; e^{\,j(\frac{q\pi}{b})^2 \frac{z}{2k}}\; H_p(x,\,z)\; \cos(\frac{q\pi}{b} y) \tag{6.25}$$

where

$$H_p(x,\,z) = \int_{-\infty}^{+\infty} e^{\,-\frac{1}{4}(k_x/\rho)^2}\; He_p(k_x/\rho)\; e^{\,-jxk_x} e^{\,j\frac{z}{2k}k_x^2}\, dk_x \tag{6.26}$$

The integral in (6.26) can be performed analytically (see Appendix D) resulting in

$$H_p(x,\,z) = (-j)^p A(z)\; e^{\,-\frac{1}{4}t^2}\; He_p(t)\; e^{\,-j\phi_p} \tag{6.27a}$$

where

$$A(z) = 2\sqrt{\pi}\,\rho\,(\,1 + \zeta^2\,)^{\,-\frac{1}{4}} \tag{6.27b}$$

$$\zeta = \frac{2\rho^2}{k}\, z \tag{6.27c}$$

$$t = \frac{2\rho x}{\sqrt{1+\zeta^2}} \tag{6.27d}$$

$$\phi_p = \frac{\zeta}{4}\, t^2 - \frac{1}{2}\,(2p+1)\,\tan^{-1}\zeta \tag{6.27e}$$

From orthogonality of the Hermite polynomial in (6.22), it is easy to show that the functions $H_p(x,\,z)$ also satisfy the orthogonality property expressed by

$$\int_{-\infty}^{+\infty} H_p\; H_r^*\, dx = (2\pi)^{3/2}\,\rho\; p!\; \delta_{pr} \tag{6.28}$$

where * denotes the complex conjugate.

The electric field components E_x and E_y can be written in the form

$$E_x = \sum_{p,q} A_{pq}\, f_p(x, z)\, e^{-j\theta_{pq}(x,z)} \sin(\frac{q\pi}{b}y) \tag{6.29}$$

$$E_y = \sum_{p,q} B_{pq}\, f_p(x, z)\, e^{-j\theta_{pq}(x,z)} \cos(\frac{q\pi}{b}y) \tag{6.30}$$

where

$$f_p(x, z) = (-j)^p k\, A(z)\, e^{-\frac{1}{4}t^2} He_p(t) \tag{6.31}$$

$$\theta_{pq}(x, z) = kz - (\frac{q\pi}{b})^2 \frac{z}{2k} + \frac{\zeta}{4} t^2 - \frac{1}{2}(2p+1)\tan^{-1}\zeta \tag{6.32}$$

These are the transverse components of the fields that comprise the propagating wave beams between the parallel plates. From (6.31) it is seen that the amplitude of the wave beam modes has a Gaussian variation along the x axis.

6.3- Discussion of the energy concentration in the beam

The power transmitted by a single mode through an area $-x_0 \le x \le x_0$, $-y_0 \le y \le y_0$ is given by

$$P_{pq}(z) = -\frac{1}{2}\sqrt{\varepsilon/\mu} \int_{-x_0}^{x_0}\int_{-y_0}^{y_0} f_p^2(x, z) \cos^2(\frac{q\pi}{b}y)\, dx\, dy \tag{6.33}$$

which is proportional to $\int_0^{t_0} e^{-\frac{1}{2}t^2} He_p^2(t)\, dt$, where

$$t_0 = \frac{2\rho x_0}{\sqrt{1+\zeta^2}} \tag{6.34}$$

Equation (6.33) shows that the transmitted power, and therefore the energy density at each cross section, changes with z. Fixing the parameter y_0, one can find a relation between x_0 and z such that as z varies, the power transmitted through the specified cross section remains constant. This requires t_0 be constant and therefore (6.34) gives the appropriate relation between x_0 and z which may be written in the form

$$x_0^2 = (\frac{t_0}{2\rho})^2 \left[1 + (\frac{2\rho^2}{k} z)^2 \right] \tag{6.35}$$

This equation is independent of the mode numbers and hence the following discussion applies to all the beam modes.

Since the power transmitted through each cross section is assumed to be constant, a minimum value of x_0 in (6.35) corresponds to a maximum power density. This equation can be written in the normalized form

$$\xi^2 = 1/C + C\ \eta^2 \tag{6.36}$$

where $\xi = x_0 / \xi_0$ and $\eta = z/z_0$ with

$$\xi_0 = \sqrt{\frac{z_0}{2k}}\ t_0 \tag{6.37}$$

and

$$C = 2\rho^2 \frac{z_0}{k} \tag{6.38}$$

Equation (6.36) is plotted in Fig. 6.1 for various values of C along with its envelope $\xi = \sqrt{2 \mid \eta \mid}$. From this figure it is seen that for a given C, the highest energy concentration in the modes (which corresponds to minimum x_0 or ξ) occurs at the $z = 0$ plane and continuously falls as one moves towards the $z = \pm z_0$ planes (i.e. $\eta = \pm 1$) which locate the phase correcting devices in a beam waveguide. It is easy to show that at the $z = \pm z_0$ planes, the minimum value of ξ or x_0 which corresponds to the maximum energy density is achieved when $C = 1$, resulting in

$$\rho_0 = \sqrt{\frac{k}{2z_0}} \tag{6.39}$$

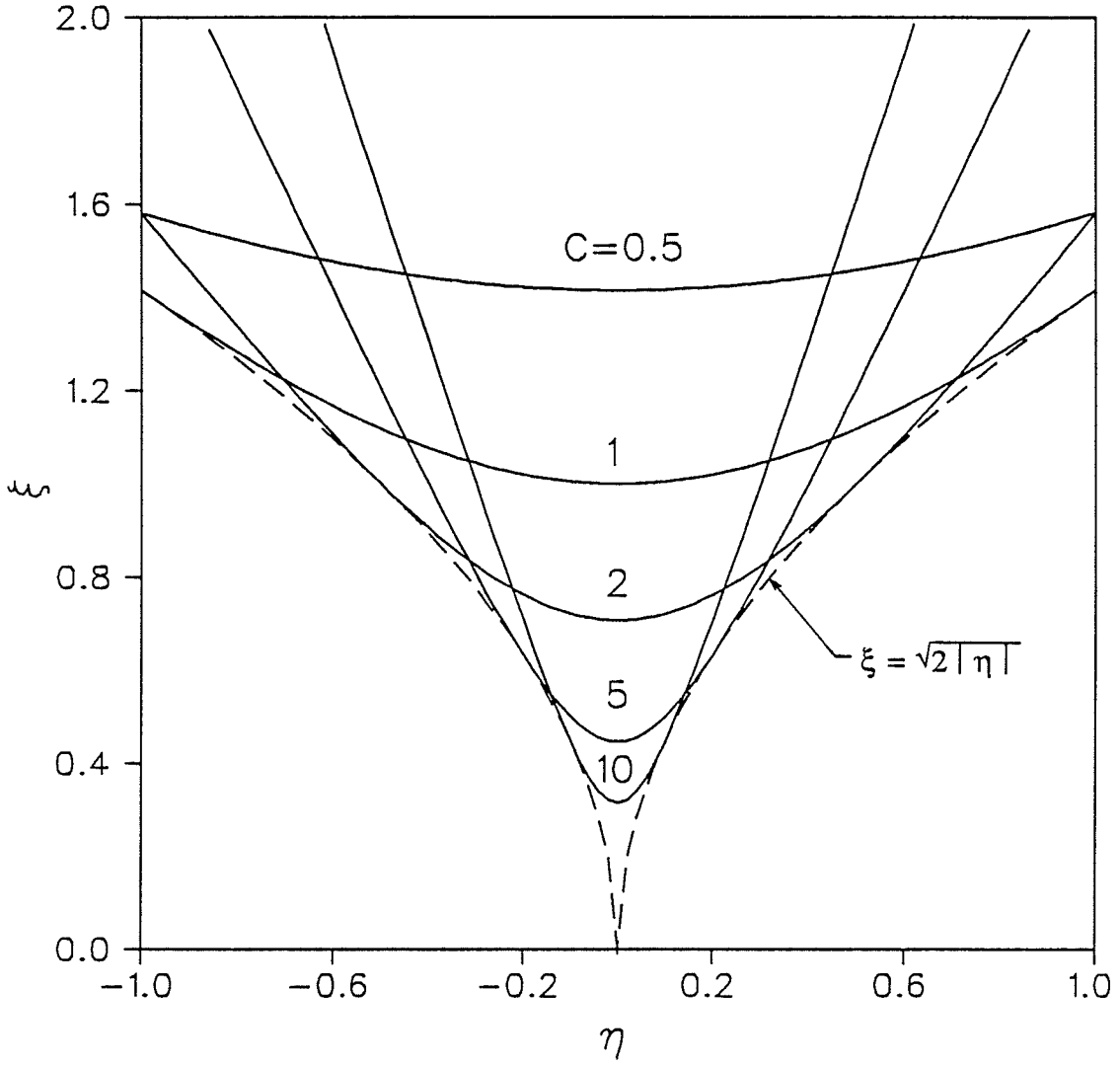

Fig. 6.1- Plot of $\xi^2 = 1/C + C\ \eta^2$ for various values of parameter C.

6.4- Structure of the Gaussian-cavity resonator

The Gaussian-cavity resonator is constructed from a beam waveguide by placing short circuits along the two constant-phase surfaces that are separated by $l\pi$, $l = 0, 1, 2, \cdots$ radians of phase shift. From (6.32) it is seen that at $z = 0$, the phase function θ_{pq} vanishes and therefore the $z = 0$ plane is a surface of constant phase. This surface is chosen here as the front wall of the cavity which contains the radiating slot (see Fig. 6.2). The back wall of the cavity must lie along a constant-phase surface which satisfies $\theta_{pq}(x, z) = l\pi$ at the operating frequency. Thus the equation of the back-wall surface is given by

$$S(x, z) = kz - (\frac{q\pi}{b})^2 \frac{z}{2k} + \frac{2\rho^4 x^2 z}{k(1 + \frac{4\rho^4}{k^2} z^2)}$$

$$- \frac{2p+1}{2} \tan^{-1}(\frac{2\rho^2}{k} z) - l\pi = 0, \quad l = 0, 1, 2, \cdots \tag{6.40}$$

Substituting the value of ρ given by (6.39) yields

$$kz - (\frac{q\pi}{b})^2 \frac{z}{2k} + \frac{k x^2 z}{2(z_0^2 + z^2)} - \frac{2p+1}{2} \tan^{-1}(\frac{z}{z_0}) - l\pi = 0 \tag{6.41}$$

If we define z_0 as the cavity depth at $x = 0$, then from (6.41)

$$z_0 = \frac{0.5(p + 4l + 0.5)\pi k}{2k^2 - (q\pi/b)^2} \tag{6.42}$$

The contour of the surface in (6.40) is plotted in Fig. 6.3 for various values of the parameter ρ including $\rho = \rho_0$. In this figure for each value of the independent variable x, the corresponding value of z is obtained by using a numerical routine for finding the real zeros of a real function. It is observed that the cavity depth z_0 is almost independent of ρ.

6.5- Restrictions on cavity dimensions

As mentioned earlier, from the wave beam condition one should have $|k_x| \ll k$. Thus it is necessary for the amplitude function in the integrand of (6.26) to decrease rapidly outside this range in order to make it possible to perform the integration over k_x from $-\infty$

to $+\infty$. Let $|k_x| \leq K_x$ where $K_x \ll k$ is a constant. The amplitude of the integrand decreases exponentially with the inverse of $-\rho^2$. In this section we calculate the upper limit on the value of ρ which results in a reasonably small amplitude at $k_x = k$. For this amplitude to be proportional to $e^{-\nu}$ with ν an arbitrary real number, one should have $(\frac{k}{2\rho})^2 = \nu$ and therefore a value $\rho \leq \frac{k}{2\sqrt{\nu}}$ serves the purpose. This inequality can be expressed in terms of the cavity depth z_0 by using the condition of maximum energy concentration in the beam given by (6.39) which results in

$$z_0 \geq \frac{\nu}{\pi} \lambda \tag{6.43}$$

Thus to obtain the maximum energy concentration in the beam at $z = \pm z_0$ and yet maintain the validity of the calculations, the cavity depth at a given frequency should be larger than a certain value implied by (6.43). On the other hand, from (6.16) one should have

$$z_0 \leq 8\pi^2 [\, K_x^2 + (q\pi/b)^2 \,]^{-1} / \lambda \tag{6.44}$$

These requirements put a restriction on the allowable mode numbers p, q and l as obvious from (6.42). For example when the values of p and q are determined from the type of excitation and transverse dimension of the cavity, the parameter l should be chosen such that the conditions on z_0 are satisfied.

The wave beam approximation used in deriving the fields also requires that $q\pi/b \ll k$. For a finite value of b this condition can only be satisfied for a limited number of q values. However, one may choose a small value for b such that the fields become essentially independent of the y variable which corresponds to the $q = 0$ modes. On the other hand, although in theory the cavity length extends to infinity along the x axis, we note that the fields inside the cavity are negligible at points sufficiently far from $x = 0$ plane. Thus in practice it is possible to construct an antenna of finite length with no appreciable reflection from the open ends.

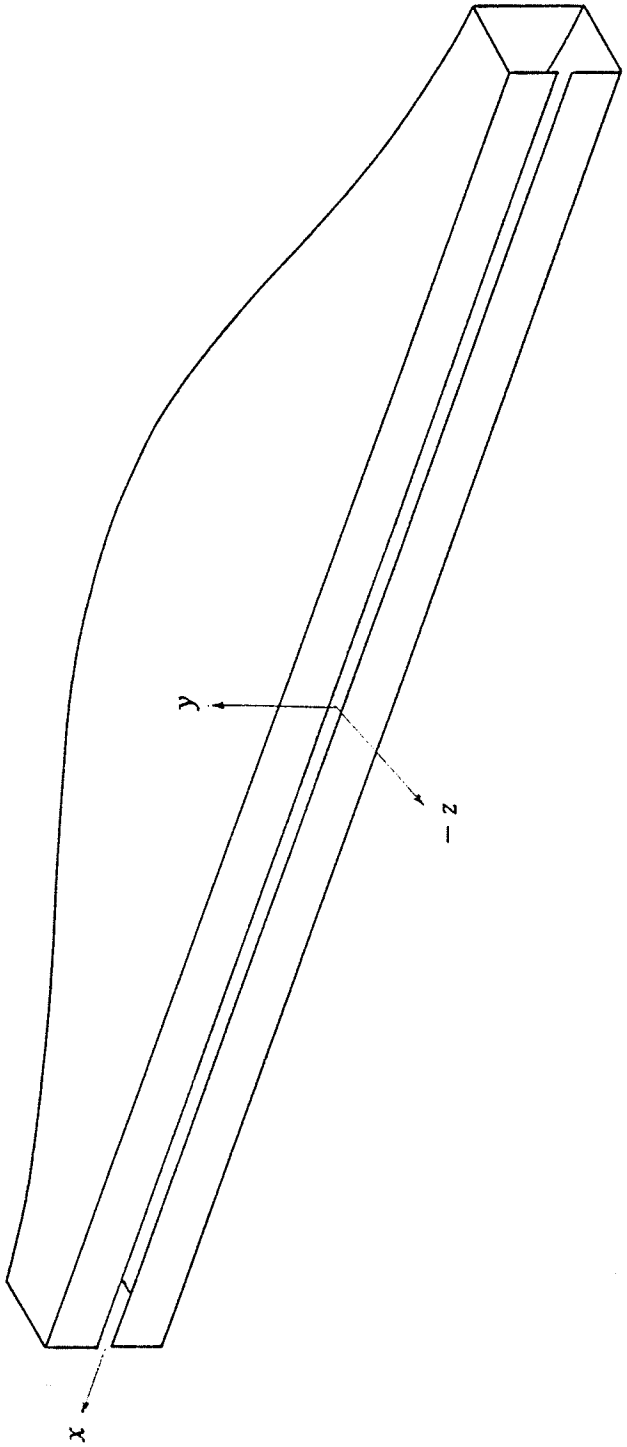

Fig. 6.2- Geometry of Gaussian cavity-backed slot antenna.

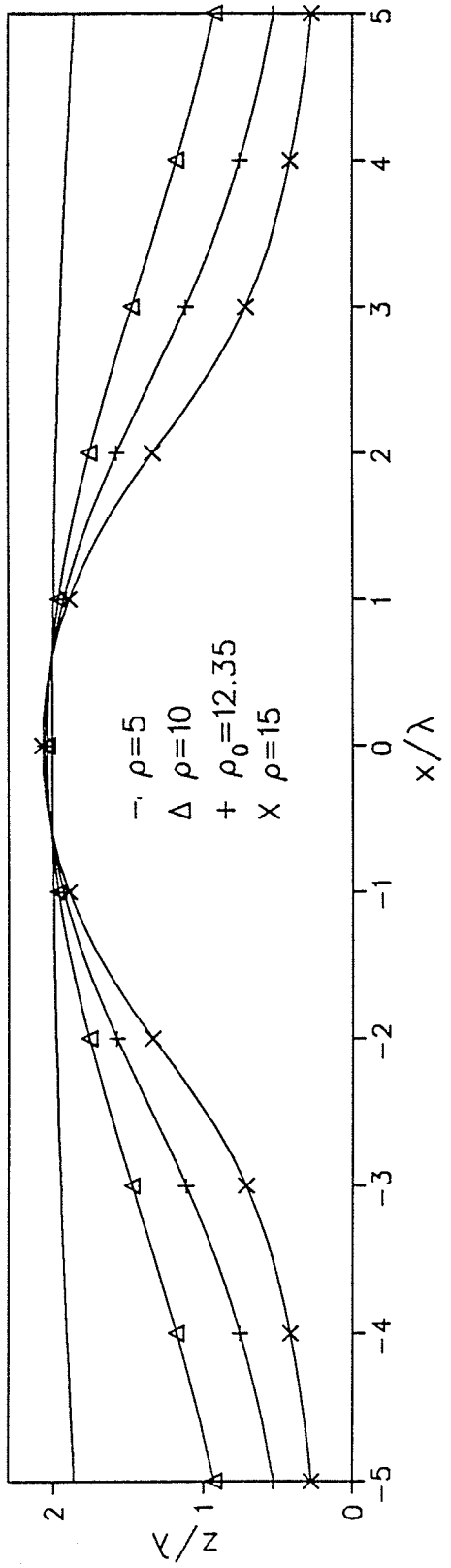

Fig. 6.3- Contour of back-wall of a Gaussian cavity of length 10 λ with $b = 0.2\ \lambda$ and $w = 0.1\ b$ for different values of parameter ρ.

6.6- Formulation of the integral equation for the electric field in the slot

In the non-radiating cavity resonator, the waveguide fields in the $\pm z$ directions combine to form a standing wave which has a sinusoidal z dependence to satisfy the boundary condition at the $z = 0$ plane. However, when the cavity is radiating through a slot, one should consider the addition of the individual propagating waves in a more general sense. For example, the y component of the electric field at every point in the cavity would be

$$E_y = E_y^+ + E_y^- \tag{6.45}$$

where

$$E_y^{\pm} = \sum_{p,q} B_{pq}^{\pm} f_p(x, z)\, e^{? j\theta_{pq}(x,z)} \cos(\frac{q\pi}{b} y) \tag{6.46}$$

At $z = 0$ i.e. in the aperture plane, we have $\theta_{pq} = 0$ and thus the electric field becomes

$$E_y^a(x, y) = 2\sqrt{\pi}\, k\rho \sum_{p,q} B_{pq}\, (-j)^p e^{-\frac{1}{4}(2\rho x)^2} He_p(2\rho x) \cos(\frac{q\pi}{b} y) \tag{6.47}$$

From this equation it is seen that for each mode, the x variation of the field amplitude is proportional to $e^{-\rho^2 x^2}$. Thus with the value of ρ given by (6.39) for maximum energy concentration in the beam, the field amplitude decreases exponentially with $(x/z_0)(x/\lambda)$ along the x axis in the transverse plane. Multiplying both sides of (6.47) by

$$e^{-\frac{1}{4}(2\rho x)^2} He_r(2\rho x) \cos(\frac{s\pi}{b} y)$$

and integrating from $-\infty$ to $+\infty$ over x and from $-b$ to $+b$ over y yields,

$$B_{pq} = \frac{(j)^p}{\pi\sqrt{2}kb\ p!} \int_{-b}^{+b} \int_{-\infty}^{+\infty} e^{-\frac{1}{4}(2\rho x)^2} E_y^a(x, y)\, He_p(2\rho x) \cos(\frac{q\pi}{b} y)\, dxdy \tag{6.48}$$

where we have used the orthogonality of the Hermite polynomial and the cosine function. It is observed that the mode amplitudes vary as $\frac{1}{p!}$ and therefore the higher order modes have little effect on the fields.

From (6.19), (6.47) and (6.48), the corresponding component of the magnetic field in the aperture can be written in the form

$$\lim_{z \to 0^+} H_x^{(1)}(x, y) = \frac{-\sqrt{2/\pi}\,\rho}{\sqrt{\mu/\varepsilon}\, b} \int_A E_y^a(x', y')\, G_c(x', y' \mid x, y)\, dx' dy' \qquad (6.49)$$

where

$$G_c(x', y' \mid x, y) = \sum_{p,q} \frac{1}{p!}\, e^{-\rho^2(x^2 + x'^2)}\, He_p(2\rho x')\, He_p(2\rho x)\, \cos(k_y y')\cos(k_y y) \qquad (6.50)$$

and the integration is performed over the aperture area due to the fact that outside the slot, $E_y^a(x, y)$ is zero on the conducting screen.

The magnetic field in region (2) i.e. $z < 0$ can be expressed in terms of an integral over the tangential electric field in the aperture. The x component of this field $E_x^a(x, y)$ is assumed to be negligible for the type of excitation to be considered here. Hence,

$$\lim_{z \to 0^-} H_x^{(2)}(x, y) = \frac{j}{2\pi\omega\mu} \int_A E_y^a(x', y') \left(k_0^2 + \frac{\partial^2}{\partial x^2}\right) G_0(x', y' \mid x, y)\, dx' dy' \qquad (6.51)$$

where G_0 is the free space Green's function given by

$$G_0(x', y' \mid x, y) = \frac{e^{-jk_0[(x - x')^2 + (y - y')^2]^{1/2}}}{[(x - x')^2 + (y - y')^2]^{1/2}} \qquad (6.52)$$

We assume the structure to be excited by a current distribution $J_y^a(x, y)$ over the slot. Thus, the continuity of the tangential magnetic field in the aperture requires that

$$\lim_{z \to 0^-} H_x^{(2)}(x, y) - \lim_{z \to 0^+} H_x^{(1)}(x, y) = -J_y^a(x, y) \qquad (6.53)$$

This condition is used to obtain an integral equation for the electric field in the aperture $E_y^a(x, y)$, namely

$$\int_A E_y^a(x', y')\, K(x', y' \mid x, y)\, dx' dy' = -J_y^a(x, y) \qquad (6.54)$$

where the kernel K is given by

$$K(x', y' \mid x, y) = C_a\ G_c(x', y' \mid x, y) + C_b\ (k_0^2 + \frac{\partial^2}{\partial x^2}) G_0(x', y' \mid x, y) \qquad (6.55)$$

with $C_a = \dfrac{\sqrt{2/\pi}\ \rho}{\sqrt{\mu/\varepsilon}\ b}$ and $C_b = \dfrac{j}{2\pi\omega\mu}$.

To solve the integral equation in (6.54) for the electric field in the aperture, we assume a separable solution in the form

$$E_y^a(x, y) = X(x)\ Y(y) \qquad (6.56)$$

where $X(x)$ is an unknown function and $Y(y)$ is given by,

$$Y(y) = \frac{1/\pi}{\sqrt{w^2 - y^2}} \qquad (6.57)$$

This choice of the function Y is in accordance with the narrow slot assumption and accounts for the proper field behavior at the slot edges [21]. The unknown function $X(x)$ may be expanded in terms of suitable known basis functions as

$$X(x) \simeq \sum_{n=1}^{N} V_n\ X_n(x) \qquad (6.58)$$

Substituting (6.56) and (6.58) into (6.54) yields

$$\sum_{n=1}^{N} V_n \int_A X_n(x')\ Y(y')\ K(x', y' \mid x, y)\ dx'dy' \simeq -\ J_y^a(x, y) \qquad (6.59)$$

To obtain a system of N linear equations for the unknowns V_n, we multiply the above equation by a suitable weighting function $W_m(x, y)$ and integrate over the slot aperture. The result may be written in the matrix form

$$[y_{mn}]\ [V_n] = [c_m] \qquad (6.60)$$

where in the expression for matrix elements i.e. $y_{mn} = C_a\ a_{mn} + C_b\ b_{mn}$, we have

$$a_{mn} = \int_A \int_A W_m(x, y)\, X_n(x')\, Y(y')\, G_c(x', y' \mid x, y)\, dx'dy'dx\ dy \tag{6.61}$$

$$b_{mn} = \int_A \int_A W_m(x, y)\, X_n(x')\, Y(y')\, (k_0^2 + \frac{\partial^2}{\partial x^2}) G_0(x', y' \mid x, y)\, dx'dy'dx\ dy \tag{6.62}$$

and the source vector elements are given by

$$c_m = -\int_A W_m(x, y)\, J_y^a(x, y)\, dx\ dy \tag{6.63}$$

For the case of a finite slot, one may choose the piecewise basis and testing functions similar to those introduced in Chapter 4 and proceed with the solution for V_n in (6.60). However, in a slot of finite length the waves reflect from the two shorted ends and constitute a standing wave pattern along the slot which obscures the desired features produced by the Gaussian cavity. To preserve the favorite Gaussian behavior of the electric field in the aperture, it is necessary that the slot length extend along the x axis as shown in Fig. 6.2. Thus, at least in the ideal case of an infinitely long cavity, there is no reflection from the two ends to disturb the Gaussian field distribution in the slot.

Unlike the sub-domain basis and testing functions which are very useful in the moments method solution of a finite slot, the infinitely long slot in the present problem calls for the use of entire-domain functions. The best choice would be a function which is closely related to the actual field distribution in the aperture, and in this case a Gauss-Hermite function in the form $e^{-\rho^2 x^2} He_n(2\rho x)$. This choice is especially useful as it allows the orthogonality property in (6.22) to be applied to the expression for a_{mn} in (6.61) resulting in,

$$a_{mn} = \frac{\pi}{2\rho^2} \sum_{p,q} \frac{(m-1)!\ (n-1)!}{p!}\ \delta_{(m-1)p}\ \delta_{(n-1)p}\ J_0(\frac{q\pi}{b}w)$$

$$= \begin{cases} \dfrac{\pi(m-1)!}{2\rho^2} \displaystyle\sum_q J_0(\frac{q\pi}{b}w), & m = n \\ 0, & m \neq n \end{cases} \tag{6.64}$$

where we have used the relations

$$X_n(x) = e^{-\rho^2 x^2} He_{n-1}(2\rho x) , \quad n=1, 2, \cdots, N \tag{6.65}$$

$$W_m(x, y) = e^{-\rho^2 x^2} He_{m-1}(2\rho x)\, \delta(y) , \quad m=1, 2, \cdots, N \tag{6.66}$$

The numerical computation of b_{mn} in (6.62) is more demanding in the sense that it involves a triple integral two of which have infinite limits, namely

$$b_{mn} = \int_{-\infty}^{+\infty} e^{-\rho^2 x'^2} He_{n-1}(2\rho x')\, Q_m(x')\, dx' \tag{6.67}$$

where

$$Q_m(x') = \int_{-\infty}^{+\infty} e^{-\rho^2 x^2} He_{m-1}(2\rho x)\, P(x, x')\, dx \tag{6.68}$$

and

$$P(x, x') = (k_0^2 + \frac{\partial^2}{\partial x^2}) \int_{-w}^{+w} Y(y') \frac{e^{-jk_0[(x-x')^2+y'^2]^{1/2}}}{[(x-x')^2+y'^2]^{1/2}}\, dy' \tag{6.69}$$

Applying the so-called reduced kernel approximation, the integral in (6.69) reduces to [21]

$$G(x, x') = \frac{e^{-jk_0R}}{R} \tag{6.70}$$

where

$$R = [(x-x')^2 + (w/2)^2]^{1/2} \tag{6.71}$$

Thus upon performing the differentiation, (6.69) becomes

$$P(x, x') = \left[(x-x')^2(-k_0^2R^2+3+3jk_0R) - (-k_0^2R^2+1+jk_0R)\, R^2\right] \frac{e^{-jk_0R}}{R^5} \tag{6.72}$$

The procedure of numerical integration of the above integrals is explained in Sec. 6.7.

For calculating the source vector elements in (6.63), we will consider the excitation by a current source connected to the slot edges. Assuming a uniform current distribution of

width $2d$ and flowing in the y direction, we have

$$J_y^a(x) = \begin{cases} \dfrac{I_0}{2d}, & \text{for} \quad |x - x_s| \le d \\ 0, & \text{for} \quad |x - x_s| > d \end{cases} \tag{6.73}$$

where x_s denotes the source location. Thus the integral in (6.63) reduces to

$$c_m = \frac{-I_0}{2d} \int_{x_s - d}^{x_s + d} e^{-\rho^2 x^2} He_{m-1}(2\rho x)\, dx \tag{6.74}$$

The voltage distribution along the slot is given by

$$V(x) = -\int_{-w}^{+w} E_y^a(x, y)\, dy \tag{6.75}$$

From (6.56) to (6.58) and (6.65), it is easy to show that

$$V(x) \approx \sum_{n=1}^{N} V_n\, X_n(x) = e^{-\rho^2 x^2} \sum_{n=1}^{N} V_n\, He_{n-1}(2\rho x) \tag{6.76}$$

With the values of the matrix and source vector elements given by (6.64), (6.67) and (6.74), one can obtain the expansion coefficients V_n from (6.60) and thus the voltage distribution along the slot from (6.76).

6.7- Numerical results

In this section we first present a number of computational notes regarding the numerical integration of the integrals encountered in the matrix elements. In spite of the infinite limits of the integrals in (6.67) and (6.68), the exponential factor in the integrand results in the fast convergence of the numerical integration process. However, the function $P(x, x')$ in (6.72) has a weak singularity at $x = x'$ and therefore the integral in (6.68) should be performed with due care. To this end and for the actual numerical computations, the integral is written in the form

$$Q_m(x') = \int_{-x'+\Delta}^{+\infty} F_m(-x, x')\,dx + \int_{x'-\Delta}^{x'+\Delta} F_m(x, x')\,dx + \int_{x'+\Delta}^{+\infty} F_m(x, x')\,dx \quad (6.77)$$

where

$$F_m(x, x') = e^{-\rho^2 x^2}\, He_{m-1}(2\rho x)\, P(x, x') \quad (6.78)$$

and Δ is a small number in the order of 0.001 to be determined by examining the behavior of $F_m(x, x')$ to make sure that the integration is performed accurately in the vicinity of the $x = x'$ point. The interval of the two infinite integrals are divided into sub-intervals much larger than Δ, say 100Δ, as the integrand is fairly smooth in these regions. A 20 point Gaussian quadrature is then applied for integration over each sub-interval and the results are added. The upper limits of the infinite integrals are continuously increased until a certain number of accurate digits is achieved. Before attempting the numerical integration in (6.67), it is imperative to know the behavior of $Q_m(x')$. This function is even for $m = 1, 3, \cdots$, odd for $m = 2, 4, \cdots$ and its amplitude decreases very rapidly as x' deviates from $x' = 0$, a fact which is shown in Fig. 6.4 by plotting $\log | Q_m(x') |$ for typical values of $\rho = 12.35\ m^{-1}$, $w = 1\ mm$, $k = k_0 = 62.8\ rad/m$ and $m = 1, 2$. From this information, it is not difficult to see that the integrand in (6.67) is well-behaved and the convergence of integration is very rapid. To further facilitate the computation of b_{mn}, one may write the integral in the form

$$b_{mn} = \int_0^{\infty} e^{-\rho^2 x'^2}\, He_{n-1}(2\rho x')\, U_m(x')\,dx' \quad (6.79)$$

where

$$U_m(x) = \begin{cases} Q_m(x) + Q_m(-x), & n = odd \\ Q_m(x) - Q_m(-x), & n = even \end{cases} \quad (6.80)$$

and then proceed with numerical integration.

The amplitude and phase (dashed lines) of the voltage distribution along the slot are shown in Fig. 6.5 for an antenna with $z_0 = 2\ \lambda$, $b = 0.2\ \lambda$, $2w = 0.1\ b$ and operating at $f = 3\ GHz$. The slot is excited by a strip-line of width $2d = 0.02\ \lambda$ and $I_0 = 1\ mA$

located at the slot center, i.e. $x_s = 0$. The presence of riples in the voltage amplitude is expected as they correspond to the number of terms in the expression for the voltage given by (6.76) which in turn determines the degree of the Hermite polynomial in the expansion. As the number of terms increases, the riples approach an exponential envelope which represents the actual voltage distribution along the slot. This point is shown in Fig. 6.6 where the voltage amplitudes corresponding to $N = 9$ and $N = 11$ in (6.76) are plotted.

The convergence of the solution can be examined from Table 6.1 where the amplitudes of the complex expansion coefficients V_n are compared for solutions with various number of terms in the expression for the voltage distribution. Note that for the symmetric excitation, the values of V_n with $n = 2, 4, \cdots$ vanish and are not shown in the Table. For the case of skew-symmetric excitation, i.e. when two current sources of equal amplitude and opposite phase are located at $\pm x_s$, we have $V_n = 0$ for $n = 1, 3, \cdots$ and there is always a null in the voltage amplitude at $x = 0$, as shown in Fig. 6.7.

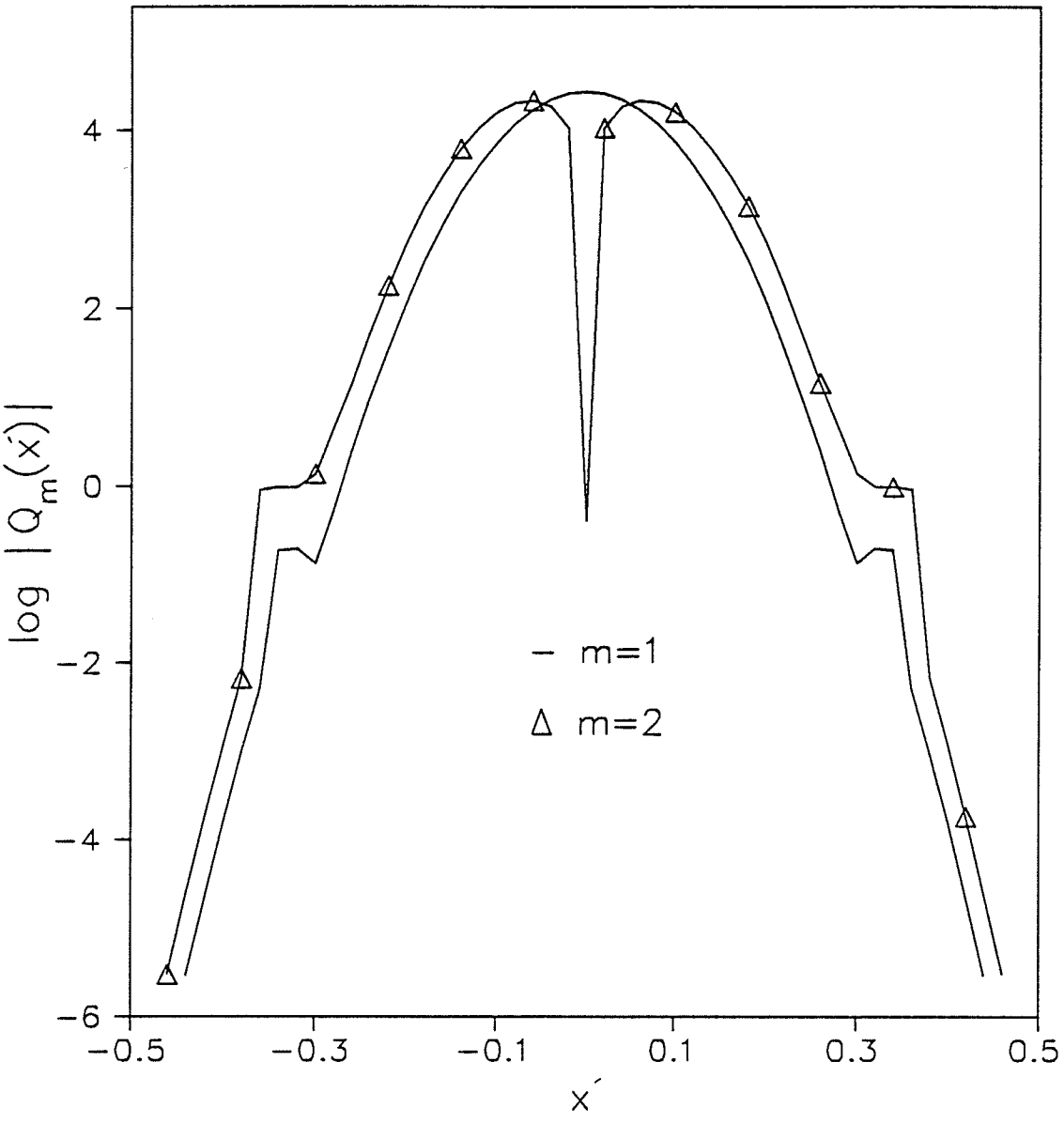

Fig. 6.4- Behavior of function $Q_m(x')$ in Eq. (6.68).

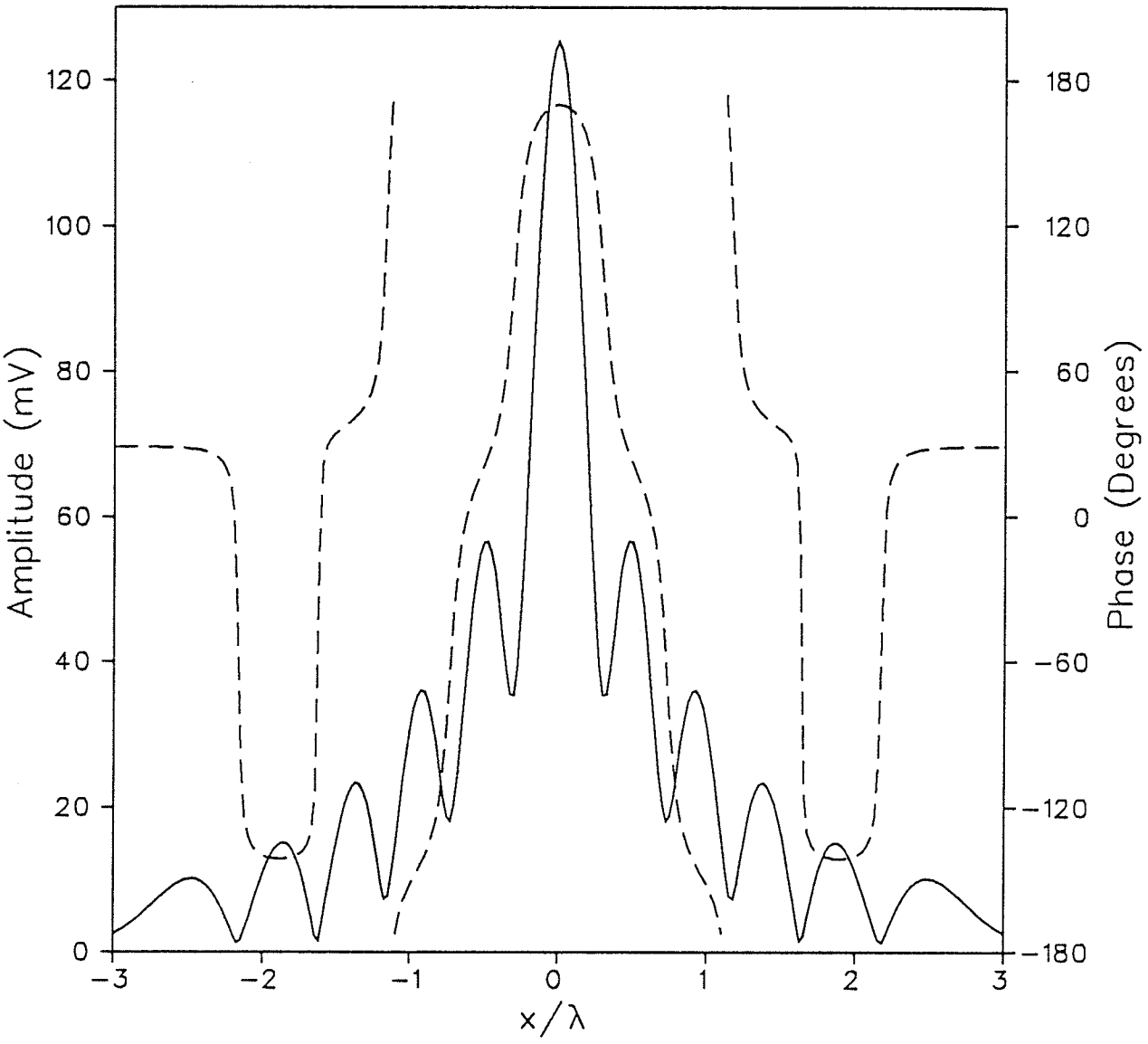

Fig. 6.5- Amplitude and phase (dashed line) of voltage distribution along the aperture of a Gaussian cavity- backed slot with symmetric excitation at $x_s = 0$.

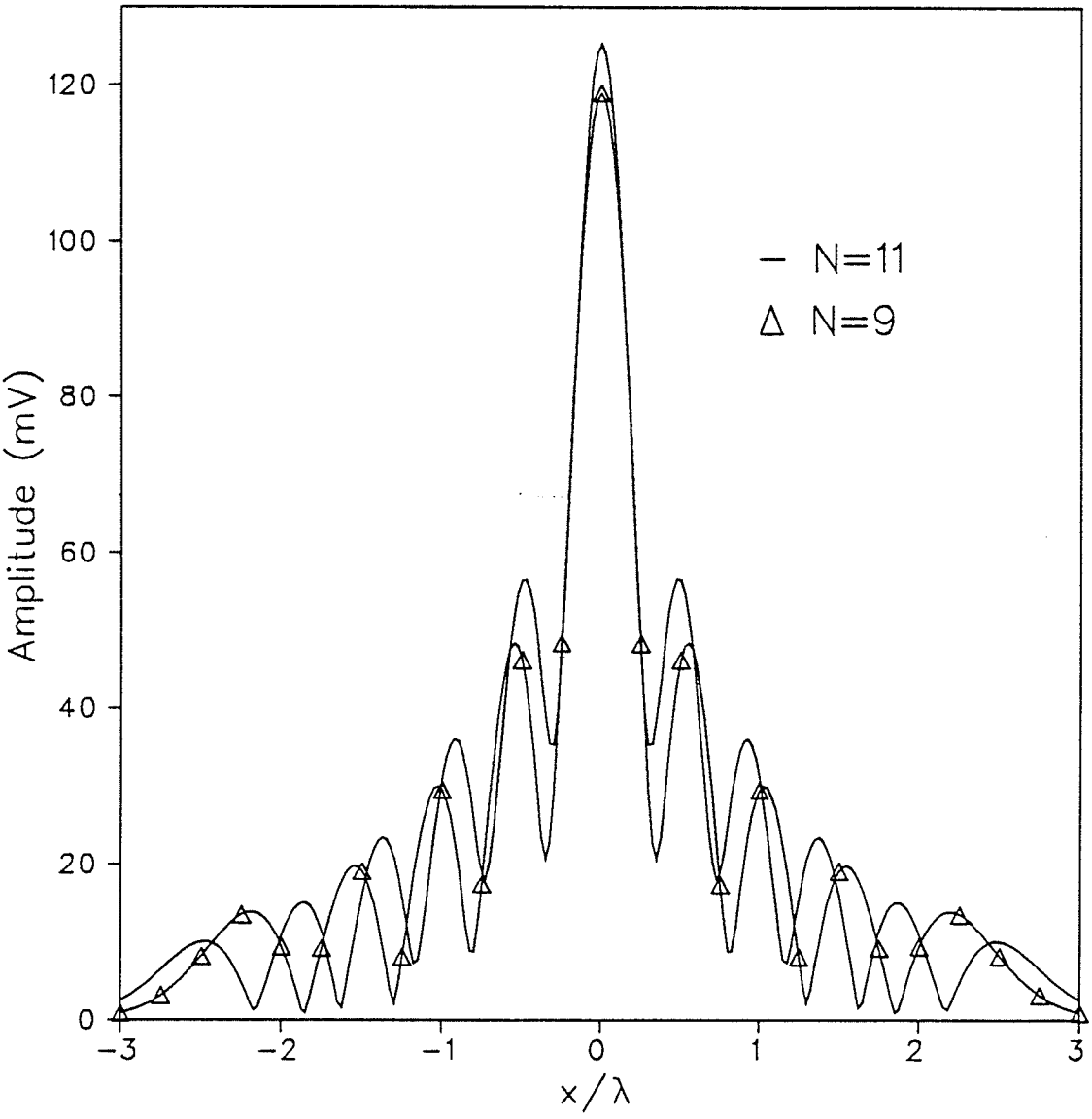

Fig. 6.6- Convergence of the solution for $N = 9$ and $N = 11$.

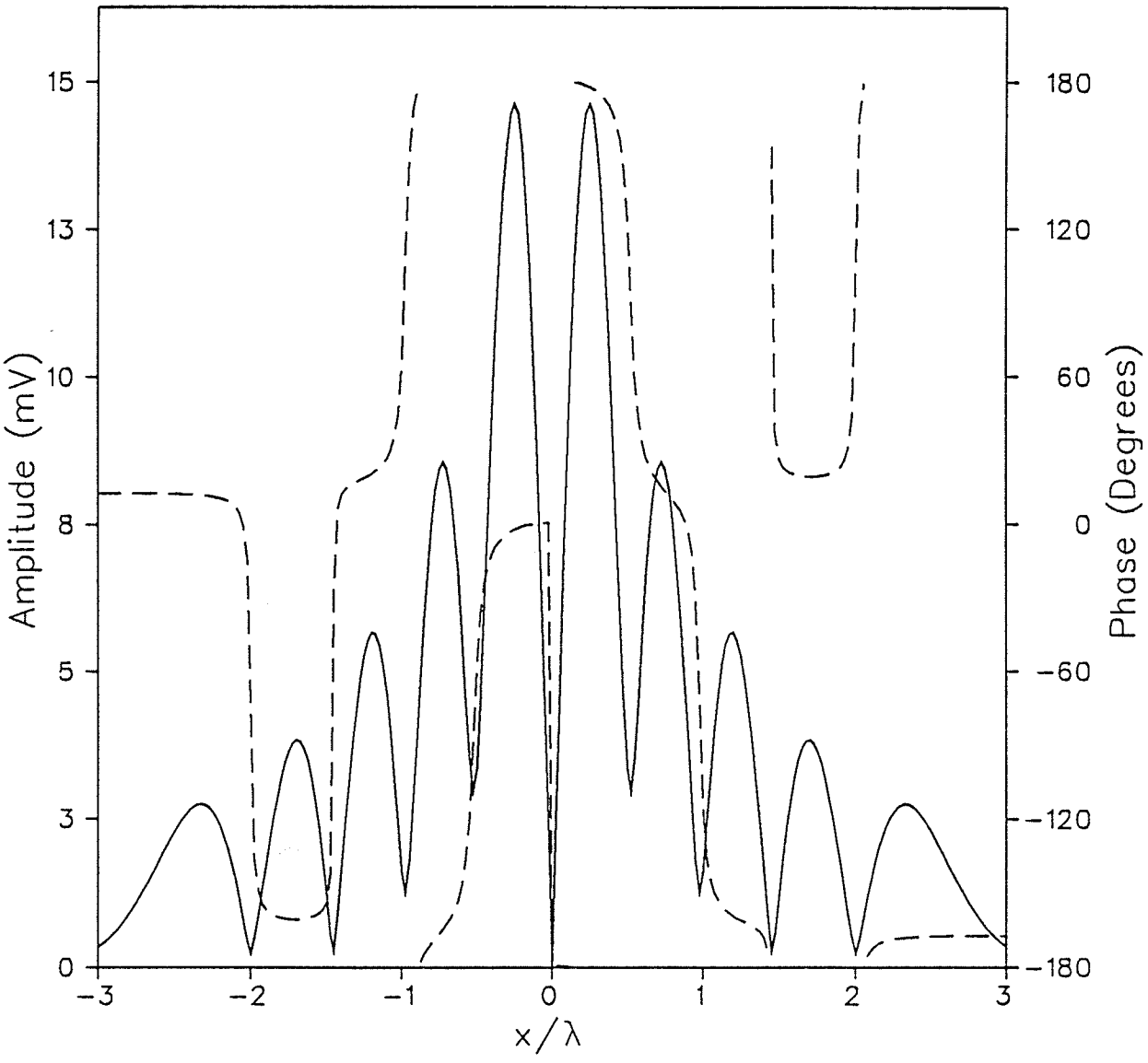

Fig. 6.7- Amplitude and phase (dashed lines) of voltage distribution along the aperture of a Gaussian cavity-backed slot with skew-symmetric excitation at $x_s = \pm \lambda/4$.

Table 6.1

N	$\lvert V_1 \rvert$	$\lvert V_3 \rvert$	$\lvert V_5 \rvert$	$\lvert V_7 \rvert$	$\lvert V_9 \rvert$	$\lvert V_{11} \rvert$
1	36.11					
3	37.11	20.91				
5	37.17	22.80	6.226			
7	37.15	22.95	7.232	1.268		
9	37.14	22.78	7.151	1.509	0.186	
11	37.16	22.68	6.889	1.372	0.202	0.018

CHAPTER 7

SUMMARY AND GENERAL CONCLUSIONS

In this thesis a unified view based on the equivalence principle is presented for analyzing various types of slot radiators. These include the open slot and also slots which are backed by cavities for the purpose of confining the radiation or to produce a certain field distribution in the slot aperture. For each case a general formulation of the problem is given which can be applied to arbitrary shaped apertures or cavities. The results are then specialized to geometries with practical importance such as radiating elements in the form of narrow slots. From the computational point of view, the emphasis is on accurately determining the voltage distribution along the slot. Once this quantity is known, other radiation and circuit parameters of the antenna may be obtained in a standard fashion.

The voltage distribution along the aperture of a narrow open slot satisfies Pocklington's equation. A technique based on the method of moments is utilized for the numerical evaluation of this integro-differential equation [37]. The elements of the moments matrix are transformed into the Fourier domain to eliminate the differential operator and also the singularity of the integrand. The effect of the slot dimensions on the parameters of interest, namely the input impedance, resonance frequency, and bandwidth are examined. The results show that the product of the resonance frequency and the slot length is a constant number. It is also found that in general a shorter and wider slot has a wider bandwidth while the radiation resistance drops as the slot width increases. The excitation source location has a significant effect on the voltage distribution along the slot and thus the radiation pattern and input impedance. This property can be used as a convenient means for matching the antenna to the source.

In most applications it is necessary to restrict the radiation from the slot to one half-space which may be achieved in practice by using a conducting enclosure to back the slot. An accurate evaluation of the aperture field in this problem requires the fields in the cavity

to be known. These fields may be expressed in terms of volume integrals over the sources in the cavity and a surface integral over the boundary area and include the appropriate dyadic Green's functions of the bounded region [38]. A system of coupled integral equations is obtained for the electric field in the aperture and specialized to the problem of a narrow slot backed by a rectangular cavity. The method of moments with piecewise sinusoids for basis and testing functions is applied for numerical evaluation of the voltage distribution along the slot. A current source in the form of a two-wire or coaxial line connected to the slot edges may be used to excite the structure. Similar to the open slot antenna, the feed-point location has major effect on the voltage distribution in the slot; a fact which is useful for the purpose of impedance matching.

The introduction of the cavity to back the slot intensifies the resonance behavior of the isolated slot, resulting in higher resonance frequencies and lower bandwidths. There are many physical parameters such as the cavity and slot dimensions, location of the slot center and excitation source, as well as the material in the cavity that contribute to the behavior of the antenna as a radiator and more importantly as a circuit element [58]. For example, the resonance frequency and bandwidth can easily be controlled by varying the cavity depth through a sliding back-wall. In general, a larger cavity width or slot width results in a wider bandwidth at the expense of reduced radiation resistance and efficiency. One of the interesting features of CBS antennas is their loading capability. In fact dielectric loading of the cavity has the effect of reducing the physical size and thus weight of the antenna which is desirable in airborne applications, especially at the lower range of operating frequencies. However, the numerical results show that an increase in the dielectric constant of the material in the cavity drastically reduces the bandwidth of the antenna while increasing the radiation resistance.

For the case where the CBS radiator is excited by a coaxial-line probe inside the cavity, one may model the probe by a filamentary current source and find the voltage distribution along the slot. As the probe is moved towards the cavity wall containing the slot, the induced voltage in the slot increases. Similar behavior is observed when the probe length is

increased. The assumption of a filamentary source results in an infinite reactance and therefore a more realistic model of the probe should be used in the impedance calculation. We assumed a sinusoidal current distribution flowing in the axial direction on the probe surface and applied Poynting's theorem for this purpose. Note that in the absence of ohmic losses, the impedance of the closed cavity (without slot) is purely reactive and its value is mainly determined by the probe length. This may be used for adjusting the input impedance by varying the probe length. As for the resonance frequency, a deeper cavity or a longer slot results in a lower resonance frequency as expected.

In applications such as radar, it is essential to eliminate or at least minimize the sidelobes in the radiation pattern of the antenna. On the other hand, it is well-known that the radiation field is the Fourier transform of the aperture field and since the Fourier transform of a Gaussian function is also a Gaussian, one concludes that a Gaussian field distribution in the aperture should in principle produce the desired radiation pattern. In a CBS radiator, it is possible to obtain the appropriate voltage distribution along the slot by using a cavity of proper size and shape to back the slot. To this end, the general solution for the electromagnetic fields between two conducting parallel plates are expressed as a continuous spectrum of plane waves. The so-called wave-beam conditions are then applied to obtain approximate solution for the fields that are confined to a small solid angle about the principal axis of the system. The field amplitudes are expanded in terms of Gauss-Hermite functions whose orthogonality property is used to obtain the expansion coefficients.

To construct a cavity resonator from the beam-waveguide one may short circuit two suitable constant-phase planes by conducting surfaces. The $x-y$ plane is taken as the plane of the front wall and the equation for surface of the cavity back-wall is obtained. In theory the cavity length extends to infinity along the x axis; however, it is shown that the amplitude of the propagating modes attenuate exponentially off the $x=0$ plane and therefore in practice one may use a cavity of finite length without noticeable reflection from the open ends. A narrow slot is cut in the front wall of the cavity and an integral equation is obtained for the voltage distribution along the slot. To preserve the favorable Gaussian

field distribution in the aperture, it is essential that the slot length extend to infinity. Thus, in the numerical evaluation of the integral equation, we have used the entire-domain basis and testing functions. The numerical results for the voltage distribution clearly show the Gaussian behavior of the aperture field for both symmetric and skew-symmetric excitations. It is also observed that for the case of skew-symmetric excitation, there is always a null in the voltage distribution at the slot center as expected.

APPENDIX A

FOURIER TRANSFORM OF $G(\xi)$ IN EQ. (2.20)

The Fourier transform of $G(\xi)$ is defined by

$$\tilde{G}(\alpha) = \int_{-\infty}^{+\infty} G(\xi)\, e^{-j\alpha\xi}\, d\xi \tag{A.1}$$

Substituting $G(\xi)$ from (2.20) and changing the order of integrations yields

$$\tilde{G}(\alpha) = \frac{4}{\pi} \int_{0}^{\pi/2} K_0(z \sin\theta)\, d\theta \tag{A.2}$$

where $z = w\sqrt{\alpha^2 - k^2}$ and we have used the result [59, p. 26]

$$\int_{-\infty}^{+\infty} e^{-j\alpha\xi}\, \frac{e^{-jk[\xi^2 + c^2]^{1/2}}}{[\xi^2 + c^2]^{1/2}}\, d\xi = 2\, K_0(\,|\,c\,|\,\sqrt{\alpha^2 - k^2}\,) \tag{A.3}$$

It can also be shown that [42, p. 485]

$$\int_{0}^{\pi/2} K_0(z \sin\theta)\, d\theta = \frac{\pi}{2}\, J_0(j\frac{z}{2})\, K_0(\frac{z}{2}) \tag{A.4}$$

Thus $(A.2)$ becomes

$$\tilde{G}(\alpha) = 2\, J_0\,(j\frac{w}{2}\sqrt{\alpha^2 - k^2}\,)\, K_0(\frac{w}{2}\sqrt{\alpha^2 - k^2}\,) \tag{A.5}$$

or

$$\tilde{G}(\alpha) = \begin{cases} 2\, I_0(\frac{w}{2}\sqrt{\alpha^2 - k^2}\,)\, K_0(\frac{w}{2}\sqrt{\alpha^2 - k^2}\,), & \alpha > k \\ 2\, J_0(\frac{w}{2}\sqrt{k^2 - \alpha^2}\,)\, K_0(j\frac{w}{2}\sqrt{k^2 - \alpha^2}\,), & \alpha < k \end{cases} \tag{A.6}$$

where I_0 is the modified Bessel function of the first kind and zero order.

APPENDIX B

CALCULATION OF THE SERIES IN EQS. (3.37)

To calculate a series in the form

$$S = \sum_{p=1}^{\infty} \frac{\cos(bp)}{P(p)} \tag{B.1}$$

where $P(p)$ is a rational even function of p, we define the function

$$f(z) = \frac{e^{jbz}}{P(p)(e^{j2\pi z}-1)} \tag{B.2}$$

and evaluate the contour integral $\int_{C_R} f(z)\,dz$ where $C_R: |z| = R$, $\text{Im}\, z \geq -\xi$ and ξ is a fixed real number. If $P(z)$ is of the order R^{ε}, $\varepsilon > 1$ as $|z| = R \to \infty$, then from Jordan's Lemma [60] we have

$$\lim_{R\to\infty} \int_{C_R} f(z)\,dz = 0$$

and therefore from Cauchy's integral formula, the sum of all the residues of $f(z)$ is equal to zero, namely

$$\sum_{p=-\infty}^{\infty} \frac{e^{jbp}}{j2\pi P(p)} + \sum [\textit{ residues of } f(z) \textit{ at zeros of } P(z)\,] = 0 \tag{B.3}$$

The first term in (B.3), which is in the form of the desired series, is due to infinite simple poles of $(e^{j2\pi z}-1)$ at $z = \pm p$, $p = 0, 1, 2, \cdots$ and clearly shows the reason for introducing this factor in (B.2).

For the special case of $P(p) = p^2 - a^2$, there are simple poles at $z = \pm a$ and from (B.3) we have

$$\sum_{p=1}^{\infty} \frac{\cos(bp)}{p^2 - a^2} = \frac{1}{2a^2} - \frac{\pi}{2a} \frac{\cos[(b-\pi)a]}{\sin(\pi a)} \tag{B.4}$$

This result can be used in calculating the series

$$S_1 = \sum_{p=1}^{\infty} \frac{\sin(k_p z') \sin(k_p z)}{k_p^2 - K_{mn}^2} \tag{B.5}$$

with $k_p = p\pi/c$. We first write S_1 in the following form

$$S_1 = \frac{1}{2}\left(\frac{c}{\pi}\right)^2 \left[\sum_{p=1}^{\infty} \frac{\cos(bp)}{p^2 - a^2} - \sum_{n=1}^{\infty} \frac{\cos(\bar{b}p)}{p^2 - a^2} \right]$$

where

$$a = \frac{c}{\pi} K_{mn}$$

$$b = \pi (z' + z) / c$$

$$\bar{b} = \pi (z' - z) / c$$

Substitution from (B.4) yields

$$S_1 = \frac{c}{2K_{mn} \sin(K_{mn} c)} \begin{cases} \sin[K_{mn}(c - z')] \sin(K_{mn} z), & z < z' \\ \sin(K_{mn} z') \sin[K_{mn}(c - z)], & z > z' \end{cases} \tag{B.6}$$

In a similar fashion, for the series

$$S_2 = \sum_{p=0}^{\infty} \frac{\cos(k_p z') \cos(k_p z)}{k_p^2 - K_{mn}^2} \tag{B.7}$$

we obtain

$$S_2 = -\frac{1}{2K_{mn}^2} - \frac{c}{2K_{mn} \sin(K_{mn} c)} \begin{cases} \cos[K_{mn}(c - z')] \cos(K_{mn} z), & z < z' \\ \cos(K_{mn} z') \cos[K_{mn}(c - z)], & z > z' \end{cases} \tag{B.8}$$

Other summations in Eqs. (3.37) can be obtained by taking the first or second derivatives of S_1 and S_2.

APPENDIX C

COMPONENTS OF THE ELECTRIC AND MAGNETIC-TYPE DYADIC GREEN'S FUNCTIONS OF A RECTANGULAR CAVITY

From Eq. (3.42), the components of the electric-type dyadic Green's function $\overleftrightarrow{G}_e(\vec{r}' \mid \vec{r})$ for a rectangular cavity and $\vec{r} \neq \vec{r}'$ are given by:

$$G^e_{xx} = -\sum_{m,n} C_{mn}(k_m^2 - k^2)\cos(k_m x')\sin(k_n y')\cos(k_m x)\sin(k_n y) f_{mn}(z, z')$$

$$G^e_{xy} = -\sum_{m,n} C_{mn} k_m k_n \cos(k_m x')\sin(k_n y')\sin(k_m x)\cos(k_n y) f_{mn}(z, z')$$

$$G^e_{xz} = -\sum_{m,n} C_{mn} k_m \cos(k_m x')\sin(k_n y')\sin(k_m x)\sin(k_n y)\frac{\partial f_{mn}}{\partial z}$$

$$G^e_{yx} = -\sum_{m,n} C_{mn} k_m k_n \sin(k_m x')\cos(k_n y')\cos(k_m x)\sin(k_n y) f_{mn}(z, z')$$

$$G^e_{yy} = -\sum_{m,n} C_{mn}(k_n^2 - k^2)\sin(k_m x')\cos(k_n y')\sin(k_m x)\cos(k_n y) f_{mn}(z, z')$$

$$G^e_{yz} = -\sum_{m,n} C_{mn} k_n \sin(k_m x')\cos(k_n y')\sin(k_m x)\sin(k_n y)\frac{\partial f_{mn}}{\partial z}$$

$$G^e_{zx} = -\sum_{m,n} C_{mn} k_m \sin(k_m x')\sin(k_n y')\cos(k_m x)\sin(k_n y)\frac{\partial g_{mn}}{\partial z}$$

$$G^e_{zy} = -\sum_{m,n} C_{mn} k_n \sin(k_m x')\sin(k_n y')\sin(k_m x)\cos(k_n y)\frac{\partial g_{mn}}{\partial z}$$

$$G^e_{zz} = -\sum_{m,n} C_{mn} k_{mn}^2 \sin(k_m x')\sin(k_n y')\sin(k_m x)\sin(k_n y) g_{mn}(z, z')$$

In these equations a, b, and c are the cavity dimensions and

$$f_{mn}(z, z') = \begin{cases} \sin[K_{mn}(c - z')]\sin(K_{mn} z), & z < z' \\ \sin(K_{mn} z')\sin[K_{mn}(c - z)], & z > z' \end{cases}$$

$$g_{mn}(z, z') = \begin{cases} \cos[K_{mn}(c - z')] \cos(K_{mn} z), & z < z' \\ \cos(K_{mn} z') \cos[K_{mn}(c - z)], & z > z' \end{cases}$$

$$K_{mn}^2 = k^2 - k_{mn}^2, \quad k_{mn}^2 = k_m^2 + k_n^2, \quad k_m = m\pi / a, \quad k_n = n\pi / b$$

$$C_{mn} = \varepsilon_m \varepsilon_n \left[abk^2 K_{mn} \sin(K_{mn} c) \right]^{-1}$$

with

$$\varepsilon_m = \begin{cases} 1, & m = 0 \\ 2, & m \neq 0 \end{cases}$$

Similarly, for the components of the magnetic-type dyadic Green's function of a rectangular cavity $\overleftrightarrow{G}_m(\vec{r}' \mid \vec{r})$, from Eq. (3.47) we have

$$G_{xx}^m = \sum_{m,n} C_{mn}(k_m^2 - k^2) \sin(k_m x') \cos(k_n y') \sin(k_m x) \cos(k_n y) g_{mn}(z, z')$$

$$G_{xy}^m = \sum_{m,n} C_{mn} k_m k_n \sin(k_m x') \cos(k_n y') \cos(k_m x) \sin(k_n y) g_{mn}(z, z')$$

$$G_{xz}^m = -\sum_{m,n} C_{mn} k_m \sin(k_m x') \cos(k_n y') \cos(k_m x) \cos(k_n y) \frac{\partial g_{mn}}{\partial z}$$

$$G_{yx}^m = \sum_{m,n} C_{mn} k_m k_n \cos(k_m x') \sin(k_n y') \sin(k_m x) \cos(k_n y) g_{mn}(z, z')$$

$$G_{yy}^m = \sum_{m,n} C_{mn}(k_n^2 - k^2) \cos(k_m x') \sin(k_n y') \cos(k_m x) \sin(k_n y) g_{mn}(z, z')$$

$$G_{yz}^m = -\sum_{m,n} C_{mn} k_n \cos(k_m x') \sin(k_n y') \cos(k_m x) \cos(k_n y) \frac{\partial g_{mn}}{\partial z}$$

$$G_{zx}^m = -\sum_{m,n} C_{mn} k_m \cos(k_m x') \cos(k_n y') \sin(k_m x) \cos(k_n y) \frac{\partial f_{mn}}{\partial z}$$

$$G_{zy}^m = -\sum_{m,n} C_{mn} k_n \cos(k_m x') \cos(k_n y') \cos(k_m x) \sin(k_n y) \frac{\partial f_{mn}}{\partial z}$$

$$G_{zz}^m = \sum_{m,n} C_{mn} k_{mn}^2 \cos(k_m x') \cos(k_n y') \cos(k_m x) \cos(k_n y) f_{mn}(z, z')$$

APPENDIX D

CALCULATION OF THE INTEGRAL IN EQ. (6.26)

From Eqs. 7.388–2, 4 in [44] and with appropriate modifications, we have

$$\int_0^\infty e^{-\frac{t^2}{2x^2}} He_{2n+1}(t)\,\sin(\frac{y}{x}t)dt=\sqrt{\pi/2}(-1)^n x\,(x^2-1)^{n+\frac{1}{2}} e^{-\frac{1}{2}y^2}\, He_{2n+1}(\frac{xy}{\sqrt{x^2-1}}) \quad \text{(D.1)}$$

$$\int_0^\infty e^{-\frac{t^2}{2x^2}}\, He_{2n}(t)\,\cos(\frac{y}{x}t)\,dt = \sqrt{\pi/2}\,x(1-x^2)^n\, e^{-\frac{1}{2}y^2}\, He_{2n}(\frac{xy}{\sqrt{x^2-1}}) \quad \text{(D.2)}$$

Let $x^2 = \dfrac{2}{1-ja}$ and $\dfrac{y}{x} = b$. Thus,

$$x = \sqrt{2}\,(1+a^2)^{-\frac{1}{4}}\, e^{j\frac{1}{2}\tan^{-1}a}$$

$$y^2 = \frac{2b^2}{1+a^2} + j\frac{2ab^2}{1+a^2}$$

$$\frac{xy}{\sqrt{x^2-1}} = \frac{2b}{\sqrt{1+a^2}}$$

$$1-x^2 = -\frac{1+ja}{1-ja} = -\,e^{j2\tan^{-1}a}$$

Substituting the above quantities in (D.1) and (D.2) and noting that $He_m(t)$ is an odd function for odd m and an even function for even m, the two equations may be combined and written in the general form

$$\int_{-\infty}^{+\infty} e^{-\frac{1}{4}t^2}\, He_m(t)\, e^{-jbt}\, e^{j\frac{a}{4}t^2}\, dt = 2(-j)^m\,\sqrt{\pi}\,(1+a^2)^{-\frac{1}{4}}\, e^{-\frac{b^2}{1+a^2}}$$

$$He_m(\frac{2b}{\sqrt{1+a^2}})\, e^{-j\frac{ab^2}{1+a^2}}\, e^{j(m+\frac{1}{2})\tan^{-1}a} \quad \text{(D.3)}$$

which is valid for even or odd m.

REFERENCES

[1] Lord Rayleigh, "On the passage of waves through apertures in plane screens and allied problems," Philosophical Magazine, Series 5, vol. 43, 1897, pp. 259-272.

[2] Bouwkamp, C. J., "Diffraction theory," Rep. Prog. Phys., vol. 17, 1954, pp. 35-100.

[3] Butler, C. M., Rahmat-Samii, Y. and Mittra, R., "Electromagnetic penetration through apertures in conducting surfaces," IEEE Trans. Electromagnetic Compatibility, vol. EMC-20, Feb. 1978, pp. 82-93.

[4] Skwirzynski, J. K. (Ed.), "Theoretical Methods for Determining the Interaction of Electromagnetic Waves with Structures," Sijthoff & Noordhoff Int. Publishers, The Netherlands, 1981.

[5] Bouwkamp, C. J., "Theoretical and numerical treatment of diffraction through a circular aperture," IEEE Trans. Antennas Prop., vol. AP-18, March 1970, pp. 152-176.

[6] Bethe, H. A., "Theory of diffraction by small holes," Physical Review, vol. 66, 1944, pp. 163-182.

[7] Millar, R. F., "An approximate theory of diffraction of an electromagnetic wave by an aperture in a plane screen," Proc. IEE, vol. 103 (C), 1956, pp. 177-185.

[8] Keller, J. B., "Diffraction by an aperture," J. Appl. Phys., vol. 28, 1957, pp. 426-444.

[9] Keller, J. B., "Geometrical theory of diffraction," Journal of the Optical Society of America, vol. 52, 1962, pp. 116-130.

[10] Van Bladel, J., "Small apertures in cavities at low frequencies," Archiv fur Electronik und Ubertragungstechnik (AEU), Band 26, 1971, pp. 481-486.

[11] Fikhmanas, R. F. and Fridberg, P. S., "Theory of diffraction at small apertures: Computation of upper and lower bounds of the polarizability coefficients," Radio Engineering and Electronic Physics (USSR), vol. 18, 1973, pp. 824-829.

[12] Knott, E. F. and Senior, T. B. A., "Comparison of three high frequency diffraction techniques," Proc. IEEE, vol. 62, 1974, pp. 1468-1474.

[13] Mittra, R., Rahmat-Samii, Y. and Ko, W. L., "Spectral theory of diffraction," Applied Physics, vol. 10, 1976, pp. 1-13.

[14] De Meulenaere, F. and Van Bladel, J., "Polarizibility of some small apertures," IEEE Trans. on Antennas and Propagation, vol. AP-25, March 1977, pp. 198-205.

[15] Menendez, R. C. and Lee, S. W., "On the role of the geometrical optics field in aperture diffraction," IEEE Trans. Antennas Prop., vol. AP-25, Sep. 1977, pp. 688-695.

[16] Van Bladel, J., "Field penetration through small apertures: The first order correction," Radio Science, vol. 14, 1979, pp. 319-331.

[17] Wilton, D. R. and Dunaway, O. C., "Electromagnetic penetration through apertures of arbitrary shape: Formulation and numeriacl solution procedure," Air Force Weapons Lab., Albuquerque NM, Tech. Rep. AFWL-TR-74-192, Jan. 1975.

[18] Harrington, R. F. and Mautz, J. R., "A generalized network formulation for aperture problems," IEEE Trans. Antennas Propagation, vol. AP-24, Nov. 1976, pp. 870-873.

[19] Harrington, R. F. and Mautz, J. R., "Electromagnetic transmission through an aperture in a conducting plane," AEU, Band 31, 1977, pp. 81-87.

[20] Suzuki, M., "Diffraction of plane electromagnetic waves by a rectangular aperture," IEEE Trans. on Antennas and Propagation, vol. AP-4, April 1956, pp. 149-156.

[21] Butler, C. M., "A formulation of the finite-length narrow slot or strip equation," IEEE Trans. on Antennas and Propagation, vol. AP-30, Nov. 1982, pp. 1254-1257.

[22] Collin, R. E. and Zucker, F. J., "Antenna Theory: Part 1," McGraw-Hill, New York, 1969, Chapter 14.

[23] Booker, H. G., "Slot aerials and their relation to complementary wire aerials," J.I.E.E. (London), vol. 93, part IIIA, 1946, pp. 620-626.

[24] Cohen, M. H., "On the bandwidth of cavity antennas," J. Appl. Phys., vol. 25, May 1954, pp. 581-587.

[25] Galejs, J., "Admittance of a rectangular slot which is backed by a rectangular cavity," IEEE Trans. on Antennas and Propagation, vol. AP-11, March 1963, pp. 119-126.

[26] Adams, A. T., "Flush mounted rectangular cavity slot antennas-Theory and design," IEEE Trans. on Antennas and Propagation, vol. AP-15, May 1967, pp. 342-351.

[27] Cockrell, C. R., "The input admittance of the rectangular cavity-backed slot antenna," IEEE Trans. on Antennas and Propagation, vol. AP-24, May 1976, pp. 288-294.

[28] Long, S. A., "Experimental study of the impedance of cavity-backed slot apertures," IEEE Trans. on Antennas and Propagation, vol. AP-23, Jan. 1975, pp. 1-7.

[29] Long, S. A., "A mathematical model for the impedance of the cavity-backed slot antenna," IEEE Trans. Antennas Propagation, vol. AP-25, Nov. 1977, pp. 829-833.

[30] Goubau, G. and Schwering, F., "On the guided propagation of electromagnetic wave beams," IRE Trans. on Antennas and Propagation, vol. AP-9, May 1961, pp. 248-256.

[31] Christian, J. R. and Goubau, G., "Experimental studies on a beam waveguide for millimeter waves," IRE Trans. Antennas Prop., vol. AP-9, May 1961, pp. 256-263.

[32] Goubau, G., "Optical relations for coherent wave beams," in Electromagnetic Theory and Antennas, Int. Series of Monographs on Electromagnetic Waves, E. C. Jordan, Ed., vol. 6, pt. 2, Pergamon Press, New York, 1963.

[33] Goubau, G. and Christian, J. R., "Some aspects of beam waveguides for long distance transmission at optical frequencies," IEEE Trans. on Microwave Theory and Techniques, vol. MTT-12, March 1964, pp. 212-220.

[34] Goubau, G. and Christian, J. R. "Loss measurements with a beam waveguide for long-distance transmission at optical frequencies," Proc. IEEE, vol. 52, 1964, p. 1739.

[35] Schwering, F., "Reiterative wave beams of rectangular symmetry," Archiv fur Electronik und Ubertragungstechnik (AEU), vol. 15, Dec. 1961, pp. 555-564.

[36] Brauer, J. R., "A rectangular beam waveguide resonator antenna," IEEE Trans. on Antennas and Propagation, vol. AP-20, Sept. 1972, pp. 595-601.

[37] Hadidi, A. and Hamid, M. "A novel treatment of Pocklington's equation applied to slot apertures," IEEE Trans. on Antennas and Propagation, (In press).

[38] Hadidi, A. and Hamid M., "Electric and magnetic dyadic Green's functions of bounded regions," Canadian Journal of Physics, vol. 66, March 1988, pp. 249-257.

[39] Weeks, W. L., "Electromagnetics for Engineering Applications," John Wiely & Sons, New York, 1964, Chapter 4.

[40] Tai, C-T., "Dyadic Green's Function in Electromagnetic Theory," Intext Publishers, Scranton, P. A., 1971.

[41] Wilton, D. R. and Butler, C. M., "Efficient numerical techniques for solving Pocklington's equation and their relationships to other methods," IEEE Trans. on Antennas and Propagation, vol. AP-24, Jan. 1976, pp. 83-86.

[42] Abramowitz, M. and Stegun, I. A. (Eds.), "Handbook of Mathematical Functions," Dover Publications, Inc., New York, 1970.

[43] Mittra, R. (Ed.), "Numerical and Asymptotic Techniques in Electromagnetics," Springer-Verlag, Berlin, 1975, Chapter 2.

[44] Gradshteyn, I. S. and Ryzhik, I. M. "Table of Integrals, Series and Products," Academic Press, Orlando, 1980.

[45] Nehari, Z., "Conformal Mapping," Dover Publications, Inc., New York, 1975.

[46] Elliott, R. S., "Antenna Theory and Design," Prentice-Hall, Inc., 1981, Chapter 7.

[47] Kurokawa, K., "The expansion of electromagnetic fields in cavities," IRE Trans. Microwave Theory Tech., vol. MTT-6, April 1958, pp. 178-187.

[48] Goubau, G., "Electromagnetic Waveguides and Cavities," Pergamon Press Inc., 1961, Chapter 2.1.

[49] Van Bladel, J., "Electromagnetic Fields," McGraw-Hill, New York, 1964, Chapter 10.

[50] Argens, E. and Kahan T., "Theory of Waveguide and Cavity Resonators," Blackie and Son Ltd., 1967, Chapter 23.

[51] Collin, R. E., "Field Theory of Guided Waves," McGraw Hill, New York, 1960.

[52] Tai, C-T. and Rozenfeld, P., "Different representations of dyadic Green's functions for a rectangular cavity," IEEE Trans. Microwave Theory Tech., vol. MTT-24, Sep. 1976, pp. 597-601.

[53] Hadidi, A. and Hamid, M., "Analysis of a cylindrical cavity resonator with absorbing wall," Int'l Journal of Electronics, vol. 63, 1987, pp. 435-442.

[54] Newman, E. H. and Thiele, G. A., "Some important parameters in the design of T-bar fed slot antennas," IEEE Trans. Antennas Prop., vol. AP-23, Jan. 1975, pp. 97-100.

[55] Crews, M. R. and Thiele, G. A., "On the design of shallow depth T-bar fed slot antennas," IEEE Trans. Antennas Propagation, vol. AP-25, Nov. 1977, pp. 833-836.

[56] Mayes, P. E., Warren, W. T. and Wiesenmeyer, F. M., "The monopole slot: A small broad-band unidirectional antenna," IEEE Trans. on Antennas and Propagation, vol. AP-20, July 1972, pp. 489-493.

[57] Roederer, A. G., "A log-periodic cavity-backed slot array", IEEE Trans. on Antennas and Propagation, vol. AP-16, Nov. 1968, pp. 756-758.

[58] Hadidi, A. and Hamid, M., "Aperture field and circuit parameters of a cavity-backed slot radiator," Proc. IEE, part H, (In press).

[59] Erdelyi, A. (Ed.), "Tables of Integral Transforms," vol. 1, McGraw-Hill, 1954.

[60] Silverman, R. A., "Introductory Complex Analysis," Dover, 1972, Chapter 12.